UNIVERSIDADE DE LISBOA

Faculdade de Ciências

Departamento de Física

Study of the Influence of a DC Electric Field on the Development of the Embryo of the Nematode *Caenorhabditis elegans*

André de Albuquerque Rino Loureiro de Amorim

Dissertação

Mestrado Integrado em Engenharia Biomédica e Biofísica
Perfil em Engenharia Clínica e Instrumentação Médica

2012

UNIVERSIDADE DE LISBOA

Faculdade de Ciências

Departamento de Física

Study of the Influence of a DC Electric Field on the Development of the Embryo of the Nematode *Caenorhabditis elegans*

André de Albuquerque Rino Loureiro de Amorim

Dissertação orientada por:
Prof. Dr. Philippe Renaud
École Polytechnique Fédérale de Lausanne
Prof. Dr. Hugo Ferreira
Faculdade de Ciências da Universidade de Lisboa

Mestrado Integrado em Engenharia Biomédica e Biofísica
Perfil em Engenharia Clínica e Instrumentação Médica

2012

aos meus pais

Contents

List of Figures

List of Tables

Physical Quantities and Constants

Quantity	**Symbol**	**Unit**
Distance	D, x	Metre (m)
Length	L, l, d	Metre (m)
Width	W, w	Metre (m)
Height	h	Metre (m)
Radius	r	Metre (m)
Diameter	d	Metre (m)
Area	A	Square metre (m^2)
Electric Field	**E**	Newton per Coulomb (N/C), Volt per metre (V/m)
Electric Current	I	Ampere (A)
Current Density	**J**	Ampere per square metre (A/m^2)
Electric Potential	V, E	Volt (V)
Potential Difference or Voltage	U, V	Volt (V)
Overpotential	η	Volt (V)
Thermal Voltage	V_t	Volt (V)
Resistance	R	Ohm (Ω)

Quantity	**Symbol**	**Unit**
Resistivity	ρ	Ohm times square metre ($\Omega.m^2$)
Conductance	G	Siemens (S), Siemens per square metre (S/m^2)
Conductivity	σ	Siemens per square metre (S/m^2)
Charge transfer Resistance	R_{CT}	Ohm (Ω), Ohm times square metre ($\Omega.m^2$)
Diffusion Resistance	R_d	Ohm (Ω), Ohm times square metre ($\Omega.m^2$)
Spreading Resistance	R_S	Ohm (Ω), Ohm times metre ($\Omega.m$)
Capacitance	C	Farad (F)
Interfacial Capacitance	C_I	Farad (F), Farad per square metre (F/m^2)
Helmholtz Capacitance	C_H	Farad (F), Farad per square metre (F/m^2)
Gouy-Chapman Capacitance	C_{GC}	Farad (F), Farad per square metre (F/m^2)
Permittivity	ε	Farad per metre (F/m)
Vacuum Permittivity	ε_0	8.8542 Farad per metre (F/m)
Relative permittivity, dielectric constant	ε_r	Dimensionless
RC Time constant	τ	Second (s)
Electric Power	P	Watt (W)

Quantity	**Symbol**	**Unit**
Faraday Constant	F	96485 Coulomb per mole (C/mol)
Electron valence	z	Dimensionless
Temperature	T	Kelvin degree (K), Celsius degree (ºC)
Gas constant	R	8.3145 Joule per mole per Kelvin (J/(mol.K))
Concentration of ion X	[X]	Mole per cubic metre (mol/m^3)
Ionic Permeability	P	Dimensionless

Symbols and Abbreviations

2D: Two dimensional

3D: Three dimensional

AC: Alternating current

AP: Antero-posterior

BioMEMS: Biological Microelectromechanical systems

***C. elegans*:** *Caenorhabditis elegans*

DC: Direct current

DIC: Differential interference contrast

DV: Dorso-ventral

***E. coli*:** *Escherichia coli*

EEM: Extraembryonic matrix

EF: Electric field

FEM: Finite element method

NEBD: Nuclear envelope breakdown

PBS: Phosphate buffered saline

PDMS: Polydimethylsiloxane

TEP: Transepithelial potential

Abstract

Bioelectricity has an impact on the development of tissues because it can influence cell polarization, essential for asymmetric cell division. This feature may be an important tool for tissue engineering and regenerative medicine applications.

The nematode *Caenorhabditis elegans* is a primitive organism, but whose physiology shares several characteristics of human biology. Its embryo is an ideal model for the study of cell division and embryogenesis, since its development is almost invariant and highly reproducible and readily observable.

This project has the objective of studying the impact of a DC electric field in the *C. elegans* embryo development and to assert if this organism is a good model for further research in this field. To accomplish it, a DC electric field is applied in a microchannel filled with PBS, where to the embryo is confined.

Embryogenesis is studied by analysing selected development stages, which are compared for control and electric field experiments. To optimize the application of the electric field to the embryo and minimize other physical phenomena which can disturb embryogenesis, a detailed physical characterization of the microfluidic system is also performed.

The results show that there are no big differences in the events of embryogenesis, suggesting that the embryo resists to the electrode field, perhaps due its eggshell. Nevertheless, small differences in embryological times suggest that the electric field can have long term effects on embryogenesis, and that a more detailed analysis should be performed.

In summary, the embryo nematode *C. elegans* is not as suited to study the impact of DC electric fields in embryogenesis as other embryo models, such as amphibians. However, there is still the possibility of studies of single isolated embryo cells. Besides, it is not discarded the possibility of applying an AC electric field or attempting to remove the eggshell in future studies.

Keywords: *C. elegans* embryogenesis; Asymmetric cell division; Bioelectricity; DC electric field; Microfluidic chip.

Resumo

A bioelectricidade pode influenciar a polarização de uma célula, responsável pela divisão assimétrica, pelo que tem um impacto significativo no desenvolvimento de tecidos ao contribuir para controlar a migração e orientação de células e também a proliferação, diferenciação e apoptose celulares. Estas propriedades da bioelectricidade em tecidos biológicos tornam-na numa ferramenta importante em engenharia de tecidos e medicina regenerativa, pois permite controlar várias respostas fisiológicas a estímulos eléctricos e usá-las para fins benéficos.

O nematóide *Caenorhabditis elegans* é um organismo primitivo, mas cuja fisiologia partilha várias características da biologia humana. Estas características, juntamente com a sua simplicidade de cultivar em grandes populações e de ser conveniente para análise e manipulação genética, tornam-no num dos organismos-modelo mais vastamente utilizados em investigação científica, existindo actualmente uma enorme quantidade de informação disponível sobre este nematóide. O embrião do *C. elegans* representa um modelo ideal para o estudo da divisão celular e da embriogénese, visto que o seu desenvolvimento é altamente reprodutível e facilmente observável. Além disso, o padrão de desenvolvimento do embrião é praticamente invariável, tornando possível construir um diagrama que representa toda a sua linhagem celular, o que facilita imensamente a análise da embriogénese.

A motivação deste projecto surge do conhecimento de que vários seres vivos, como a hidra ou a salamandra, possuem uma grande capacidade de regeneração que está grandemente relacionada com a bioelectricidade. Compreender e controlar os seus mecanismos será certamente um grande avanço na área de engenharia de tecidos e terá como consequência o surgimento de diversas potenciais aplicações.

Este projecto tem como objectivo aplicar a aplicação de um campo eléctrico DC num organismo vivo, de forma a induzir uma resposta por parte dele. Devido às suas características, o embrião do nematóide *C. elegans* foi escolhido como organismo modelo para a aplicação deste estímulo eléctrico. A principal assumpção é que o campo eléctrico aplicado ao longo do eixo antero-posterior do embrião do nematóide *C. elegans*, induza uma acumulação de carga oposta nas suas extremidades anterior e posterior com o intuito de alterar o potencial de membrana, onde se levantou a hipótese

de poderem induzir respostas celulares diferentes em cada extremidade, causando alterações na embriogénese. A ideia surge de uma analogia à aplicação de um gradiente de temperatura ao longo desse mesmo eixo, sabendo-se actualmente que induz uma resposta relativamente à duração de ciclos celulares, visto que é fortemente dependente da temperatura.

Através dos resultados, pretende-se também avaliar a utilidade deste embrião como um organismo-modelo para o estudo do impacto de campos eléctricos DC em tecido vivo, visto que outros embriões, como de anfíbios ou pintos, apresentam grandes distúrbios no seu desenvolvimento quando estimulados com campos eléctricos contínuos, com consequências catastróficas no organismo final.

A tecnologia dos micro-sistemas permite controlar eficazmente o ambiente celular de uma forma bastante precisa. Assim, um sistema microfluídico é usado como plataforma para estudar o impacto da aplicação do campo eléctrico ao embrião. Este é colocado no interior de um microcanal contendo PBS (tampão fosfato-salino), um bom electrólito e ao mesmo tempo biocompatível para o seu desenvolvimento. Recorrendo a eléctrodos de platina, é aplicada uma diferença de potencial nas extremidades do canal, o que torna possível a existência de uma corrente eléctrica que deverá resultar numa acumulação de carga oposta nas extremidades do embrião, visto que a sua resistividade deverá ser superior à do PBS. A largura e altura do canal são semelhantes à espessura do embrião, o que garante que o campo eléctrico passa através do embrião ou que seja desviado por ele, no caso de este ser isolante.

Tendo em conta que o campo eléctrico propaga-se através do canal em direcção ao embrião, é necessário saber qual a sua magnitude à volta dele. Além disso, interacções físicas como o efeito de Joule e reacções redox entre os eléctrodos e o electrólito podem alterar a temperatura e o pH no interior do canal e comprometer o desenvolvimento do embrião de forma indesejada. Assim é também efectuada uma caracterização física detalhada do sistema microfluídico, com o intuíto de saber quais os principais fenómenos físicos que podem ocorrer no interior do canal durante a aplicação do campo eléctrico. Esta caracterização permite tomar as medidas necessárias para minimizar estes efeitos secundários que possam perturbar o normal desenvolvimento do embrião.

A caracterização física do sistema consiste essencialmente numa análise das interacções dos eléctrodos de platina com uma solução de cloreto de sódio, o principal

constituinte do PBS e em determinar a relação entre a corrente eléctrica no canal e a diferença de potencial aplicada. Para isso são efectuadas medições experimentais e simulações recorrendo ao software de elementos finitos *COMSOL Multiphysics*.

O procedimento experimental para a análise do impacto do campo eléctrico no embrião começa com a recolha de um embrião de um nematóide hermafrodita adulto, proveniente de uma cultura em pratos de agarose semeados com *Escherichia coli* como fonte de alimento. O embrião escolhido deve estar no início do desenvolvimento, de preferência após a meiose, de forma a poder ser estimulado o mais cedo possível. Sabe-se que perturbar os eventos iniciais da embriogénese pode ter consequências em todo o restante desenvolvimento, visto que este depende grandemente das primeiras divisões celulares.

Recolhido o embrião, este é inserido no microcanal, onde é fixado e permanece durante todo o ensaio experimental. De seguida, o campo eléctrico é aplicado através da aplicação de uma diferença de potencial nos eléctrodos em contacto com as extremidades do canal. Pontes salinas de agarose são utilizadas em algumas experiencias para evitar a contaminação do electrólito com produtos das reacções químicas que ocorrem na superfície dos eléctrodos. O desenvolvimento do embrião é observado através de microscópios invertidos equipados com contraste de fase. Imagens de *time-lapse* são capturadas e posteriormente analisadas recorrendo ao software *ImageJ*. Eventos da embriogénese seleccionados para análise são comparados para embriões em experiencias de controlo e embriões estimulados com o campo eléctrico. Métodos de análise estatística são efectuados para auxiliar a comparação. Parâmetros a observar e comparar são os tempos de ocorrência dos eventos seleccionados e orientação e posição de células no embrião. O comportamento da minhoca juvenil após o nascimento também pode fornecer informação relativamente à embriogénese, pelo que também é analisado.

A caracterização do chip revelou que uma tensão de 5V é apropriada para criar um campo eléctrico com dimensões fisiológicas (cerca de 0.3mV/μm), não aumentando a temperatura para valores fora dos limites de desenvolvimento normal do embrião. Alterações do pH foram minimizadas através da utilização das pontes salinas inseridas nas entradas do canal.

A comparação entre embriões de controlo e embriões estimulados revela que não existem grandes diferenças entre os eventos da embriogénese de embriões de controlo e

embriões estimulados pelo campo eléctrico, o que sugere que o embrião resiste ao campo eléctrico, talvez devido à barreira de permeabilidade presente na sua carapaça. Pequenas diferenças nos tempos embriológicos entre embriões de controlo e estimulados sugerem que o campo eléctrico possa ter efeitos a longo prazo na embriogénese, retardando os seus eventos mais tardios. As diferenças são demasiado pequenas para se poder tirar alguma conclusão, contudo, os resultados sugerem que deveria ser feita uma análise mais detalhada ao ciclo celular de certas células do início da embriogénese, o que não foi possível com o equipamento disponível.

Comparando estes resultados com os de outros estudos com embriões, como por exemplo em anfíbios ou pintos, conclui-se que o impacto do um campo eléctrico DC no desenvolvimento do embrião do nematóide *C. elegans* não é tão significativo como nesses modelos, o que os torna preferíveis para estudos com embriões intactos. No entanto, existe ainda a possibilidade de estudos a nível de células isoladas extraídas do embrião e também não é de descartar a hipótese de aplicar um campo eléctrico AC ou de tentar remover a carapaça do embrião em futuras investigações.

Palavras chave: Embriogenese do *C. elegans*; Divisão assimétrica; Bioelectricidade; Campo eléctrico DC; Chip microfluídico.

Acknowledgements

First of all, I have to thank my parents and siblings for all the help, support and motivation they gave me during the roughest times when I was writing this thesis.

I am really grateful to Professor Philippe Renaud who gave me a unique opportunity and continuously provided helpful suggestions when my project faced an apparent dead end.

I am also grateful to Professor Abel Oliva, without him I would never had this opportunity.

I sincerely thank my supervisor at EPFL, Robert Meissner, from whom I a have learnt a lot during this year. I am grateful for his constant availability and for all the times he explained or taught me about something I didn't know or wasn't familiar with. Without him, I would be permanently lost in the lab.

I would like to thank Hugo Ferreira, for his almost instantaneous suggestions to solve a particular problem and for all the help and patience while I was writing the report.

I have to thank Sophie Baranek for teaching me about *C. elegans*, Harald van Lintel and Arnaud Bertsch for the help with every type of devices and their sense of humour, and the remaining crew of LMIS4. I also thank Pierre Gönczy, Coralie Busso, Aitana Neves, Alexandra Bezler and Simon Blanchoud from the SV lab, who were always available to help me with *C. elegans*.

I thank Wyllian Hasenkamp and Daniel Duplat, the two whom I could speak portuguese in the middle of that sea of foreigner languages.

I would also like to thank the professors of IBEB, Alexandre Andrade and Eduardo Ducla Soares, and also to Giomar Evans.

Finally, I thank the friends I have made in Lausanne, namely Mafalda, Ricardo, Aleksey and Arthur, with whom I shared the final moments during my stay in Switzerland.

1. Electricity of Life

1.1. What is Bioelectricity?

Electricity is everywhere in our lives. Everything we see, hear, fell, touch or think is electricity. Our sense of reality is in fact the interpretation of electric signals by the brain, making our perception of life how it is. But electricity is not only in our senses. It is everywhere in our body. Our heart beats because of electricity. We move and speak because of electricity. We grow and reproduce because of electricity. If electricity did not exist, life would not exist. Electricity is present in every single cell that makes part of us and all other living beings.

Bioelectricity is the electricity produced by or occurring in living cells, tissues and organisms. The first evidence of how electricity can affect living organism goes back to the XVIII century, when the french clergyman Jean-Antoine Nollet caused 180 of the King's guards to leap simultaneously by having them all hold hands and then connecting the man at the end of the line to the discharge from a Leyden jar [1]. The italian anatomist and physician Luigi Galvani was one of the pioneers to investigate experimentally the phenomenon that came to be named "bioelectrogenesis", the ability of a living organism to generate electricity. In 1794, he proved that animals could generate electricity when he demonstrated that the cut end of a frog sciatic nerve from one leg induced contractions when it touched the muscles of the opposite leg (Fig. 1.1), introducing the concept of "animal electricity" [2]. Galvani's famous experiments helped to establish the basis for the biological study of neurophysiology and neurology [2].

In 1843, the swiss-german scientist Emil Heinrich Du Bois-Reymond measured a small current flowing out of a cut in his own finger [1] and five years later he used a galvanometer (named after Galvani) to detect what he called an "action current" in the frog's nerve, later called by "action potential". Reymond's work created the field of scientific electrophysiology as the science that studies bioelectricity, which greatly

contributed to reduce physiology to applied physics and chemistry, a trend that has dominated physiology and medicine ever since [2].

In modern times, the measurement of bioelectric potentials has become a routine practice in clinical medicine. Electrical effects originating in active cells of the heart and the brain, for example, are commonly monitored and analyzed for diagnostic purposes.

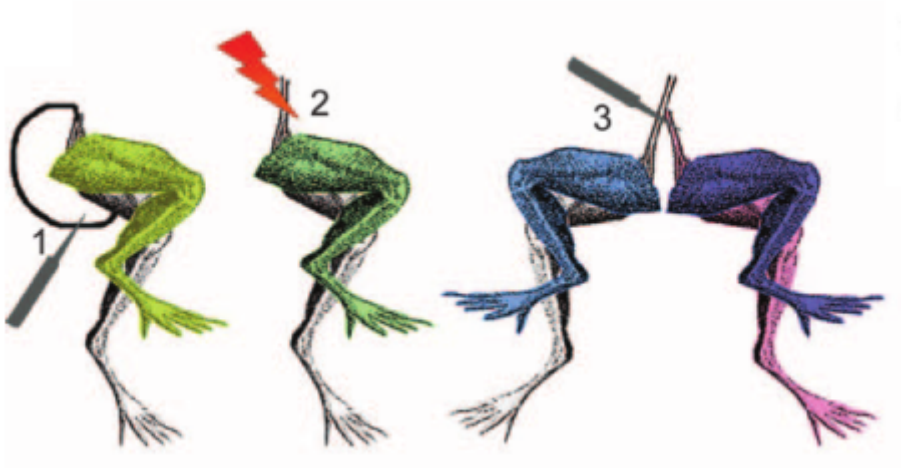

Fig. 1.1: Galvani's experiments using a frog leg preparation. The leg contracted when the cut end of the sciatic nerve touched the leg muscle (1) or when the electrical discharge was applied directly to the nerve (2). When the surface of a section of the right sciatic nerve touched the intact surface of the left sciatic nerve, both legs contracted (3). (Image taken from [1])

Currently, bioelectricity is defined as electric potentials and currents produced by or occurring within living organisms. Bioelectric potentials are identical to the potentials produced by devices such as batteries or generators, but are instead generated by a variety of biological processes and are also weaker, generally ranging in strength from only one to a few hundred millivolts [3]. The most famous bioelectric potential is the action potential, used to transfer information in animals and playing a central role in cell-cell communication. Bioelectric currents, on the other hand, are always ionic, differing completely from the electron currents flowing in metal wires. In animals, bioelectric currents occur due to the movement of ions through the interstice, cytoplasm and across cell membranes, through ion channels. Their strengths usually range from hundreds of nanoamperes to hundreds of microamperes.

The potential across the cell membrane i.e. the difference between the potential inside the cell and the potential outside the cell is called the membrane potential (V_m). No single ion species is distributed equally on the two sides of a cell membrane. There are four most abundant ions found on either side of it: Na^+ and Cl^- are more abundant outside the cell and K^+ and organic negative anions are more concentrated inside. The cell is impermeable to organic ions due to their size, but not to the other three ions, which are allowed to move across the membrane through ion channels. The membrane potential that results from the total contribution of those three ions is given by the Goldman equation [4]:

$$V_m = \frac{RT}{zF} \ln \frac{P_K \left[K^+\right]_o + P_{Na} \left[Na^+\right]_o + P_{Cl} \left[Cl^-\right]_i}{P_K \left[K^+\right]_i + P_{Na} \left[Na^+\right]_i + P_{Cl} \left[Cl^-\right]_o} \tag{1.1}$$

P_X is the permeability of the membrane to the ion X. This permeability results from the activity of specific ion channels and may be influenced by voltage gradients, chemical gradients and mechanical stress. Therefore, the activity of these channels may change due to internal stimulus induced by the cell or external stimulus induced near it.

At a specific potential, the currents from all the ions cancel each other and the total current at the membrane is zero ($I_K + I_{Na} + I_{Cl} = 0$). In this situation, the membrane is said to be at rest, and its potential is called the resting membrane potential (V_r). Almost all cell membranes are polarized at rest, since V_r is never equal to zero. However, the activity of a cell may change when its polarization (i.e. its membrane potential) changes from the rest situation, due to a stimulus.

Cell membranes also show a capacitive effect. This is extremely important, because the membrane is very thin and thus highly capacitive [5]. A capacitive or displacement current is responsible for charging the membrane when electrical stimuli are applied to it, and thus changing the membrane potential. It is crucial for the propagation of the action potential, for example.

$$I_C = C_m \frac{dV_m}{dt} \tag{1.2}$$

C_m is the membrane capacitance. At rest, the capacitive current (I_C) is zero since V_m does not change with time.

Ionic currents do not exist only at the cell membrane. They exist also inside the cell, in the cytoplasm, and outside the cell, in the interstice, and may cross the cell membrane, creating electric circuits. Ionic currents may also flow away from a cell and cross entire tissues, due to electric fields gradients induced by the membrane potential of various cells. These electric fields are responsible for many regenerative and growth processes.

1.2. Asymmetric Cell Division and Tissue Growth and Development

Bioelectricity has a great impact in tissue development and growth, because it can influence cell polarization. Cell polarity does not refer to membrane charge gradients, but instead to spatial differences in the shape, structure, and function of cells. A complete organism is not symmetric. Mammals have a head at their rostral extremity and two feet at their ventral extremity. The human heart is on the left side and not on the right. How can this happen if all animals started as a unique round egg cell? Also, how can a vertebrate have a nervous system and a skeleton, two completely different tissues, if both of them came from the same cell? The answer is asymmetric cell division.

Asymmetric cell division is the process that allows one cell, called stem cell, to divide into two daughter cells with different fates (Fig. 1.3). These divisions allow cellular diversity, an essential feature of the development of any multicellular organism [6]. Through asymmetric divisions, stem cells can both generate differentiating cells that will constitute the bulk of the tissues, and self renew, thereby maintaining a constant

pool of stem cells (Fig. 1.2). Two distinct mechanisms (or a combination of them) can lead to asymmetric cell divisions [6]:

- Extrinsic mechanisms: two daughter cells are born equal but an asymmetry is subsequently induced in one of the daughters by the cell environment or cell niche;

- Intrinsic mechanisms: two daughter cells are born different after determinants are segregated asymmetrically before division. The three main events required for such process to occur are polarization of the mother cell, unequal distribution of cell fate determinants along the polarity axis and proper alignment of the mitotic spindle in the axis of polarity. Cell polarity is the trigger for the other two events that occur after. It arises primarily through the localization of specific proteins to specific areas of the cell membrane.

Protein localization requires both the recruitment of cytoplasmatic proteins to the cell membrane and polarized vesicle transport along cytoskeletal filaments to deliver transmembrane proteins from the Golgi apparatus. Examples include the PAR complex (Cdc42, PAR3, PAR6, atypical protein kinase C), Crumbs complex (Crb, PALS, PATJ, Lin7), and Scribble complex (Scrib, Dlg, Lgl) [7]. Most of them are common among several different organisms.

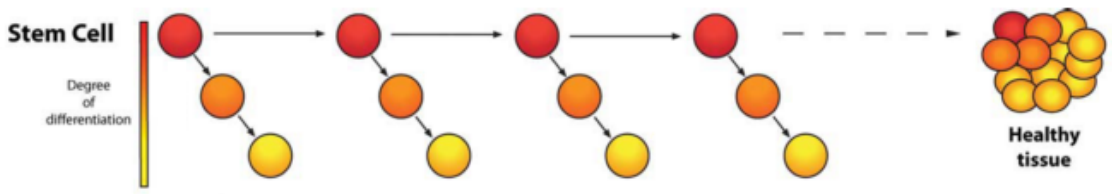

Fig. 1.2: A stem cell divides asymmetrically originating two daughter cells with different fates. The daughters may differentiate and proliferate or remain stem cells to divide asymmetrically again. A healthy tissue is composed by several differentiated cells. (Image taken from [6])

After an asymmetric division, the two daughter cells may have completely different fates. They can differentiate and proliferate to form various tissues or remain

undifferentiated. They can migrate to different places and orient to different directions. They may even be destined to die by apoptosis.

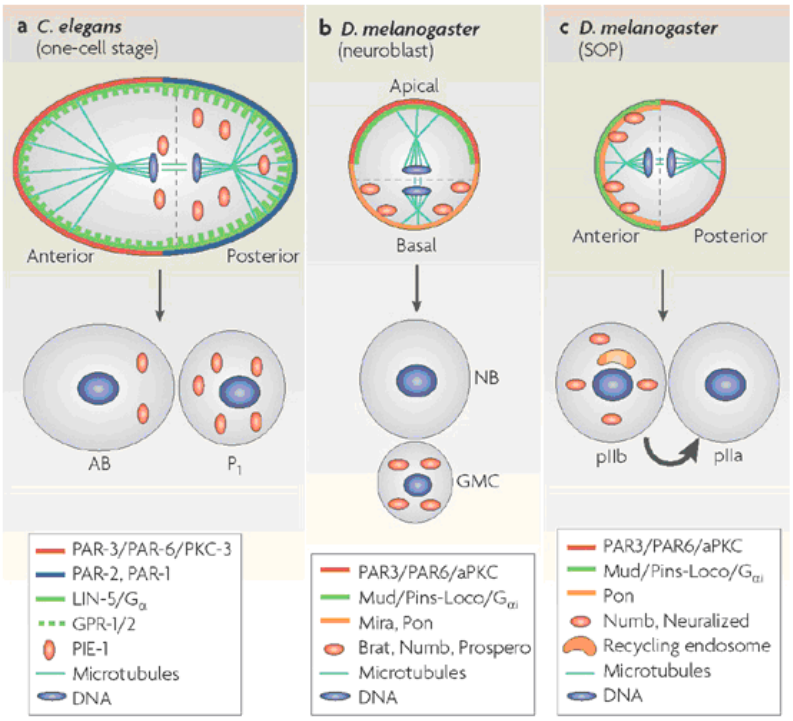

Fig. 1.3: Asymmetric division of the egg-cell of three different organisms. This is the first mitotic division of embryogenesis. The polarized mother cell during anaphase is shown at the top of each panel, whereas the daughter cells that are produced by asymmetric division are shown at the bottom of each panel and are named below. The distribution of several components that are important for polarity establishment, spindle positioning and cell-fate determination is illustrated for the mother cell, and the distribution of cell-fate determinants is shown for daughter cells immediately after mitosis. Note that many of them are the same for the three organisms. Directional signalling between the anterior cell (pIIb) and the posterior cell (pIIa), whereby the Delta ligand from pIIb signals to the Notch receptor on pIIa, is denoted by a thick arrow in panel c. This is an example of an extrinsic mechanism of fate determination. (Image and description taken from [8])

1.3. The Impact of Bioelectricity in Regeneration and Development

By affecting cell polarization, bioelectricity contributes to control cell fate, as the cell orientation, directionality of cellular migration and differentiation. DC electric signals control re-epithelisation, neural and muscle tissue growth, angiogenesis and

inflammation responses. This level of physiological control allows coordinating complex regenerative responses, as the wound healing in humans or limb regeneration in salamanders.

The transepithelial potential (TEP) is the potential difference across an intact epithelium and arises from its impermeability due to tight junctions between cells that block the flow of ionic currents. After an injury, the epithelium is interrupted creating a current leak at the wound site causing an immediate collapse of the TEP at the wound. This injury current creates a steady voltage drop that decreases within the distance to the wound, which, by its turn, creates an extracellular DC voltage gradient, strongest at the wound region and weaker as the distance to the wound increases (Fig. 1.4). Injury currents were first observed during Galvani's experiments with the frog nerve, but also may occur at other tissues that have a TEP, such as the skin, as showed by Du-Bois Reymond [1].

The wound induced endogenous DC electric field may be present for hours, days, or even weeks during both development and regeneration [1]. The regeneration mechanism eventually involves adult stem cell divisions and differentiation in order to recreate the missing tissue. The electric fields are though to be involved mainly in the cell orientation and migration mechanisms, a phenomenon termed electrotaxis. It consists in the movement of charged receptor molecules, exposed on the outer surface of the cell membrane lipid bilayer, due to the physical action of a physiological electric field. This results in a created receptor asymmetry between cathodal and anodal facing membranes, that in turn induce asymmetries in the cellular response (by signal transduction), that may affect the cell division [9].

As an example is the division of human corneal epithelial cells, whose cleavage plane orients perpendicularly to an artificially applied DC electric field [10] (Fig. 1.5). It was also shown that they tend to migrate in direction to the cathode, when submitted to an electric field [11]. Other studies showed that wounded rat corneal epithelium regenerated differently when the endogenous injury electric field was manipulated. The rate and degree of wound healing was proportional to the magnitude of the electric field that was increased or decreased by changing the transcorneal potential difference through chemical treatments that altered the epithelium permeability to ions, such as

Na^+ and Cl^-, that are needed to create injury currents [12, 13, 14]. These results showed that disrupting the injury currents alters tissue regeneration.

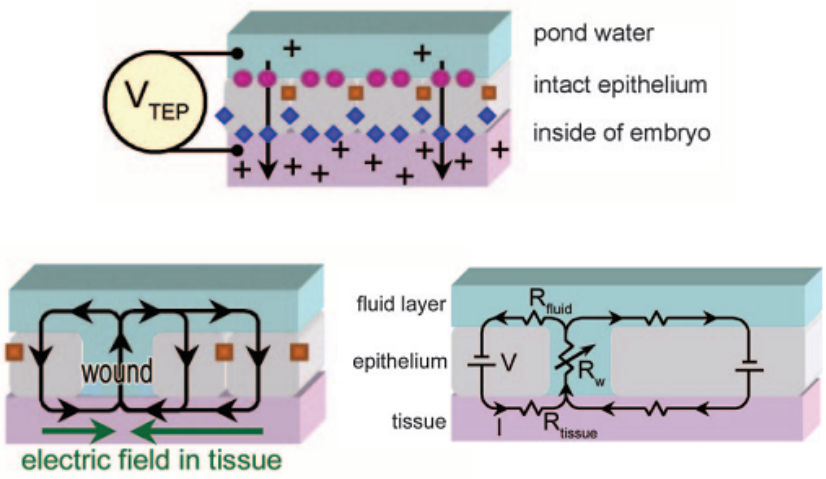

Fig. 1.4: Top: skin epithelium of the *Xenopus* embryo. The transepithelial potential results from active transport and passive diffusion of ions across the basal and apical membranes of epithelial cells. Thigh junctions avoid the passage of ions outside the cells. Bottom left: wounding of an epithelial sheet (or localized disruption of tight junctions) creates a current leak at the wound site causing the immediate, catastrophic collapse of the TEP at the wound. The TEP is not affected distally, where the epithelial integrity and ion transport properties remain intact. Na^+ leak out the wound, resulting in an outward injury current and a lateral voltage gradient (electric field) within the embryo (green arrows) oriented parallel to the epithelial sheet. The wound site is the cathode of the EF. Bottom right: circuit model of the wounded epithelium. Each battery represents the transepithelial potential for a patch of epithelium. It differs with the distance to the wound. R_w is the resistance of the wound, R_{fluid} is the resistance of the pound water where the frog embryo develops and R_{tissue} is the resistance of the tissue underlying the epithelium. (Image taken from [1])

Experiments using neuron cultures submitted to DC electric fields demonstrated that the nerve growth was enhanced and directed by the field, showing that electrotaxis is involved in neural tissue growth [9]. Measurements in intact amphibian embryos show spatial differences in the TEP that generate electric fields within them. Altering those fields by electrical stimulation disrupts embryogenesis [15]. Large currents flowing out the cut end of a newt amputated limb were also detected and persisted during all the regeneration process. Interestingly, the currents stopped when skin grafts covered the wound region, suggesting that the regeneration ends when the skin is covering again the wound [16]. Other examples of research about the impact of bioelectricity in tissue development may be found in [1, 17 and 18].

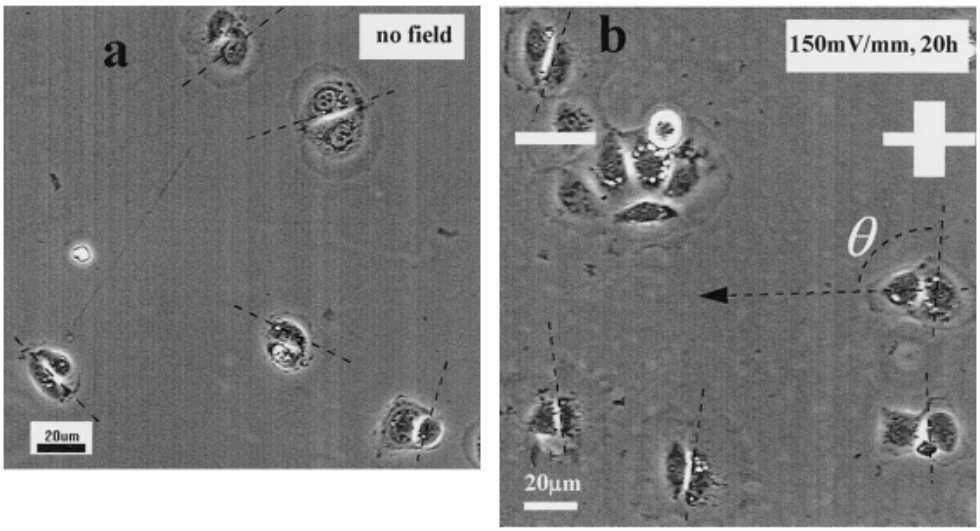

Fig. 1.5: Orientation of the cleavage plane of transformed human corneal epithelial cells was affected by applied EFs (strength and polarity as shown). (a) No field control. Cleavage furrows are evident and oriented randomly. (b) Dividing cells in an applied EF showed preferential orientation of the cleavage furrow. (Image and description taken from [10])

The response of stem cells to DC electric fields shows bioelectricity as a very important tool in tissue engineering and regeneration medicine. The potential applications of manipulating biologic tissue with these fields are apparent. Once understood their mechanisms, one can use the interaction between bioelectricity and a tissue for beneficial ends. Chronically wounds could be healed and born body deficiencies could be minimized or completely eliminated. The most prominent potential applications nowadays are in cancer research and spinal cord regeneration.

Cancer cells have a greater negative surface charge than normal cells, and usually their membrane potential is depolarized markedly. The TEP of the skin of normal and cancer breast epithelium differs, and this is used clinically to diagnose the early onset of breast cancer in women [1, 19, 20]. There are also reports of small steady extracellular voltage gradients between cancerous tissue and neighbouring normal tissue, which could act as guidance cues promoting and directing cancer cell migration [1, 21]. In rat prostate cancer tissue, cell lines with different metastatic levels responded differently to an external applied electric field, suggesting news therapies to this disease [22].

Borgens [23, 24, 25] was able to restore some function in damaged guinea pig spinal cord with an applied DC electric field. The electric field stimulated and directed regenerative growth of large numbers of myelinated axons towards the cathode. The degree of regeneration was enough to allow certain specific reflexes to occur. Who knows if in the near the future there will exist implantable stimulating devices for entire spinal cord regeneration, or to electrically kill cancer cells and destroy tumours.

2. Motivation and Objective

When observed in other animals such as the salamander or the starfish, everybody certainly has thought at least once why limb regeneration does not happen in humans. They eventually have also wondered if in a far future technology would not be advanced enough to allow this phenomenon to occur on us. The latest advances in science are showing, however, that the so called "future technology" is not an illusion, but a possibility that may turn into reality very soon. In medicine and also in other sciences, several techniques that seemed impossible ten years ago are routine nowadays. Who knows if limb regeneration, chronic wound healing, spinal cord repair or cancer elimination will not be a reality in the next years?

This project is based on the context of tissue engineering and is concerned in understanding how bioelectricity and living tissue interact. To achieve this goal, the embryo of the nematode *Caenorhabditis elegans* will be used as model to study the impact of a DC electric field in tissue development. The embryo seems to be ideal for this particular study, since its embryogenesis is highly reproducible, allowing to easily observe asymmetric division and cell migration and orientation.

Furthermore, a previous study [26] showed that this particular embryo responds to a gradient of temperature applied across its antero-posterior (AP) axis, which induces a change in its development pattern. In a similar way, an electric field gradient across the embryo might induce a change in embryogenesis, due to the electrically induced polarizations in the embryo cells.

The objective of this project is to apply a DC electric field to the embryo of *C. elegans* and analyse whether responses in it occur or not. The hypothesis assumed here is that, applying a DC the electric field across the AP axis of the embryo, an excess of negative charge will accumulate on one side of the embryo and an excess of positive charge will accumulate on the other side, resulting in a different cell membrane polarity at different parts of the embryo. In an analogous way to electrotaxis, it is expected that possible cellular responses resulting in abnormal cell polarizations will change asymmetric division mechanisms and alter the development of the embryo.

In order to successfully apply the electric field to the embryo, a microchannel filled with conductive and biocompatible medium will be used. Due to its small and rectangular dimensions, the field can be easily directed and focused to the AP direction of the embryo. Some physical processes occurring in the channel may disturb the embryo development, so a detailed characterization of the physics at the channel will also be performed. To accomplish that, experimental measurements, simulations and a theoretical analysis will be used to model the microfluidic system.

The characterized system will then be used to conduct experiments where the *C. elegans* embryo will be stimulated with a DC electric field, and any differences between normal and stimulated embryogenesis will be analysed. The experiments will be conducted under certain assumptions that depend on the system characterization and must be in accordance wit the goal of the project.

In order to correctly analyse the *C. elegans* embryo development, some details of its embryogenesis must also be asserted a priori and used as a template in which the study of the embryo will be based on.

3. *Caenorhabditis elegans* – Closer than it Looks

Biological models are widely used in research to study biological processes in a controlled manner. In tissue engineering, they range from individual cells, useful to study cell cycle and division, proliferation and differentiation, to entire organisms, namely embryos in-vitro to study embryogenesis and development and amphibians to study tissue growth and regeneration. Some invertebrates and microorganisms are also widely used, since they are simpler and usually have great capacities of regeneration. Tissues in culture, on the other hand, allow studying developmental processes under simple and controllable biological conditions [27].

One of the most appropriate models to study cellular and development mechanisms is the nematode *Caenorhabditis elegans*. It is a primitive organism that shares several biological characteristics that are central problems of modern human biology. It was initially chosen as a model by Brenner in 1996 [28] due to its simplicity to culture in great numbers and being convenient for genetic analysis and manipulation. At the present, it is one of the models most used in research. It was also the first organism whose genome was entirely mapped [29].

3.1. *C. elegans* Biology

Caenorhabditis elegans is a small (about 1mm long), free-living soil nematode (roundworm) that lives in many parts of the world by feeding on microbes, primarily bacteria. The organism arises from only one cell, the egg, which suffers a complex development process, starting in an embryonic cleavage followed by morphogenesis and finally a growth till the adult stage. It produces sperms and oocites, mates and reproduces. After reproducing, it gradually ages, loses vitality and dies about 2/3 weeks after being born (Fig. 3.2). The development and function of this diploid organism are coded by around 20 000 genes [30, 31].

In the adult stage there are two genres, one hermaphrodite composed by 959 somatic cells and a male composed by 1031 somatic cells. Males are extremely rare, being only 0.05% of the total population. Despite this, sexual reproduction is preferred compared to asexual every time a male is available. The adult essentially consists in a tube which contains two smaller tubes. The outer tube (body wall) consists in the cuticle, hypodermis, excretory system, neurons and muscles, and the inner tube consists in the pharynx, intestine and, in the adult, gonads (Fig. 3.1). All these tissues are under an internal hydrostatic pressure, regulated by an osmoregulatory system [32]. Most of the animal volume consists in the reproducing system (gonads), formed by two individual tubes in the first and two thirds of the worm.

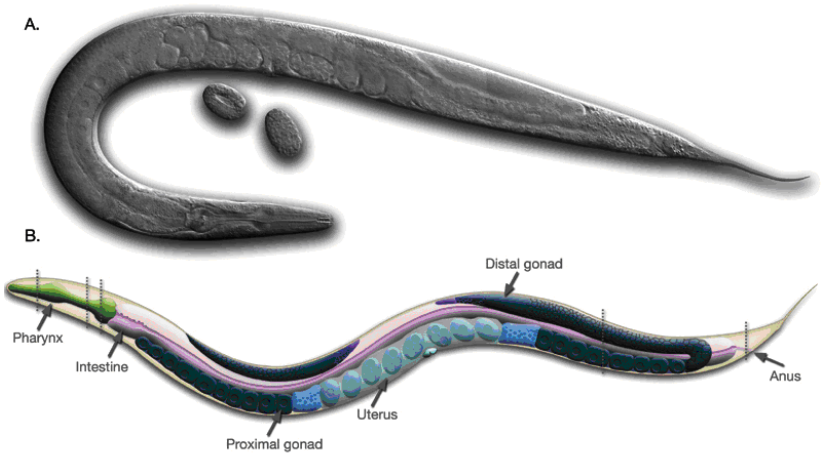

Fig. 3.1: Anatomy of an adult hermaphrodite *C. elegans* individual. A: DIC image of an adult hermaphrodite. B: schematic drawing of its anatomical structures. (Image taken from [32])

After hatching, the animal goes through four juvenile stages (L1 – L4) (Fig. 3.3), then enters to the adult stage, highlighted by the beginning of the reproduction. In starving or overpopulation conditions, the worm at the L2 stage, instead of passing to L3, metamorphoses to an alternative stage called the *Dauer* state (L2d) [33]. Here, the juvenile nematode delays its development to adapt itself to the extremely adverse environments. It does not age or reproduce and can stay in the *Dauer* stage for more than 3 months, about four times its normal life span. After exiting the *Dauer* state, the individual enters the L4 stage (Fig. 3.2).

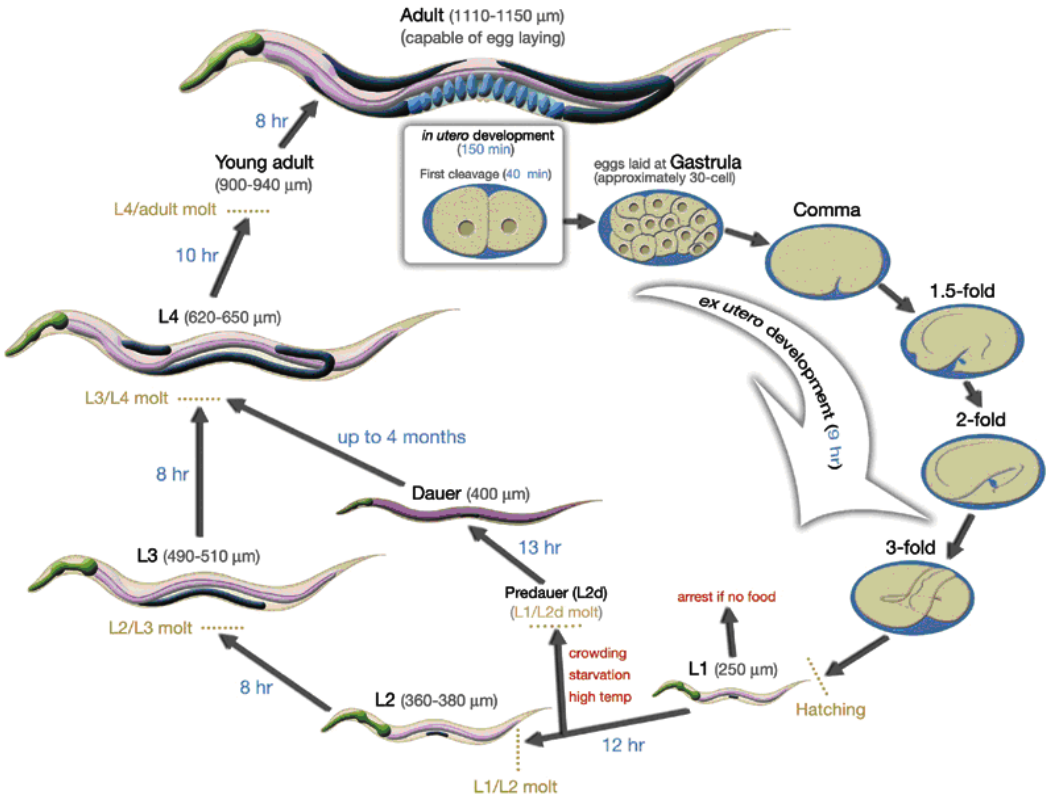

Fig. 3.2: Life cycle of *C. elegans* at 22ºC. The time of fertilization is set to 0. Numbers in blue along the arrows indicate the length of time the animal spends at a certain stage. The first cleavage occurs at about 40min after fertilization. Eggs are laid outside at about 150min after fertilization, during the gastrulation stage. The length of the animal at each pos-embryonic stage is marked next to the stage name in micrometers. *C. elegans* embryogenesis will be presented in the next section. (Image and description taken from [32])

Despite its simple anatomy, the *C. elegans* displays many different behaviours including locomotion, foraging, feeding, defecation, egg laying, metamorphosis, sensory responses to touch, smell, taste and temperature as well as some complex behaviours like male mating, social behaviour, learning and memory and dependence [34, 35].

More detailed descriptions of the *C. elegans* biology can be found in [29, 32, 36, 37, 38, 39] and various other literature easily available through a simple search for the term “c elegans”.

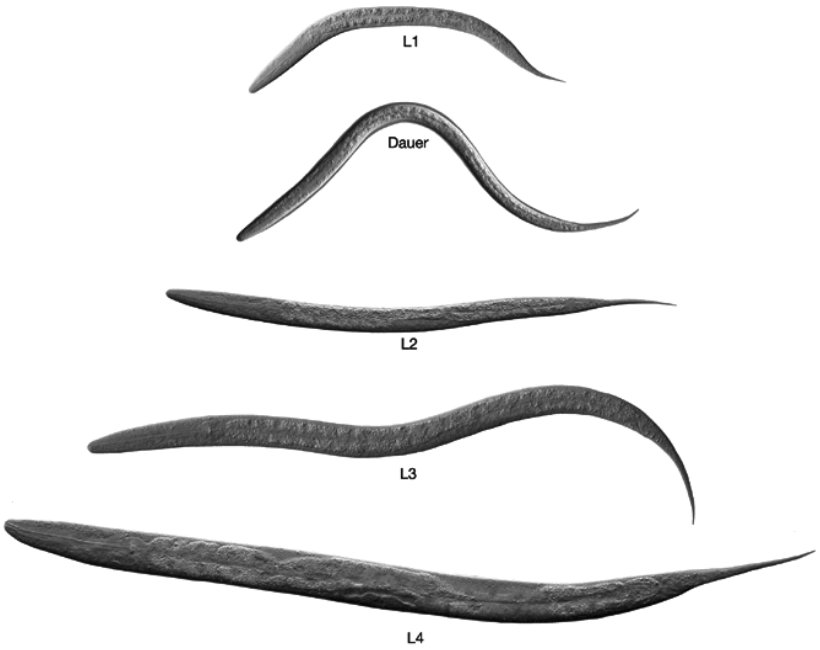

Fig. 3.3: DIC images of the larval stages of *C. elegans*. (Image taken from [32])

3.2. *C. elegans* as a Model

There are a lot of reasons to use *C. elegans* as a model organism. As already stated, it is a primitive organism, thus simple to analyse, and possesses a lot of biological characteristics present in human beings. Among them are embryogenesis, morphogenesis, organogenesis, growth, aging, nervous function, behaviour, all of them determined by genes that can be manipulated [30]. In addition, its short life span makes it very useful for research about aging. All 959 somatic cells are transparent and visible with an optical microscope equipped with differential interference contrast (DIC)[1], which allows examining the nematode till the cellular level in living preparations,

[1] DIC (Differential interference contrast microscopy or Nomarski microscopy) is an optical microscopy technique used to enhance the contrast in unstained, transparent samples, which contain little or no optical contrast when viewed using brightfield illumination. DIC is widely used to visualize cellular features, most notably nuclei and nucleoli, but also microtubules, chromosomes and cytokinesis furrows. Cells above or below the DIC focal plane are not visible, making this technique perfect to observe and follow individual cells. Reviews about DIC microscopy can be found at [40]. A more detailed description of this technique is in Appendix D.

turning it easier to study cellular differentiation and other processes about development inside an intact living organism [41].

Together with these features is its easiness of culture and observation (Fig. 3.4). The nematode can be cultured in Petri plates with agar seeded with *Escherichia coli* (bacteria) as food source. If only one *C. elegans* hermaphrodite individual is placed in a Petri plate with food, more than 500 000 individuals can be produced in one week [42]. Self fertilization of the hermaphrodite allows for homozygous worms to generate genetically identical progeny and male mating facilitates the isolation and maintenance of mutant strains as well as moving mutations between strains [32]. *C. elegans* can also endure harsh environmental conditions.

All these characteristics present in a simple organism and its easiness to culture provide the researcher the perfect compromise between the complexity and treatability. Being one of most used biological models of actuality, *C. elegans* is used for several applications in the field of cellular and molecular biology, biotechnology, biomedical engineering (such as neurosciences), genetics, embryology and biology of the development, immunology; also for modelling of physiological systems, such as the digestive system or the reproducing system; and even to study cellular communication, chemotaxis, thermotaxis and mechanotransduction [36, 43]. As an example, the study of *C. elegans* mechanisms allowed to acquire knowledge about cancer, Alzheimer disease, muscular dystrophy and aging in humans [44].

The scientific community has at hand several bibliographical sources and databases about *C. elegans* and also specialized portals about this and other nematodes. These portals have the advantage of also containing not officially published data. Some of the main data centres about *C. elegans* are available at [29, 32, 36, 37, 38, 39, 45, 46, 47]. They also contain a lot of multimedia information to assist in the visualization of cellular and development processes, specialized software for the analysis of those processes as well as atlas where several cells and tissues are mapped.

Fig. 3.4: *C. elegans* under microscope. The worm length is about 1mm. (Image taken from [48])

3.3. The *C. elegans* Embryo

The *Caenorhabditis elegans* embryo is a wonderful model to various fields of research, with several applications in areas such as cancer research, genetics, tissue engineering and cellular and molecular biology [6, 36, 49, 50]. It has several favourable characteristics that turn it into an ideal model for the study of embryogenesis and morphogenesis, development of tissue and organs, cellular mechanisms, the cell cycle, cell growth, proliferation and differentiation, mitosis and meiosis and also the oocyte to embryo transition [36, 49, 50]:

- It is transparent, allowing to readily visualize the internal structures in intact embryos using conventional optical microscopes;
- It develops normally outside the progenitor uterus, which allows studying it in-vitro;
- It has a small size and cell number, therefore organs and tissues are composed by only a few cells. Consequently, it is easy to follow a tissue or a single cell in this multicellular organism;

- It has only six chromosomes and short cell cycles, being perfect to study the cell cycle and division [51];

- It has an almost invariant cell lineage where cells divide at specific times within the developmental program and with the same fate map between different specimens [52, 53], providing the powerful advantage of performing several experiments under the same conditions;

- It remains healthy at room temperature which facilitates diverse types of experiments.

A huge collection of tools is readily available to help with research and experimentation. The embryo pattern of cell cleavage and differentiation are fully known and provide the foundation for the analysis of cell cycle progression at single cell resolution [49, 54]. All the cell lineage and division times have been mapped and a diagram representing the entire cell lineage of the *C. elegans* embryo has been constructed, providing a powerful model for the study of its embryogenesis [52, 53].

With these characteristics and available information, the embryo of the nematode *C. elegans* seems to be a perfect model for the study of the impact of an external stimulus on the development of a biological system. Previous research show that the embryo and its pool of cells respond to diverse types of external and internal stimulus, such as temperature [26, 55], hydrostatic pressure [56], cell-cell contact [57] and chemical treatments [58]. These results show that other techniques different than genetic modification can be used to study and control cell, tissue and organism development.

From its advantageous features, the *C. elegans* embryo was chosen as a model to study the impact of an externally applied DC electric field on biological tissue. In addition to the ones mentioned above, electricity is another type of external stimulus to which the embryo may respond, as other biological samples did.

3.4. *C. elegans* Embryogenesis

The embryogenesis of *C. elegans* produces a juvenile worm that has 558 cells at hatching [53]. The embryonic development is rapid, taking only half a day, between 12h and 14h at room temperature. However, the development (and post development) speed increases with temperature. It occurs inside a rigid eggshell, starting with one cell and ending with a complete juvenile worm that leaves the eggshell. Each egg has approximately an ellipsoid shape, with dimensions around 30µm × 30µm × 60µm (Fig. 3.5 and Fig. 3.6).

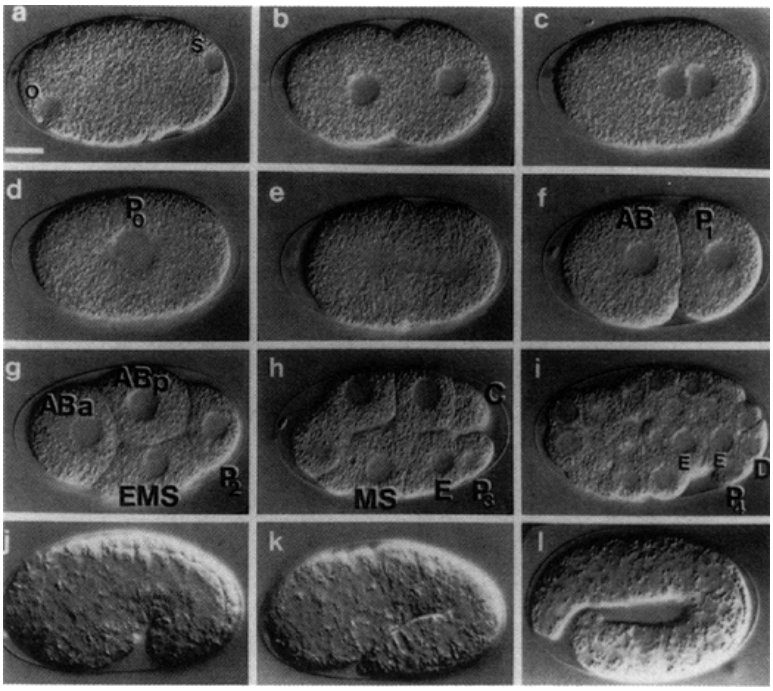

Fig. 3.5: Main stages of *C. elegans* embryogenesis. Cell names are written near the respective cells. Anterior is left, ventral is down. a – d: 1-cell stage, showing the pro-nuclei and their migration. The oocyte pro-nucleus is signalled by (o) and the sperm pro-nucleus is signalled by (s). e: start of the first mitosis. f: 2-cell stage. g: 4-cell stage. h: 8-cell stage (one of the AB descendants is not visible. i: start of the gastrulation. j: comma stage. k: 1.5-fold (tadpole) stage. l: 3-fold (pretzel) stage. (Image taken from [54])

Considering the embryo development as approximately invariant, an event diagram summarizes the main events of the development and their times under normal conditions (Fig. 3.6).

Embryogenesis in *C. elegans* is roughly divided into two stages [52]. The first stage is the proliferation, starting after fertilization and ending about 350 minutes later. This stage involves all cell divisions of embryogenesis. The initial 150 minutes occur inside the progenitor uterus and then the embryo is laid outside at about the 30-cell stage, at the time gastrulation occurs. At the proliferation stage there is a considerable rearrangement of cells, at first due to short range shuffling, and once gastrulation begins, due to specific cell migrations. By the end of proliferation, the embryo is organized into the three germ layers: ectoderm, mesoderm and endoderm [32].

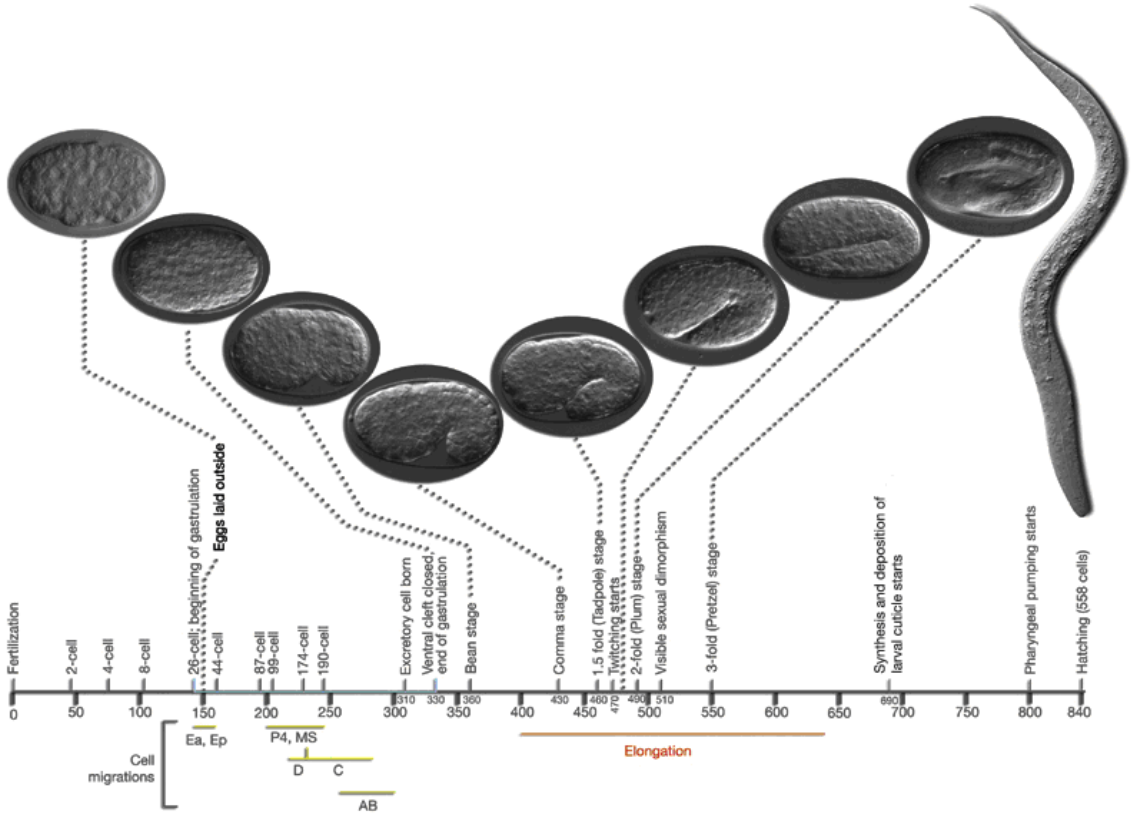

Fig. 3.6: Embryonic stages of development. The numbers below the horizontal axis show approximate time in minutes after fertilization at 22ºC. The yellow bars indicate the period of time during which cells from a certain lineage migrate towards the inside of the embryo through the entry zone (the gastrulation cleft or ventral cleft) during gastrulation (blue bar). Red bar indicates elongation of the embryo that takes place between 400-640min due to circumferential contraction within the hypodermis. During elongation,

the embryo becomes threefold thinner and its length increases about fourfold. The stages, number of nuclei, marker events and DIC images of the embryos and a newly hatched larva are shown above the horizontal axis. (Image and description taken from [32])

The second stage encompasses the organogenesis and morphogenesis. It starts at about 5.5h to 6h after fertilization. During it, there are no more cell divisions, but instead, their differentiation occurs. The embryo elongates threefold (comma fold) and takes form of an animal with fully differentiated tissues and organs. Organogenesis ends between the first and half and second folds (when the embryo looks like a lima bean) and morphogenesis starts. The first muscle twitches (small movements) are observed at about 430 minutes after the first cleavage. In the late 3-fold stage, the worm is able to move inside the egg in a coordinated fashion, indicating advanced motor system development. Finally, it hatches at about 800 minutes after the first cleavage [32, 52].

At the end of the embryogenesis, the main body plan of the animal is already established and does not change during the postembryonic development. Post embryonic development is triggered by the start of feeding of the larva: cell divisions resume and the postembryonic developmental program begins about 3 hours after hatching [32, 59].

3.5. The *C. elegans* Eggshell

Oocytes from all animal species have a special coat of extracellular matrix whose assembly is triggered by fertilization and that, between others, has the function of avoiding polyspermy and to generate a covering to protect the zygote. In nematodes, that coat is the eggshell. It is a structure distinct from the embryo, existing a space between it and the plasma membrane of the embryo [60]. Far from being simply a passive physical support, the eggshell is a key player in many early developmental events, such as meiotic chromosome segregation, anterior–posterior polarization and organization of the embryo cell membranes and cortical proteins. It provides mechanical rigidity, prevents polyspermy and is impermeable to small molecules [56, 58, 61, 62].

The *C. elegans* eggshell is about 0.3–0.4μm thick, except at the anterior pole, where it has a total thickness greater than 2μm (Fig. 3.7). [63]. Inner to the eggshell is the extraembryonic matrix (EEM), the space between the embryo plasma membrane and the eggshell. It must provide an ideally cushioned and buffered environment for embryonic development.

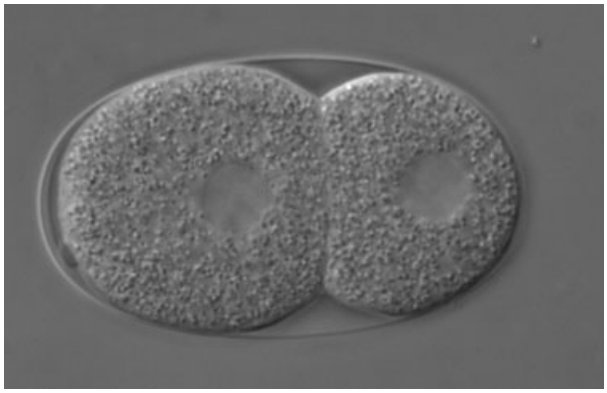

Fig. 3.7: 2-cell stage embryo, where the eggshell is clearly visible surrounding the embryo. (Image taken from [64])

There is a distinct envelope that assembles between the eggshell and the embryo plasma membrane, called the permeability barrier. It is responsible for avoiding the passage of small molecules that the eggshell does not block and maintaining proper osmotic conditions inside it [61].

A more detailed description about the *C. elegans* embryogenesis and the embryo eggshell is in Appendix C.

4. System Characterization

Microsystems create new opportunities for the control of cell growth and stimulation by combining surfaces that mimic complex biochemistries and geometries of the cellular microenvironment. The control of cellular microenvironments via microfluidic systems potentially represents a valuable tool for fundamental studies of cell biology. Microfluidics applies when chamber and channel dimensions are at the micro scale. Most BioMEMS[2] contain microchannels and microcompartments to manipulate fluids at the microscale. Biological insight into the pathways that control cell phenotype and behaviour can be gained by monitoring cellular responses to controlled perturbations in the extracellular environment. A wide range of microsystems are therefore emerging with the express aim of facilitating the basic study of biochemical pathways, cell fate decisions and tissue morphogenesis. Some cell based microsystems simply represent miniaturized versions of conventional laboratory techniques, whereas others exploit the advantages of small length scales and low Reynolds numbers, such as favourable scaling of electrical fields and the ability to create well controlled laminar flows. Highly integrated microdevices show great promises for basic biomedical and pharmaceutical research [65].

Te goal of this project involves, someway, the application of an electric field to a biological sample of the size of about one cell. Therefore it is necessary to be sure that the electric field hits the embryo in an effective way, so that the embryo may respond to that stimulus. It must also be assured that no kind of significant stimulus, other than the DC electric field, affects the embryo in any way that might compromise the study of the influence of the electric field on it. Therefore, and due to the potentialities of microdevices as enounced above, a microfluidic system is going to be used in order to effectively apply the electric field to the embryo. This option was chosen principally

[2] BioMEMS (biological microelectromechanical systems) are microelectromechanical systems that interact with biological systems. They may be just a measurement or stimulation device used in biological samples, but they can also be composed themselves by biological matter for applications in biomimetics.

because it allows confining the embryo to a small space with dimensions close to the dimensions of embryo, so that the electric field can be scaled and focused to it.

The system must satisfy the necessary conditions to assure that the embryo is properly stimulated by the electric field, and that other factors such as temperature and pH do not compromise its development. The speed of mitotic events in *C. elegans* is faster at higher temperatures and abnormalities occur above 25ºC [41, 55]. *C. elegans* is also sensitive to the pH of the surrounding environment, surviving between a pH range of 3.1 to 11.9 during 24 hours [66]. Due to the embryo eggshell, there are no mechanical concerns, but the environment medium solute concentration may influence the activity of the osmotic barrier, so an appropriate medium must be chosen. Therefore, the microfluidic system to be used must satisfy to the following:

- The dimensions of the channel must focus the electric field to the embryo, i.e., almost all of the field lines must cross the embryo or be deflected by it in case the embryo is insulating;
- The device must afford the application of a constant electric field for at least 14 hours, and whose magnitude is in the physiological range;
- The channel must be filled with a good electrolyte to conduct the electric current necessary for stimulation, and at the same time be biocompatible with the normal development of the embryo;
- The solute concentration must avoid osmosis across the eggshell that may dry the embryo. Also, the system must remain humid to avoid the channels to dry, and thus osmosis out of the eggshell to occur;
- Any fluid flow must be minimized, so that the embryo stays static and is not disturbed by shear stresses or other hydraulic forces;
- The temperature of the electrolyte must be inside the normal embryogenesis range and stay approximately constant;
- The pH of the microenvironment must also be inside the normal embryogenesis range and preferentially stay approximately constant. A neutral microenvironment would be preferred;

- The device must be optically transparent at the embryo region to allow proper visualization by microscopy;

- Finally, the device must allow an easy and quick injection of the embryo inside the channel and an easy application of the electric field to it, so that the stimulation can start still at the 1-cell stage.

The chosen device seems to be able satisfy all these conditions if enough care is taken. In order to have an accurate idea of the type and magnitude of the stimulus and what must be done to satisfy them, it is necessary to perform a physical characterization of the system. It is important to find out the magnitude of the current and electric field present in the channel near the embryo and also to have an idea of the temperature and pH of the electrolyte. At constant room temperatures, the temperature of the electrolyte may change mainly due to the Joule heating effect, where a current passing through a resistive conductor causes its temperature to increase. The pH may change due to electrochemical reactions occurring at the interface electrode/electrolyte, releasing charged products that can move to the embryo region by convection or electrophoresis (Fig. 4.1). Therefore, the types of flow of the electrolyte or its solutes in the channel must also be taken into consideration.

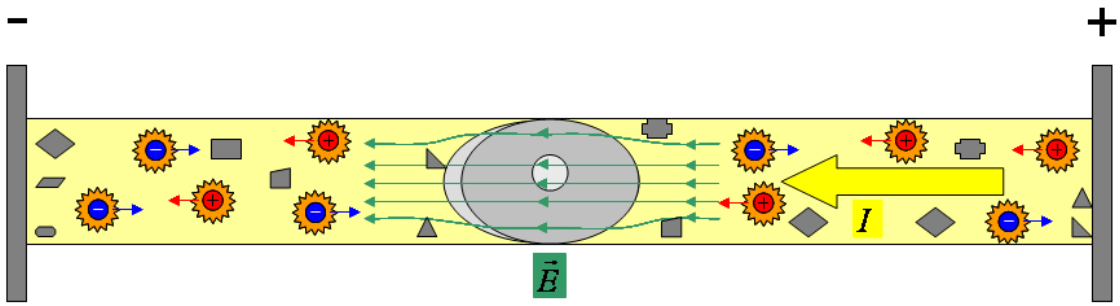

Fig. 4.1: Schematic representation of the main physical processes that may have an impact on the efficiency of the experiments. The embryo is the light grey ellipse (includes the eggshell and the nucleus) at the centre of the channel filled with a light yellow electrolyte. A potential difference across the channel induces an EF that moves the ions of the electrolyte across the channel, creating an electric current (yellow arrow). The expected field lines across the embryo are depicted in green. The ions interact with the resistive electrolyte increasing its temperature through joule heating (orange). The two electrodes at the channel extremities react with the electrolyte releasing redox products that may change the pH of the solution (dark grey).

This section has the goal of characterizing the microfluidic system used for the embryo stimulation. The first sections will introduce some relevant concepts about electricity and electrodes, necessary to understand the physical processes occurring in the system. The next sections are dedicated to the characterization itself, presenting the methods used and the results obtained and conclusions taken. Finally, the relevant characteristics of the system will be summarized and an explanation of how it may influence the embryo will be provided.

4.1. Relevant Concepts about Electricity

In order to achieve the goal of this project, a physical phenomenon must occur at certain places of the device: movement of electric charge. For a charge to move, it needs an impulsive force and a conductor necessary for the movement. This project explores the electric force as the agent to move charge to stimulate the embryo and an electrolyte as the conductor.

Any electric charge is surrounded by a force field, called the electric field. It is a vector field that describes the electric force acting on another charge at any position in space. The electric field (***E***) generated by a charged particle is conservative and depends only on the charge creating it and the position relatively to that charge. When conservative, the electric field is the negative of the gradient of the electric potential, independently of the total charge configuration [67]:

$$\vec{E} = -\nabla V \tag{4.1}$$

The electric potential (V) expresses the effect of an electric field of a source in terms of the location within the electric field, being a measure of the potential energy per unit charge [68]. The electrical potential difference or voltage (U) is the difference in electric potential energy per unit charge between two points.

The electric current (*I*) is the flow of electric charge through a conductive medium. The electric current is driven by a voltage through a conductor in an analogous way a fluid flow is driven by a pressure difference through a channel. The charge is carried by charge carriers, which are typically moving electrons in conductors such as wires and ions in electrolytes. The current density is a measure of the flux of electric charge through a conductor. It is an important concept to the design of electrical systems. Contrary to the current, witch is a scalar, the current density (***J***) is defined as a vector whose magnitude is the ratio of the magnitude of current flowing in a conductor with the cross-sectional area (*A*) perpendicular to the current flow and whose direction is the same of the electric field [69]:

$$\vec{J} = \frac{dI}{d\vec{A}} \tag{4.2}$$

The electrical resistance (*R*) of a conductor is the opposition to the passage of an electric current through it. The inverse of the resistance is the electrical conductance (*G*), the ease at which an electric current passes. The resistance of an electric conductor is related with the current passing through it and the potential difference between its extremities in the direction the current flows, by Ohm's Law [69]:

$$R = \frac{1}{G} = \frac{U}{I} \tag{4.3}$$

Not every electrical component obeys this law. Components that obey Ohm's Law are called ohmic, and components which do not obey are called non-ohmic.

The primary cause of the resistance is the scattering of charged carriers due to interaction with the atoms of the conductor. For electrolytic conductors, the ion atoms collisions are related to viscous forces. Every ohmic material has a characteristic resistivity that depends on the properties of the material and on its temperature [69]. It is

a measure of how strongly a material opposes the flow of electric current. The electric resistance depends on the resistivity and the geometric properties of the conductor. An object of uniform cross section has a resistance proportional to its resistivity (ρ) and length (L) and inversely proportional to its cross-sectional area (A) (Fig. 4.2) [67]:

$$R = \rho L / A \tag{4.4}$$

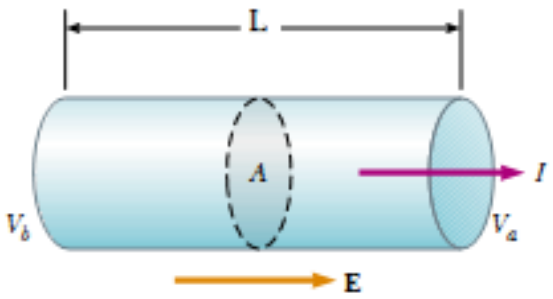

Fig. 4.2: Uniform conductor of length L and cross-sectional area A. A voltage $U = V_b - V_a$ maintained across the conductor sets up an electric field $\boldsymbol{E}$, and this field produces a current I that is proportional to the potential difference. The resistance of the conductor is given by Eq.(4.4) and is related with the voltage and current by Eq.(4.3). (Image taken from [69])

Ohm's Law can also be written in terms of the electric field ($\boldsymbol{E}$) and current density ($\boldsymbol{J}$). If there is an electric field inside a material, it will cause an electric current to flow. For a given material, the magnitude of the electric field is proportional to the magnitude of the current density and the constant of proportionality is the resistivity (ρ) [69]:

$$\vec{E} = \rho \vec{J} \tag{4.5}$$

This relationship is Kirchhoff reformulation of Ohm's Law.

In typical resistive circuits, energy is transferred from a source such as a battery to the resistive elements, increasing their temperature. Charged carriers in an electric circuit are accelerated by the electric field but give up some of their kinetic energy each time they interact with an atom. The increase in the kinetic or vibrational energy of the atoms manifests itself as heat (internal energy) and a rise in the temperature of the conductor. This phenomenon is called Joule or resistive heating [69]. Joule heating is proportional to the electrical power (P) of the resistive element. This way, increasing the electric current or the applied voltage will result in an increase of Joule heating.

4.2. Relevant Concepts about Electrodes

In the point of biological applications, an electrode functions as a transducer between a physiologic system and an electronic system, for two possible applications: recording of physiological electric signals and electrical stimulation of physiological systems. Small signals are mainly used for recording applications, whereas large signals are used of stimulation. [70]. The following discussion applies for metal electrodes immersed in ionic solution electrolytes.

4.2.1. The Electrode/Electrolyte Interface – The Double Layer

When a metallic object is placed into an ionic solution, there occur electrochemical reactions between the metal surface and the electrolyte. In the simplest form [70]:

$$D \Leftrightarrow A^{+} + e^{-} \tag{4.6}$$

The electron donor D is oxidized and forms an electron acceptor A and an electron e^{-}. These reactions involve the dissolution of metal of the electrode surface in the aqueous

electrolyte to form metal ions and also an accumulation of excess electrons in the metal surface. Consequently, as the reaction proceeds, a potential builds up originating an electric field that induces the reverse reaction. After reaching the equilibrium, the net current of electrons across the interface is zero, $I_{ox} = I_{red}$ [70].

The ions that accumulate at the solution to counter the surface charge of the metal vary in concentration, from a maximum value at their closest approach to the metal, to their bulk concentration relatively far away from the influence of the electrode (Fig. 4.3). For metal electrodes, the closest approach of the cations to the electrode surface is determined by the hydration sheath of the electrode, a layer of oriented water molecules in contact with the surface of the metal. This layer, also called Stern or Helmholtz layer, therefore comprises ions adsorbed directly onto the object [70].

A second layer outward from the electrode consists of hydrated cations. It is composed by ions attracted to the surface charge via coulomb forces, screening electrically the first layer. This layer is loosely associated with the object, because it is made of free ions that move in the fluid under the influence of electric attraction and thermal motion rather than being firmly anchored to the electrode surface. It is thus called the diffuse or Gouy-Chapman layer [70]. Part of the diffuse layer can move under the influence of tangential stress. A conventionally introduced slipping plane separates the mobile part of the electrolyte from the one that remains attached to the electrode surface (Fig. 4.3).

A voltage drop occurs across this double layer and is quantified by assuming a reference point in the bulk fluid far away from the interface, where the potential is zero. Under this convention, the potential at the metal surface is the highest potential of the interface and is called the surface potential. The potential at the Stern layer is called Stern potential and the potential at the slipping plane is called zeta potential (Fig. 4.3).

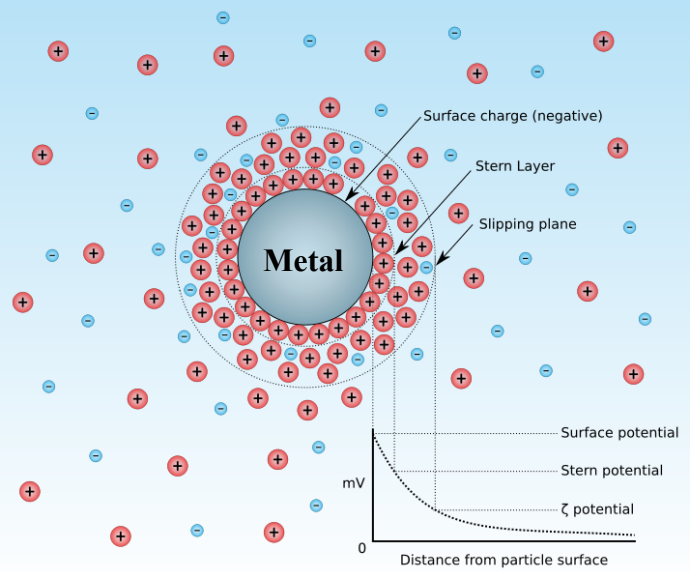

Fig. 4.3: The electric double layer. The innermost layer of positive ions is the Stern layer, where the ions are attached to the electrode surface. The outer layer of positive ions is the diffuse layer, where some negative ions from the bulk solution are present in hydrated form (here represented by the negative ions between them). After the slipping plane, the cations of the diffuse layer can move when submitted to a tangential stress. (Image taken from [71])

4.2.2. Interfacial Capacitance

In equilibrium there is an electric field and thus a voltage drop across the double layer, but since $I_{ox} = I_{red}$ there is no net current in it. Consequently, charge is stored by the solution to create the electric field and a capacitance arises at the double layer. The Stern model is the most accepted nowadays to explain this interfacial capacitance. It assumes a series combination of two capacitances [70]:

$$C_I = \left(\frac{1}{C_H} + \frac{1}{C_{GC}} \right)^{-1} \tag{4.7}$$

C_I is the interface capacitance, C_H is the Helmholtz capacitance and C_{GC} is the Gouy-Chapman capacitance (or diffuse capacitance). For large signals, $C_{GC} >> C_H$ and consequently $C_I \approx C_H$, where [70]:

$$C_H = \frac{A\varepsilon_0\varepsilon_r}{d} \tag{4.8}$$

ε_0 is the dielectric permittivity of free space, ε_r is the relative permittivity of the medium and d is the distance between the inner and outer Helmholtz planes[3].

4.2.3. Resistive Mechanisms at the Electrode Surface

As was said before, a potential arises due to the redox events that occur at a metallic surface. There is a difference between the resultant potential at which the redox event is experimentally observed (E) and each individual half reaction's equilibrium potential thermodynamically determined (E_{eq}). This difference is called polarization and quantified in terms of overpotential (η) [72]:

$$\eta = E - E_{eq} \tag{4.9}$$

This means that the movement of charge into or out the electrode requires a shift in its potential from its equilibrium value E_{eq} to a new value E and this shift is referred as the overpotential [72].

There are various contributions to the overpotential, sometimes not very well defined. The potential component most significant is the activation overpotential (η_t) which must occur for any steady state current to flow. This component is always present and is considerably larger in magnitude than the others components at conditions near

[3] For the Stern layer, the locus of the innermost layer of water is referred to as the inner Helmholtz plane. For the diffuse layer, a line drawn through the locus of centres of the hydrated cations is referred as the outer Helmholtz plane [70].

equilibrium. Another important component is the diffusion overpotential (η_d), a function describing the mass transport limitations associated with electrochemical processes. Other contributions to the overpotential are not important for biological applications [70].

When the equilibrium between the oxidation and reduction reactions is reached, the current due to oxidation (dissolution) (I_{ox}) is equal and opposite to that of the reduction (deposition) (I_{red}). The absolute magnitude of this current in any of the directions is referred to as the exchange current (I_0). It depends on the metal surface material and the reactions taking place there (Fig. 4.4) [73]. The exchange current can be thought of as a background current to which the net current observed at various overpotentials is normalized. When passing additional (externally applied) current through the electrode, its effect on the electrode overpotential will be determined by its magnitude in respect to the exchange current [70, 73, 74].

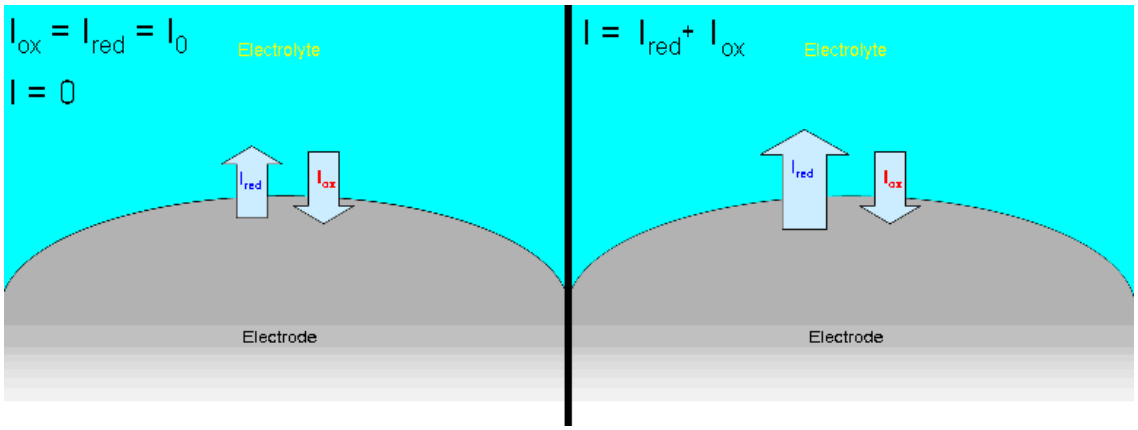

Fig. 4.4: Left panel: the electrode surface in equilibrium conditions. There is no net current I across the electrode surface, since I_{ox} and I_{red} are equal and opposite. The exchange current I_0 is a virtual background current that equals the magnitude of I_{ox} and I_{red} in equilibrium conditions. Right panel: the electrode surface in non equilibrium conditions. The net current is $I = I_{red} + I_{ox}$ and, in this case, points away from the electrode (it is positive). If $I \approx 0$, the electrode is in near equilibrium conditions.

The activation overpotential (η_t) is related to the current density by the Butler-Volmer equation (Fig. 4.5). For a non rectifying electrode system (used in most biological applications), the equation is written as [70]:

$$J = 2J_0 \sinh\left(z\eta_t / 2V_t\right) \tag{4.10}$$

J is the net current density across the electrode surface, J_0 is the exchange current density, z is the number of participating electrons of the electrode (number of electrons involved in the redox overall reaction) and V_t is the thermal voltage.

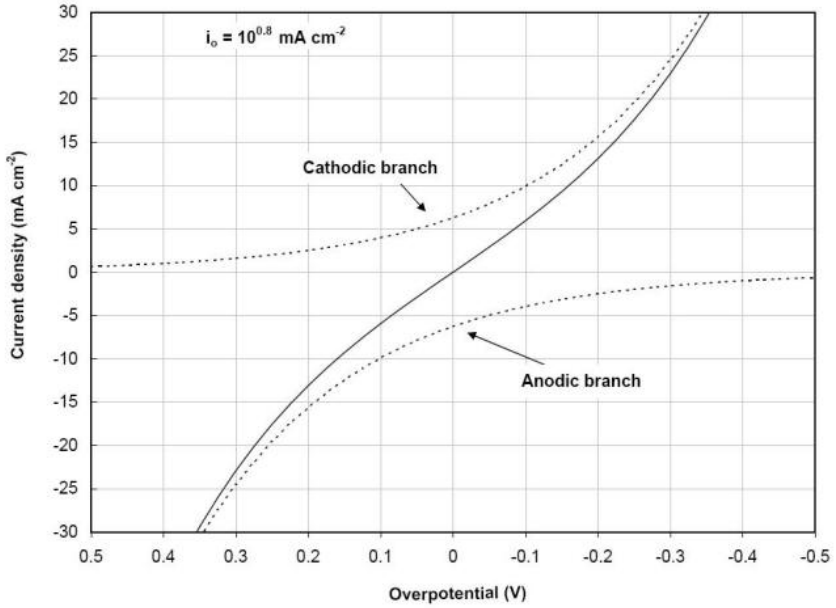

Fig. 4.5: Current vs. overpotential polarization plot (also called *I/V* relationship, where V is the overpotential) for a non rectifying system, showing both the anodic (I_{ox}) and cathodic (I_{red}) branches of the resultant current behaviour. This example is for the ferric/ferrous ion reaction on palladium. (Image taken from [72])

The activation overpotential means it is necessary more energy to induce a current across the electrode surface than thermodynamics require. This way it is reasonable to think that there is a resistance to that current, called the charge transfer resistance R_{CT}, a non-ohmic resistance given by differentiating the activation overpotential (η_t) with respect to the current [70]:

$$R_{CT} = \frac{\partial \eta_t}{\partial J} = \frac{V_t}{J_0 z}\left[\cosh\left(z\eta_t / 2V_t\right)\right] \tag{4.11}$$

When the magnitude of the voltage across the interface increases, the charge transfer resistance exhibits an exponential decrease with the applied potential (Fig. 4.6).

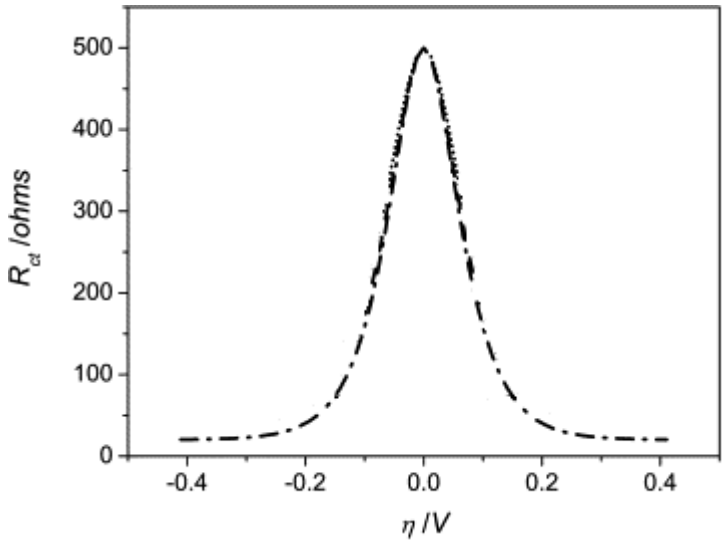

Fig. 4.6: Charge transfer resistance variation in function of the overpotential for a non rectifying system. (Image adapted from [75])

The charge transfer resistance is an undesired feature in the design of electrodes. To minimize it, it is important to use a material with an appropriate value of J_0. When needed to apply large currents it is better to choose electrode materials with a big J_0 for most electrolytes, such as gold or platinum, because they have smaller charge transfer resistances compared to other materials [70].

Near electrodes operating at high current densities there is a local decrease in the concentration of reactants relative to that in the bulk solution. For any electrode, there is a limiting current density J_s, which corresponds to the maximum rate at which reactant ions can be supplied to the electrode from the bulk solution. Under DC conditions, the

overpotential under steady state diffusion is related to the electrode current density by [70]:

$$\frac{J}{J_s} = 1 - e^{(-|\eta_d| z / V_t)} \quad , \tag{4.12}$$

which gives an incremental diffusion resistance of:

$$R_d = \frac{\partial \eta_d}{\partial J} = \frac{V_t}{z}\left[\frac{1}{J_s - J}\right] \quad , \tag{4.13}$$

where η_d is the diffusion overpotential [70].

4.2.4. Spreading Resistance

The spreading resistance (R_S) is the resistance encountered by a current spreading out from an electrode into a conductive solution. This parameter is determined by the geometric surface area of the electrode, being obtained by integrating the series resistance of shells of solution outwards from the electrode:

$$R_S = \int_{x=0}^{x=\infty} dR_S \quad , \tag{4.14}$$

where x is the distance normal to the surface [70]. The solution for a planar rectangular electrode (one side exposed) is:

$$R_S = \frac{\rho \ln(4l/w)}{\pi l} \quad , \tag{4.15}$$

where ρ is the resistivity of the solution and l and w are the length and width of the rectangle [70].

4.2.5. A Circuit Model for the Electrode/Electrolyte Interface

An electrical circuit may be used to model the electric behaviour of the electrode/electrolyte interface (Fig. 4.7). This circuit takes into account the capacitance (C_l) of the double layer, the charge transfer resistance (R_{CT}), the effects of diffusion (R_d) and the spreading resistance of the electrode (R_S). The resistive mechanisms of the interface (R_{CT} and R_d) are in parallel with the capacitive mechanisms (C_l). The spreading resistance (R_S) connects the electrode to the electrolyte.

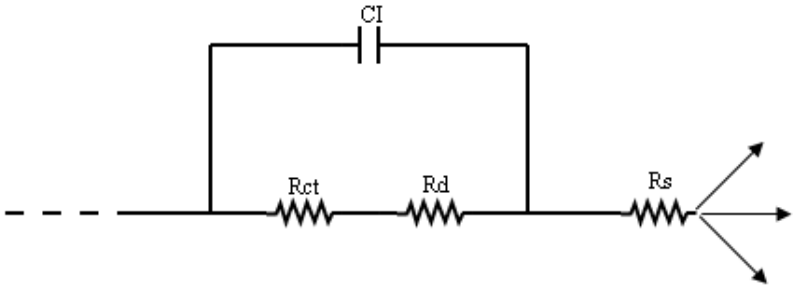

Fig. 4.7: Equivalent circuit of the electrode/electrolyte interface considering the interfacial capacitance, charge transfer resistance, diffusion resistance and spreading resistance. The electrode circuitry is to the left and the electrolyte is to the right.

4.3. System Overview

The device used for the embryo stimulation is a microfluidic chip made of PDMS and glass (Fig. 4.8). Details about its microfabrication process are in Appendix D. Each chip is composed by three systems, but only the middle one is used due to its linear geometry. From now on, only the middle system will be considered unless it is stated the contrary.

The system consists mainly in a central rectangular channel, bordered by a floor made of glass and a roof and walls made of PDMS. At each extremity of the channel, there is a floorless approximately round inlet with a diameter of 1.5mm. The two inlets have no apparent distinction, but while one functions as the inlet, the other functions as the outlet and vice versa. They will be referred together as inlets and individually as inlet and outlet. The inlets' purpose is to connect the central channel with the exterior of the system through a vertical pathway with a height of about 0.5-0.7cm, starting at the bottom of the inlet and ending at the top of the chip. It is through the inlets that the electrolyte and embryo are injected into the channel and it is also where the electrodes are placed.

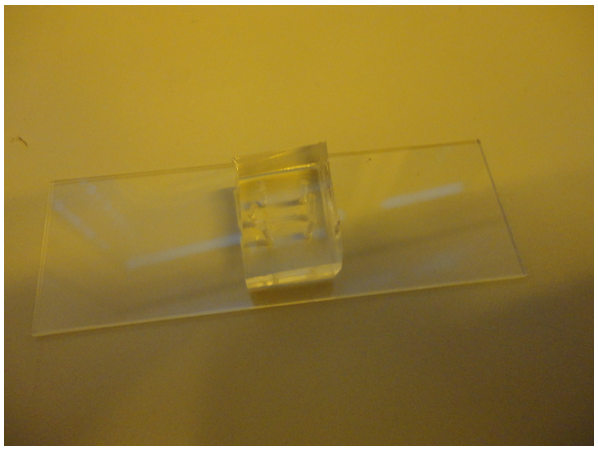

Fig. 4.8: Photography of the system used to stimulate the embryo. The glass constitutes the floor and the PDMS cube constitutes the walls and roof of the channel. The inlets are the small holes visible at the chip surface.

Each electrode is just a simple platinum wire 99.9% pure with 0.15mm of radius, which is inserted into each inlet and has approximately the same immersed length as the height of the inlet. Due to the high length and radius of the electrode, its surface area in contact with the electrolyte is big, thus minimizing the barriers to the charge transfer and providence of chemicals to its surface, and also decreasing the spreading resistance.

The central channel is approximately a parallelepiped and contains a cylindrical pillar of 20µm diameter near its centre. The pillar has the function of holding the embryo at a fixed position, since the embryo can not pass through the pillar. Although approximated by a parallelepiped, the channel does not have the same dimensions in all its length and is therefore divided into three pairs of segments with dimensions measured from its design *CleWin* file (Fig. 4.9):

- two outer segments (1 and 1'), which have the same width, and are the longest and widest of all the channel;
- two middle segments (2 and 2'), which have also the same width, but a smaller length and width compared to the outer segments;
- two small inner segments in parallel (3 and 3'), one on each side of the pillar, with the same length but different width. These segments are an approximation of the pillar section, where the pillar was approximated to a rectangle of 20µm length and 15.6µm width (about the same area of a circle of 10µm radius).

The height of the channel (h) is always 41µm. The channel dimensions are summarized in Table 4.1. The dimensions were also averaged relatively to the total length of the channel having in account the weight of the length of each segment, in order to be able to consider the channel as a parallelepiped with length equal to the sum of the lengths of all segments and width and cross sectional area equal to the averaged values. It would be advantageous to know if these average dimensions may be used for the computations of the channel ohmic parameters for simplicity, instead of dividing it into the segments mentioned above. Schemes of the device in different positions are in Fig. 4.9 and Fig. 4.10.

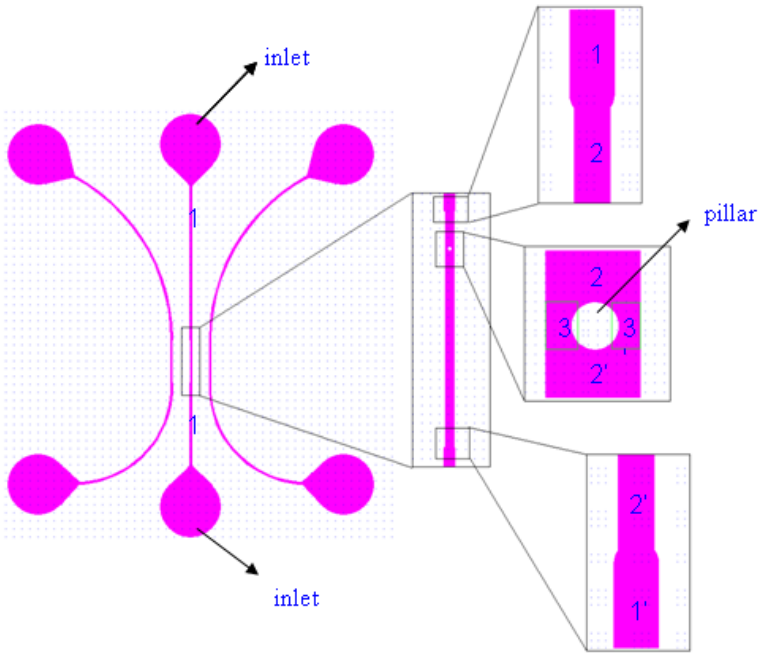

Fig. 4.9: *CleWin* design of the device (courtesy of S. Baranek). It corresponds to the system viewed from above with the PDMS roof removed. The approximate channel dimensions are in Table 4.1.

The electrolyte used is PBS (phosphate buffer saline), a saline solution that mimics the physiological environment, helps maintaining the pH constant and at the same time is a good conductor since it is an ionic solution composed mainly by sodium chloride [131].

Finally, the applied voltage is represented by V_0 and varies between 1V and 10V (assuming only integer values), It can also assume 15V, 20V and 33V in certain cases.

Table 4.1: Dimensions of the system channel

Segment	Length	Width	Height	Cross sectional area
1	$L_1 = 3.8$mm	$w_1 = 50\mu$m	h = 41µm for all segments	$A_1 = h.w_1 = 2050\mu m^2$
1'	$L_{1'} = 2.0$mm	$w_{1'} = 50\ \mu$m		$A_{1'} = h.w_{1'} = 2050\mu m^2$
2	$L_2 = 150\mu$m	$w_2 = 40\mu$m		$A_2 = h.w_2 = 1640\mu m^2$
2'	$L_{2'} = 900\mu$m	$w_{2'} = 40\mu$m		$A_{2'} = h.w_2 = 1640\mu m^2$
3	$L_3 = 20\mu$m	$w_3 = 13.2\mu$m		$A_3 = h.w_3 = 541.2\mu m^2$
3'	$L_{3'} = 20\mu$m	$w_{3'} = 11.2\mu$m		$A_{3'} = h.w_{3'} = 459.2\mu m^2$
Average	**Total length: 6.87mm**	**48.4µm**	**41µm**	**1984µm²**

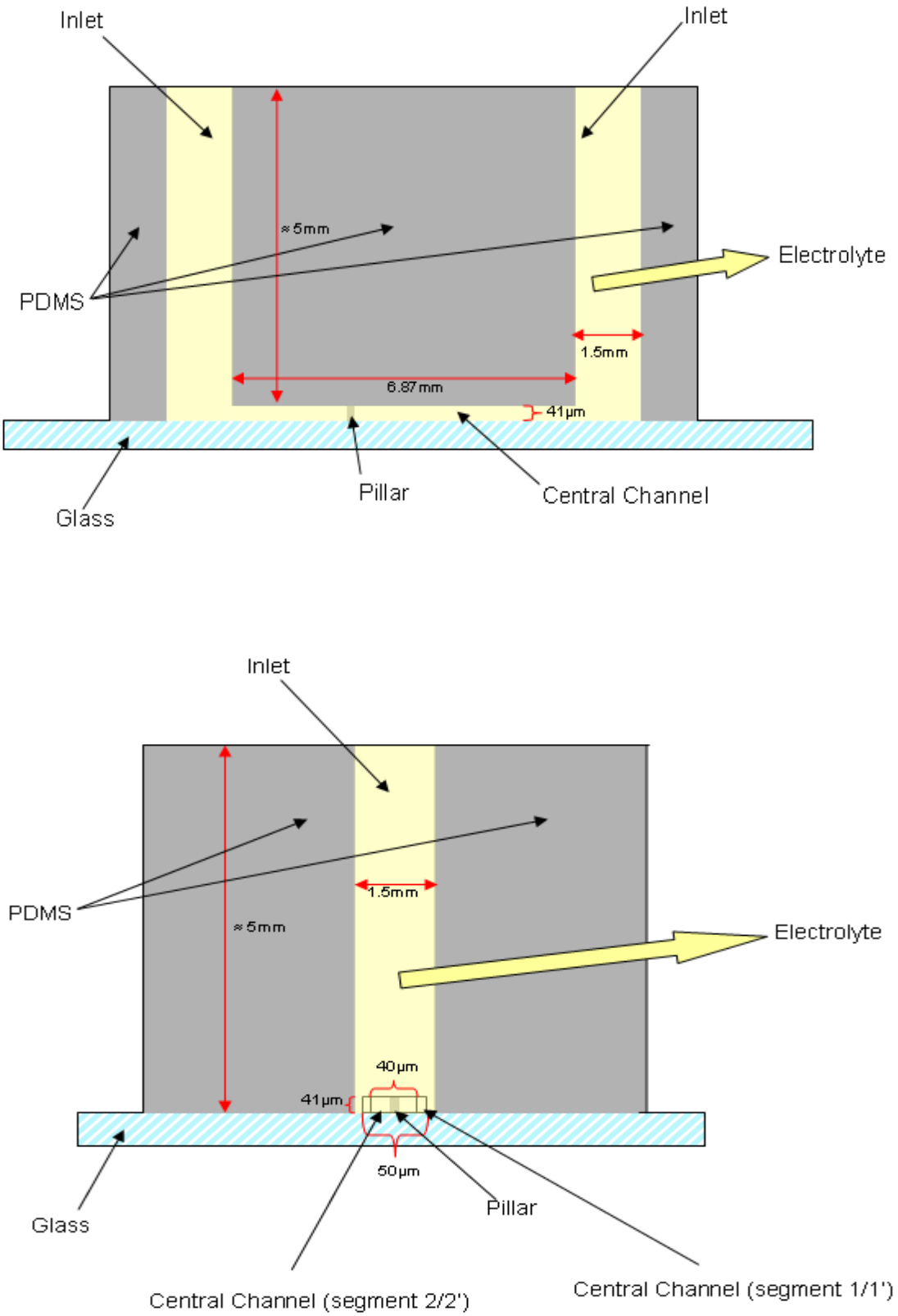

Fig. 4.10: Lateral (top) and frontal (bottom) views of the device. The block is about 5mm height. The inlets are cylinders with 1.5mm diameter. The pillar is a cylinder with 20µm diameter. The approximate channel dimensions are in Table 4.1. Note: the draws are not scaled to the system dimensions.

4.4. Methods

Note: the details of all the computations performed are in Datasheet 1 (file in the annex CD-ROM).

4.4.1. Determination of the Ohmic Parameters of the Channel

An ohmic behaviour of the system channel is intended in order to perform a proper stimulation of the test subject, the *C. elegans* embryo. The most important ohmic parameters of the channel to determine are the channel bulk ohmic resistance, the electric current and current density and the electric field and voltage drop along the channel.

The bulk (ohmic) resistance of the channel was calculated theoretically by using the dimensions presented in Table 4.1 and the resistivity of PBS (ρ_{PBS}), which was measured with a resistivity meter (*S20-K SevenEasy*™), yielding 62.10 Ω.cm at 22ºC. The channel resistances of each segment were calculated using Eq. (4.4) and then they were associated (series and parallel association) to a single total bulk resistance. The average resistance was also computed, by considering the channel as a single parallelepiped with the average dimensions presented in Table 4.1.

To confirm the theoretical results, the channel bulk resistance was also measured by impedance spectroscopy. The measurements were performed using the two wire method (see [76]) by inserting the electrodes into the inlets and connecting them to an impedance spectrometer's (*Agilent 4294 A* or *Agilent 4284 A*) terminals. The parasitic impedance due to the wiring of the system was neglected. Six measurements (n = 6) were performed and the results were averaged. The data was analysed using *MATLAB R2010a* (.m files in the annex CD-Rom).

The electric current in the channel was measured for a range of voltages from 1V to 10V. The measurements were done using again the two wire method, by inserting the

electrodes into the inlets and connecting them to the terminals of a DC power supply (*Agilent E3631A Triple Output DC Power Supply*), and connecting an ammeter in series to the circuit (Fig. 4.11). An amplifier (*Stanford SR570*) was used to help with the measurements and to filter some noise. Noise was assumed to be significant to the centesimal of the microampere. Ten measurements (n = 10) were performed for five different chips (two measurements per chip). The current obtained for all the measurements for a given voltage was averaged. The channel bulk resistance was also computed from that average for each voltage (V_0), by applying Ohm's Law (Eq. (4.3)).

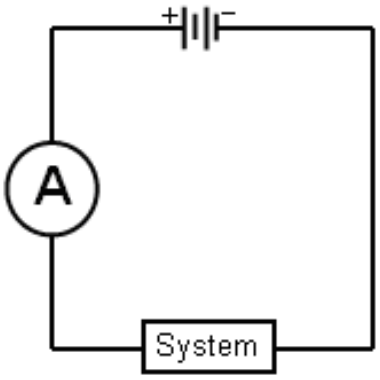

Fig. 4.11: Schematics of the setup used to measure the current and the bulk resistance of the channel. The channel is represented by a box. The instrument for the measurement may be an ammeter or an impedance spectrometer (both represented by an "A").

Since using the average dimensions of the channel instead of dividing it into segments gives an error inferior than 1% for the computation of a given ohmic parameter (see the discussion section below), the current density (J) and electric field (E) were computed by using the average dimensions, for simplicity. The magnitude of the current density (J) was computed for voltages from 1V to 10V using Eq. (4.2), where $d\boldsymbol{A}$ equals the average channel cross-section area since it is almost constant along all its length. From the current density and using the resistivity of PBS, Eq. (4.5) was used to compute the magnitude of the electric field (E).

The voltage drop along the channel was analysed only for an input voltage of 5V ($V_0 = V_{x=0} = 5V$) (for other voltages, the procedure is similar). Under the assumption that the

channel cross-section area is constant along all its length, the computed voltage drop is also expected to be constant. Consequently, the gradient of the potential Eq. (4.1) for only one dimension can be replaced by ΔV. This way, the procedure to determine the voltage drop was solving Eq. (4.1) for ΔV and making iterations of 10µm ($\Delta x = 10\mu m$), starting at one extremity of the channel ($x = 0$) where the potential is 5V, here called the first extremity, and ending at the other extremity of the channel ($x = 6870\mu m$, see Table 4.1) where the potential is 0V, here called the last extremity. Then, from the value of ΔV, the voltage at a given point every 10µm in the channel was obtained. Since the voltage decreases as one advance along the channel, the voltage is given by:

$$\begin{cases} V_0 = 5 \\ V_x = V_{x-10} - E\,\Delta x \end{cases} \tag{4.16}$$

where V_x is the voltage at distance x from the first extremity, V_{x-10} is the voltage at the distance 10µm behind ($x - 10\mu m$), $\Delta x = 10\mu m$ is the space between each iteration and E is the channel average electric field computed before (from the average current density). x assumes only values multiples of 10, from 0 to 6870. The voltage drop was normalized by dividing each obtained voltage by V_0.

4.4.2. FEM Simulation of the Channel

The channel was simulated recurring to the finite element method (FEM) software *COMSOL Multyphysics 3.5*, using the *Conductive Media DC* module. The system was draw the closest possible to the *CleWin* design. A detailed description of the simulation design and settings is in Appendix B. The input voltage chosen was 5V and the channel medium was set with the PBS resistivity. The electric field and current density at any area of the channel were available from the simulation results. Their average values were also computed having in account the weight of the length of each segment in

relation to the total channel, neglecting the contribution of region 3/3' due to its small length compared to the other segments.

The voltage drop along the channel was also computed from the electric field found in the 2D simulation in two ways. The first was using the built-in post processing function of *COMSOL* to plot the potential for a line crossing all the length of the channel, and then normalizing the values by dividing them by V_0. The second way consisted in using the average values of the electric field found from the 2D simulation and using the iterative procedure (Eq. (4.16)) to find out the voltage drop.

Since the system used in this project is tri-dimensional, the most accurate simulation of it should be also 3D. For simplicity a 2D simulation is preferred. However, it should be compared to the 3D case in order to verify if it is accurate enough and therefore validated. For this reason, a 3D simulation was also performed with the same conditions of the 2D simulation. The geometry of the 3D simulation was built starting from the 2D geometry model and extruding it for a height (h) of 41μm. The inlets and electrodes were extruded for 7mm to create the vertical pathways connecting the system to the exterior where the electrodes are inserted.

4.4.3. 2D FEM Simulation of the Channel with the Embryo Injected

The simulation of the channel with the embryo had the goal of estimating the electric field profile around the embryo, in order to have an idea of how charge distribution would occur around the embryo. The simulation was performed using the 2D *Conductive Media DC* module, the same channel geometry and physical conditions of the previous 2D simulation and an input voltage of 5V ($V_0 = 5V$). The embryo was placed at the right of the pillar as an ellipse with axis 15μm × 30μm. An estimated resistivity of 200Ω.cm was set for the embryo (this value is in the physiological range [77]).

4.4.4. Analysis of the Joule Heating Effect from the 2D FEM Simulation

The Joule heating effect was simulated by applying the *Heat Transfer* module integrated with the *Conductive Media DC* module using exactly the same setup that was used to compute the current density and the electric field. Water thermodynamic properties were used instead of PBS, since PBS is mainly composed by water. PDMS thermodynamic properties were extracted from [78] and were converted to adapt to the simulation geometry. The heat transfer coefficient was calculated from the thermal conductivity assuming the system as an entire PDMS block dissipating heat. The details of the assumptions taken are in Appendix B.

In addition to the original geometry simulation, a new geometry with closer inlets (Fig. 4.12) was also simulated and compared with the original device. For this modified device, two new inlets with 1.25mm of diameter were placed approximately near the end of segments 2/2'. The electrodes were moved to a position near the centre of the new inlets. Making closer inlets allows decreasing the channel bulk resistance and maybe also reducing Joule heating. The position of the new inlets has no influence in the direction of either the electric current or the electrolyte flow since the original inlets are not connected to the exterior and thus are a dead end for the propagation of the current and fluid flow.

All simulations were performed considering an external temperature of 24ºC. The applied voltage (V_0) varied between 1V and 15V for the original device and 1V and 5V for the modified device.

Fig. 4.12: The approximate location of the new inlets (in blue) compared to the original inlets (in purple). The blue section of the channel corresponds to the part where the electric current and fluid go, showing a decrease in both hydrodynamic and electric resistance.

4.4.5. Determination of the Electrode/Electrolyte Interface Parameters

An electrical circuit model is a simple way to visualize the physical phenomena that occurs at the electrode/electrolyte interface. In our case, it will help to visualize in which way the system deviates from the linear ohmic behaviour expected for the experiments.

The surface area of the electrode (A_S) corresponds to the area of the base of the cylinder (πr^2) in contact with the solution and all the lateral area of the cylinder immersed in the solution ($2\pi r h_i$):

$$A_S = \pi r^2 + 2\pi r h_i \tag{4.17}$$

where $h_i = 5mm$ is the height of the wire immersed in the solution and $r = 0.15mm$ is the radius of the wire. Table 4.2 summarizes the relevant properties of the platinum electrodes for the following computations.

Table 4.2: Relevant platinum electrode properties

Electrode Wire Geometric Properties	**Radius (r):**	1.50×10^{-2}cm
	Immersed length (h_i):	0.5cm
	Surface area (A_S):	$4.78\times10^{-2}cm^2$
Electrode Electrochemical Properties for PBS (assumed sodium chloride solution 0.5M)	**Exchange current density (J_0) [79]:**	$1.85\times10^{-3}A/cm^2$
	Number of participating electrons (z):	4
	Thermal voltage (V_t):	26mV
	Saturation current (I_S):	$>1.57\times10^{-5}$A*
	Vacuum permittivity (ε_0):	8.85×10^{-14}F/cm
	Dielectric constant (ε):	50
	Distance between Helmholtz planes (d):	5.00×10^{-08}cm
	Resistivity of PBS (ρ_{PBS}):	62.10Ω.cm

*maximum current that could be measured with the available equipment

Charge Transfer Resistance

The first parameter analysed was the charge transfer across the interface. The main component of PBS is NaCl (~ 0.14M) [80]. Assuming a thermal voltage of 26mV ($V_t = 0.026V$) at room temperature, Eq. (4.10) was solved for the overpotential (η_t) where J is the current density at the electrode surface, computed from the previously measured current in the channel and from the electrode surface area. The overpotential was then used do compute the charge transfer resistance (R_{CT}) using Eq. (4.11).

The charge transfer resistance was also measured by impedance spectroscopy. Since the bulk resistance is too high, it concealed the charge transfer resistance and the later could not be measured. Therefore, a similar measurement was performed using instead a recipe filled with PBS, where the electrodes could be put together. It was not a correct approach to characterize the system since the bulk resistance has also an impact on the R_{CT} (because it determines the channel current and thus the current density at the electrode surface), together with the electrode surface and exchange current density. However, for small input signals, a good estimate could be made. The R_{CT} values were

extracted from the impedance plot based on to the model plot of [81] (Fig. 4.13). Two measurements were made, the values were extracted using *MATLAB* and their average was computed.

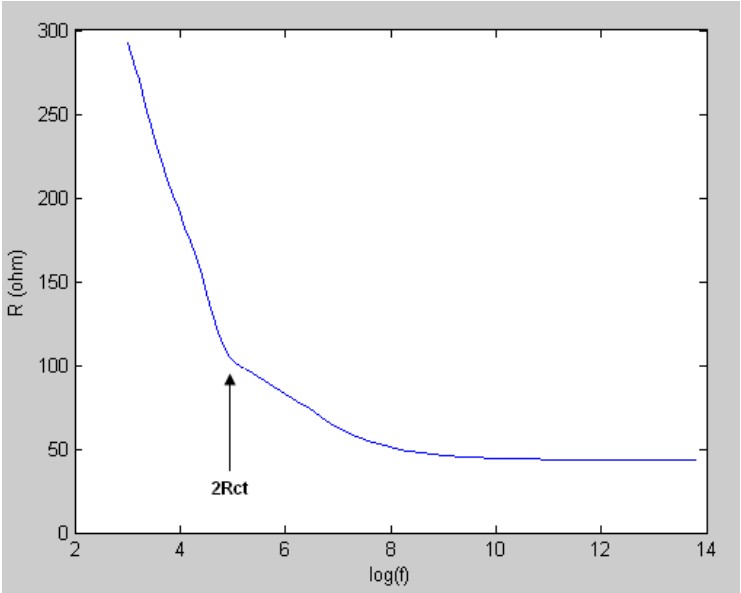

Fig. 4.13: Example of how the R_{CT} is extracted from the *MATLAB* plot.

Diffusion Resistance

The next factor to be studied was diffusion. The saturation current (I_S) was measured by increasing the applied voltage till the current saturated. However, the maximum voltage available by the power generator (model) was 33V and was not enough to reach the saturation current. Consequently, the maximum current measured was assumed as the saturation current in Eq. (4.13) to compute the diffusion resistance.

Interfacial Capacitance

The interfacial capacitance is usually neglected for DC applications. Since the interfacial capacitance is in parallel with the charge transfer resistance, after the capacitor is fully charged, no more current will flow through it and resistive mechanisms will describe completely the electrode/electrolyte interface. The interfacial

capacitance (C_I) was calculated using Eqs. (4.7) and (4.8), where C_{GC} was neglected since it is too big for the voltage range used (between 1V and 10V).

Spreading Resistance

The formula to find the spreading resistance of a cylinder is complex and the electrode was instead approximated to a planar rectangle with length equal to the electrode height ($h = 5mm$) and width equal to the electrode base perimeter ($w = 2\pi r$). This assumption was made because the inlet diameter ($d = 0.30mm$) is much bigger than the electrode diameter ($d = 1.5mm$). The base of the electrode was neglected. The width of the rectangle *is* $w = 2\pi r \approx 0.942mm$, where $r = d/2$. Eq. (4.15) was then to compute the spreading resistance (R_S), using the PBS resistivity.

4.4.6. Study of the Electroosmotic Flow and pH of the Channel

Electroosmotic flow occurs when a voltage is applied along a channel. It is proportional to the applied voltage and the electroosmotic mobility of the fluid. In a similar way to metal surfaces, when a polar or ionic solution comes into contact with a solid material, a double layer occurs at the interface. After the slipping plane, the charge on the solution side of the interface is mobile and moves parallel to an applied electric field (tangential stress). Due to viscous forces, this thin layer of mobile charge drags the neutral bulk of the solution along the channel in a plug-like manner, inducing a mass movement of the fluid.

The electroosmotic flow in the channel was analysed by observing the movement of yeast cells in suspension in the electrolyte (PBS) under the influence of the applied electric field. The direction was determined by observing in which direction the yeast cells moved and the approximate speed of the flow was estimated by counting the time a yeast cell took to migrate from one extremity of the channel to the other.

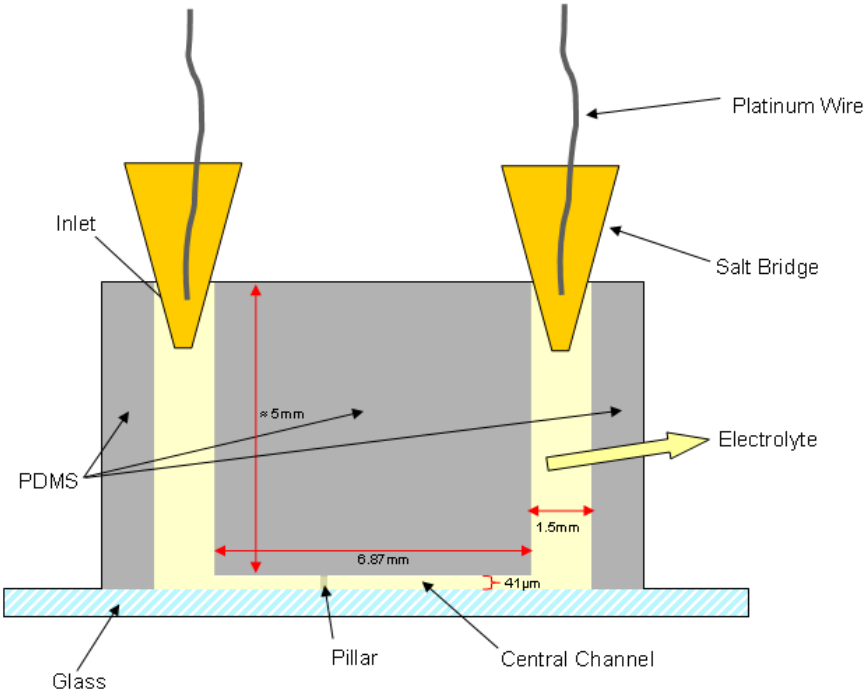

Fig. 4.14: Chip configuration using the agar salt bridges. The salt bridges are inserted in the inlets and the electrodes are placed into the salt bridges instead of directly into the inlets. This avoids the contact between the electrodes and the electrolyte, while allowing an almost unchanged electric current.

The pH of the channel was estimated by diluting phenol red[4] in the electrolyte and analysing its colour after applying the electric field. The same procedure was performed using an agar salt bridge at the inlets (Fig. 4.14) and a comparison between the two cases was done. The other channels of the same chip were used as control.

[4] Phenol red is a pH indicator. A phenol red solution exhibits a gradual transition from yellow to red over the pH range 6.8 to 8.2. Above pH 8.2, phenol red turns to a bright pink colour [137].

4.5. Results

4.5.1. Ohmic Parameters of the Channel

Channel Bulk Resistance

The bulk resistance values found theoretically and experimentally by impedance spectroscopy are in Table 4.3. The measured resistivity of PBS is $\rho_{PBS} = 62.10\ \Omega.cm$. The channel bulk resistance may be approximated by $R_{bulk} \approx 2.2\ M\Omega$.

Table 4.3: Channel bulk resistance computed theoretically and measured experimentally

Theoretically		Experimentally
Total of Segments	Average Dimensions	
2166982 Ω	2150034 Ω	2214305 ± 114538 Ω

Electric Current in the Channel

Fig. 4.15 shows the resistance obtained by applying Ohm's Law. The average of the resistances computed for each voltage is $R_{avg} = 2195986\Omega$ and may be approximated by $R_{bulk} \approx 2.2\ M\Omega$.

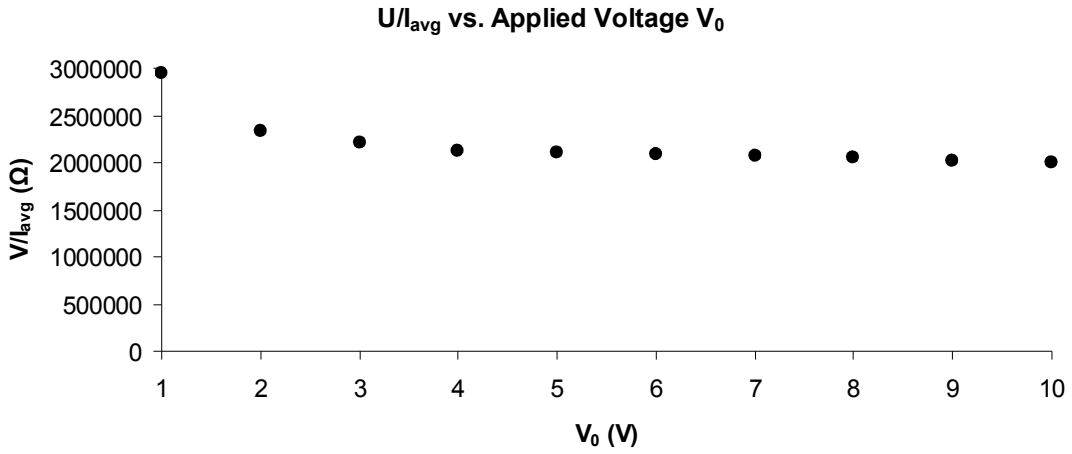

Fig. 4.15: Resistance obtained by applying Ohm's law to the measured data, in function of V_0 (two wire method).

Current Density and Electric Field

Table 4.4 presents the obtained average current densities and average electric fields from the average of the measured current using the average channel dimensions (Table 4.1), for each applied voltage.

Table 4.4: Average current density and average electric field computed from the average of the measured current using the average channel dimensions

V_0 (V)	J (nA/µm^2)	E (mV/µm)
0	0.000	0.000
1	0.171	0.106
2	0.431	0.268
3	0.683	0.424
4	0.947	0.588
5	1.199	0.745
6	1.444	0.897
7	1.706	1.059
8	1.970	1.224
9	2.240	1.391
10	2.515	1.562

Table 4.5 compares the values of the current density and electric field computed from the measurements with the average values obtained from the 2D and 3D simulations (segments 3/3' neglected) for $V_0 = 5V$. The average value was calculated by multiplying each value by the ratio between the length of the segment in question and the total channel length, and then all the values were summed to find the average value.

Table 4.5: Comparison between the values of the current density and electric field computed from the measurements versus the average values obtained from the 2D and 3D simulations (segments 3/3' neglected) for $V_0 = 5V$

J (nA/µm^2)			E (mV/µm)		
Experimental	**2D Simulation**	**3D Simulation**	**Experimental**	**2D Simulation**	**3D Simulation**
1.199	1.130	1.142	0.745	0.702	0.709

Voltage Drop along the Channel

The plot in Fig. 4.16 depicts the voltage drop as a fraction of the initial voltage in function of the channel length for the same simulation, calculated by *COMSOL*. The channel is centred in the x axis (in millimetre). The flattening of the curve at the extremities is due to the electric field being almost constant at the inlets, and thus also the voltage.

Fig. 4.17 compares the voltage drop plot computed from the average values of the electric field obtained from the measured current with the plots of the voltage drop computed using the same method, but using instead the average values obtained from the 2D and 3D simulations.

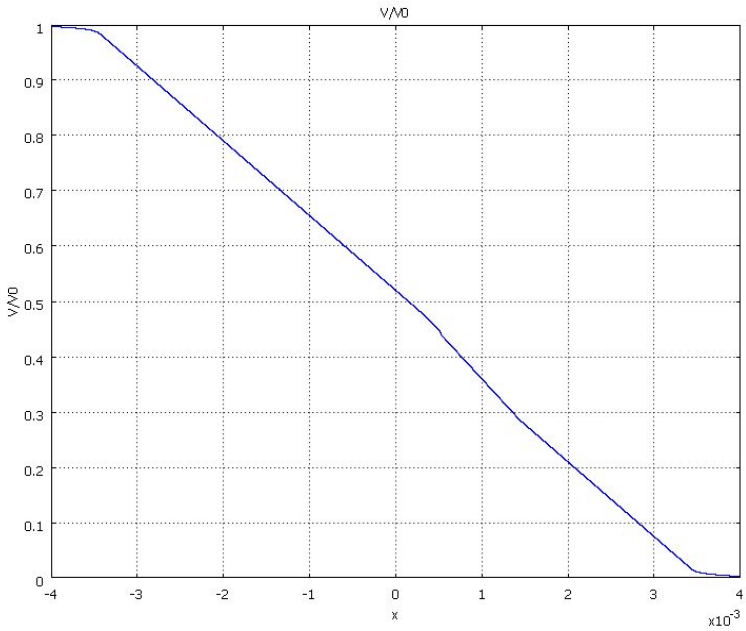

Fig. 4.16: Voltage drop as a fraction of the initial voltage in function of the channel length for 2D simulation, calculated by *COMSOL*. The *x* axis is in millimetre. The flattening of the curve at the extremities is due to the electric field being almost constant at the inlets, and thus also the voltage.

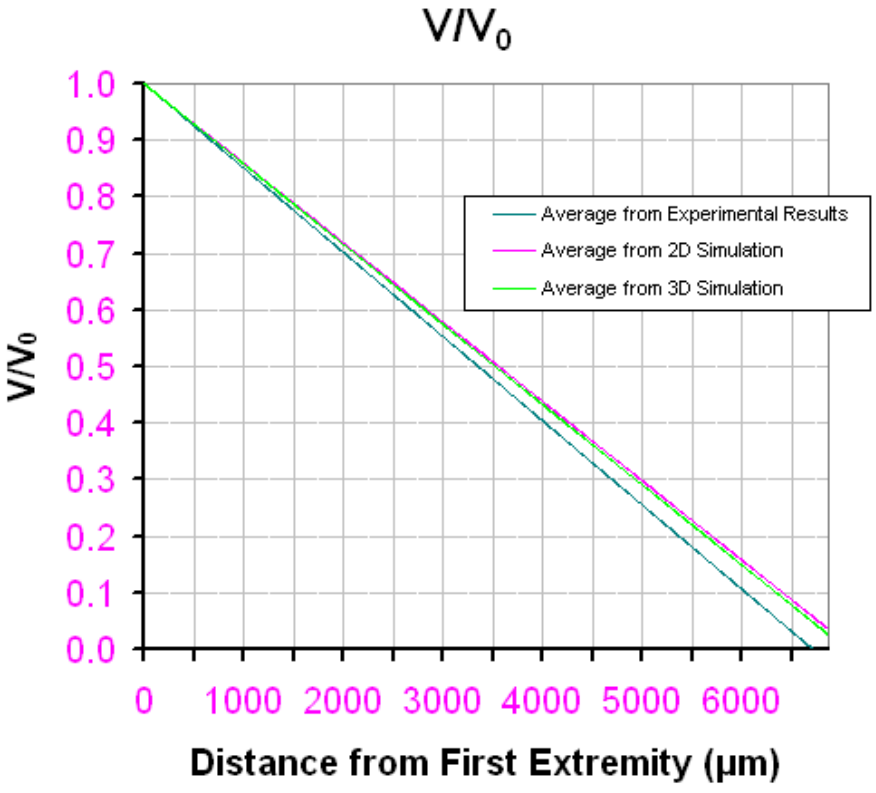

Fig. 4.17: Comparison between the voltage drop plot computed from the average values of the electric field obtained from the measured current versus the plots of the voltage drop computed using the same

method, but using the instead the average values obtained from the 2D and 3D simulations. The x axis goes from 0 to 6870µm.

4.5.2. 2D FEM Simulation of the Channel with the Embryo Injected

Table 4.6 compares the average current density and average electric field obtained from the 2D simulation with no embryo and from the 2D simulation with embryo, both for $V_0 = 5V$. Assuming a resistivity of 200Ω.cm ($\rho_{embryo} = 200\Omega.cm$), Fig. 4.18 shows the current density and electric field profiles at the embryo region, showing also the stream and field lines form the current density and electric field respectively. The scale is in nA/µm^2 for the current density and mV/µm for the electric field. Hot colours represent higher values and cold colours represent smaller values. The current goes from the left to the right.

Table 4.6: Comparison of the average current density and average electric field obtained from the 2D simulation with no embryo and with embryo, both for $V_0 = 5V$

2D Embryo no Embryo Comparison					
Current Density (J) (A/m^2)			Electric Field (E) (mV/µm)		
No embryo	Embryo	Difference (%)	No embryo	Embryo	Difference (%)
1130	1120	-0.82%	0.702	0.696	-0.87%

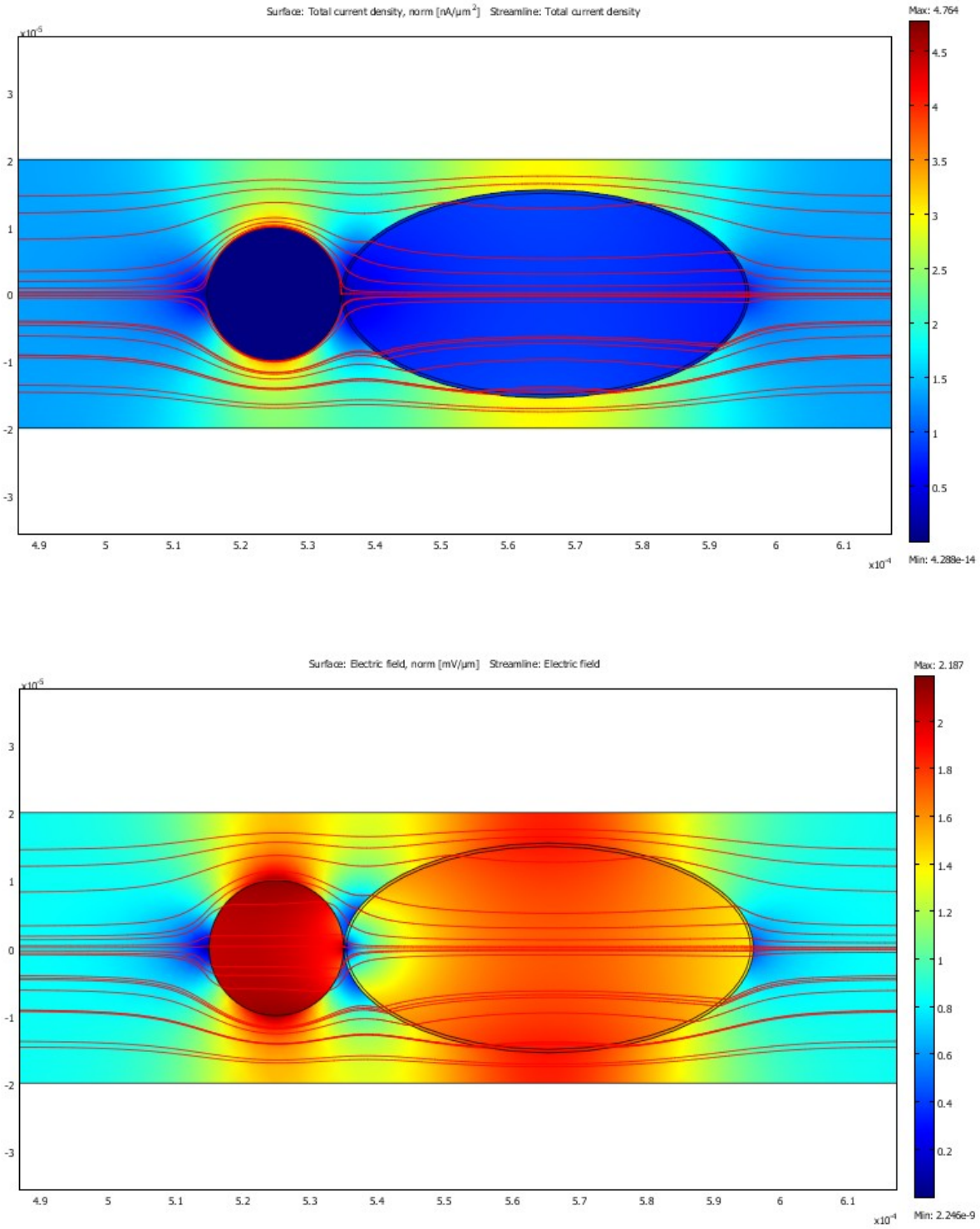

Fig. 4.18: Top: colour map of the current density profile at the embryo region. Bottom: colour map of the electric field profile at the embryo region. The stream and field lines are visible. The scale is nA/µm^2 for the current density and mV/µm for the electric field. Hot colours represent higher values and cold colours represent lower values. The size bar ranges from 0 till 4.76nA/µm^2 for the current density and 0 till 2.19mV/µm for the electric field. The current goes from the left to the right. The coordinate axes are in 10^{-4}m. Calculations performed by *COMSOL*.

4.5.3. Joule Heating Effect Simulation

Fig. 4.19 shows the relationship between the electric field and the temperature calculated at the embryo region (at the right side of the pillar). The connected points correspond to the situations with most interest:

- Grey line *(E, T = 0.843, 24.7) (mV/µm, ºC)* for the original device and *(E, T = 1.058, 24.7) (mV/µm, ºC)* for the modified device: connects the situation where the temperature arises from an applied voltage $V_0 = 5V$ of the original device with the situation where the applied voltage takes to approximately the same temperature in the modified device.

- Purple line *(E, T = 1.430, 26.0) (mV/µm, ºC)* for the original device and *(E, T = 1.802, 26.0) (mV/µm, ºC)* for the modified device: connects the limiting situations for the normal development of the embryo where the temperature is about 26ºC.

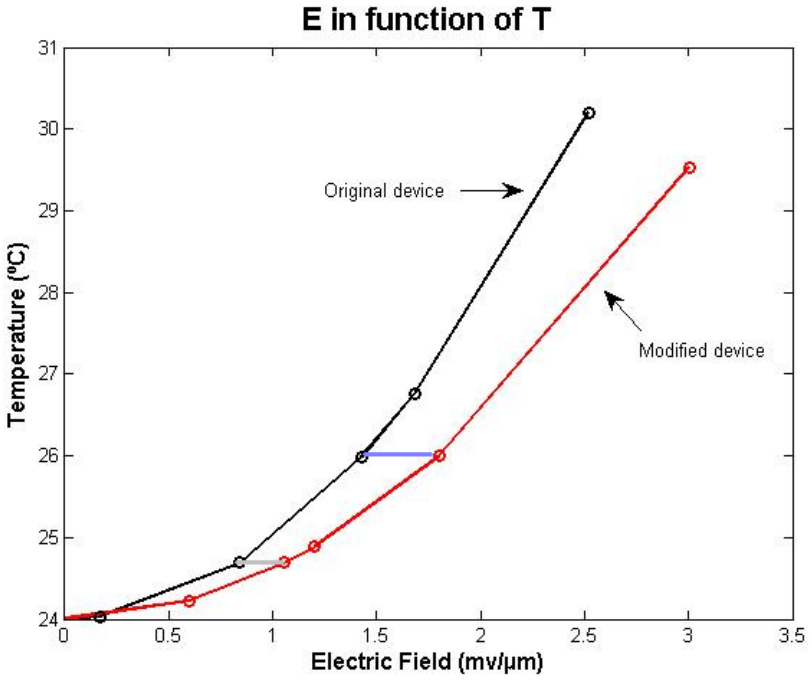

Fig. 4.19: Relationship between the electric field and the temperature calculated at the embryo region by *COMSOL*.

To evaluate the efficiency of the system in relation to the temperature, the ratio electric field/ temperature (slope of the graphs) was also computed. The efficiency at these two points was compared giving an increase of efficiency from the original device to the modified device:

- 26.0% for the points connected by the grey line.
- 25.5% for the points connected by the purple line.

4.5.4. Analytical Model of the Electrode/Electrolyte Interface

Table 4.7 shows the results of the computations of the parameters of the electrode/electrolyte interface. The time constant τ of electrode/electrolyte interface (see Fig. 4.7) was also computed by multiplying the interfacial capacitance by the charge transfer resistance.

Table 4.7: Results of the computations of the parameters of the electrode/electrolyte interface

R_{CT}:	147Ω for any V_0
R_d:	between 414Ω (V_0 = 1V) and 617Ω (V_0 = 10V)
R_S:	121Ω (planar rectangular electrode)
R_{Smax}:	1035Ω (planar circular electrode)
C_I:	4.24×10^{-6}F
τ:	6.22×10^{-4}s

Charge Transfer Resistance Measured Experimentally

The two impedance measurements yielded respectively $R_{CT} = 50\Omega$ and $R_{CT} = 36\Omega$. Their average is $R_{CT} = 43\Omega$.

4.5.5. Study of the Electroosmotic Flow and pH of the Channel

The observed direction of the electroosmotic flow was from the anode (+) to the cathode (-). Each yeast cell took between 5 and 10 seconds to run the entire channel and, from the channel length at Table 4.1, they moved at a speed of about 687μm/s to 1374 μm/s. From the average cross section area, it yields a flow rate of about 1.363nL/s to 2.726 nL/s.

After injecting the PBS solution diluted with phenol red into the channel, its colour turned to transparent with a very small tone of yellow/orange, indicating an almost neutral solution. After applying the electric field, the channel with no salt bridges started turning red, from the anode in direction to the cathode. After some minutes, the solution had a vivid pink tone. The anode inlet was vivid pink and the cathode inlet was vivid yellow. The salt bridged channel remained yellow, although the anode inlet was vivid pink and the cathode inlet was vivid yellow. The control channel and inlets remained transparent with a very small tone of yellow.

4.6. Discussion

4.6.1. Ohmic Parameters of the Channel

Bulk Channel Resistance

Comparing the bulk resistances computed theoretically and measured experimentally by impedance spectroscopy, we can say that the real channel resistance should be around 2.2MΩ. The average of the experimental values differ less than 2.2% in relation to the theoretical value. These differences may arise due to other physical phenomena other than the driving of the electric current by the applied voltage, or errors due to the rounding and measurement of the channel dimensions from the *CleWin* file.

Comparing now the theoretical values obtained with and without averaging the channel dimensions, the difference between them is less than 1%. This means that averaging the channel dimensions is a good procedure for the computations of the electrical parameters that depend on the channel dimensions, since it provides simplicity. It may be thus a good way to calculate the electric field and current density.

Measurement of the Electric Current in the Channel

The average of the measured current values obtained for each input voltage (V_0) has dimensions of the order of the microampere, which is typical in microsystems. Fig. 4.15 shows a linear relationship between the average of the current and the voltage, suggesting an ohmic circuit, despite the non-linear elements such as the electrode/electrolyte interface. These results may give an insight about the electrode/electrolyte interface, suggesting that its impact in to the U/I relationship should be small, even for small voltages like 1V.

Fig. 4.15 shows that bulk resistance computed for each voltage, by applying Ohm's law to the average of the measured current and applied voltage, is almost constant for any voltage. The average of the resistances computed for each voltage differs less than 3% from the theoretical computed resistance and less than 1% from the resistance measured by impedance spectroscopy, proving that the V_0/I relationship shown in Fig. 4.15 is accurate.

However, for $V_0 = 1V$, the resistance for this voltage is about 34% greater than the average, maybe because, since the current is small, other physical phenomena different of the driving of current by the applied voltage may become significant. In fact, from the graph, the resistance seems to decrease a little till $V_0 = 5V$, suggesting that some non-linearities are present for small voltages. However, only voltages equal or greater than 5V are going to be used for the embryo stimulation and there are no non-linearities apparent for those values.

During the measurements it was observed that the current changed randomly with an order of magnitude of 0.001A, what led to the conclusion that noise was significant to the centesimal of the microampere.

Current Density and Electric Field

The current density and electric field depend on the channel geometry and are slightly different in different segments. However, it is simpler using the average values computed using the average channel dimensions, rather than dividing the channel in segments, since there are no significant changes of the values, as seen with the bulk resistance analysis.

The magnitude of the current density indicates currents of the order of the nanoampere flowing through areas of the order of square micrometer. Both of them are typical of physiological systems, such as ionic currents flowing through ion channels [4]. As for the electric field, it indicates voltages drops varying between hundreds of microvolts and a little more than one milivolt per micrometer, or alternatively, between hundreds of milivolts and a little more than one volt per milimeter. Typical cell membrane thickness varies between 7.5nm and 10nm [82], what means that for this electric field values, the voltage drop is between about 10mV and 200mV for these distances, what is in the range of physiological values, as exemplified with the membrane potential, ranging about some teens of milivolts, sometimes reaching the hundreds.

For $V_0 = 5$, the experimental values were compared with the average values obtained by 2D and 3D simulation. The experimental and simulated values differs only about 5% to 6%. The differences may arise due to the averaging of the values computed, to the fact that the system geometry design is not exactly the same as the real geometry, to the resistance of the wires and connectors between the power supply and the system, to the rounding of the constants in the simulation, and to the neglecting of other physical phenomena such the ones occurring at the electrolyte/interface and channel walls. This small difference suggests that all physical phenomena, other than the ohmic processes, affecting the electric field and current in the channel can be neglected, as already stated above when analysing the channel bulk resistance.

Finally, the values between the 2D and 3D simulations differ only by about 2.5%, proving that a 2D model is good enough to simulate the system.

Voltage Drop for $V_0 = 5V$

The plots V/V_0 for the experimental data were built for $V_0 = 5V$, but, since we are dealing with a ratio, the behaviour of the graph is almost the same for greater voltages. The voltage at the last extremity (outlet) should be $V = 0V$ at $x = 6870\mu m$, but the plots show a small difference between this ideal situation and the real situation, showing a deviation of about 3.1%. For the voltage drop using the iterative method with simulation values, there is also a small deviation of about 3.6% for 2D and about 2.6% for 3D. The voltage drop ratio calculated by *COMSOL* for the 2D simulation corresponds to the ideal situation, since *COMSOL* used always the same conditions. These deviations may arise essentially due to measurement errors, to approximations performed at the analytical computations and to non-linearities of the system. However, they are too small proving that we can neglect all physical phenomena determining the current and electric field in the channel other than Ohm's Law, at least for $V_0 = 5V$ or greater values.

For smaller voltages, with evidence for $V_0 = 1V$, the voltage drop deviates significantly from the ideal situation. As discussed already, when analysing the current measurements, there is a deviation of the channel resistance of about 34% for 1V, compared with the average. However, 1V and voltages smaller than 5V will not be used for the embryo stimulation.

4.6.2. 2D FEM Simulation of the Channel with the Embryo Injected

From the experiments, it is known that the electric current changes due to the embryo resistance are concealed by noise, so that the impact of the embryo in the average current density and electric field in the channel should be very small. The simulation results show an impact of the embryo on the electric field and current density of less than 1%. These values seem to be in agreement with the fact that no current changes are detected after injecting the embryo, during the experiments. However, this avoids making any estimate about the resistivity of the embryo.

The first colour map of Fig. 4.18 shows that the current prefers to pass laterally to the embryo, where there are higher current densities, due to the embryo being more resistive than the electrolyte (PBS). This may be the real situation, since most cell membranes are not completely permeable to ion flow across them. The capacitive effects of the membrane, which were not considered here, may also play a role and contribute to change the membrane potential (charge it).

The second colour map of Fig. 4.18 shows that there is a higher voltage drop across the embryo region (red tone) and the pillar, which are the less conductive areas, than elsewhere in the channel. The voltage drop is greater than 120mV along all the 60µm of the embryo length. On the other hand, the electric field is inferior outside the embryo at the AP extremities (more blue tone). Consequently, there is bigger voltage gradient through the embryo, suggesting an excess of accumulation of charge at the embryo AP extremities, which is pretended for the embryo stimulation.

4.6.3. Joule Heating Effect

Making closer inlets allows decreasing the channel bulk resistance (see Eq. (4.4)), however, the proximity of the inlets also decreases the hydrodynamic resistance of the channel in the same proportion it decreases the electric resistance. This turns the liquid flow much more sensitive to mechanical stimulus, reflecting in great difficulties to place the embryo at the pillar region (it almost always flows back to the inlets). Consequently, extreme care must be taken when injecting the embryo and several tries are needed for a successful injection. The comparison between the modified device and the original device was performed to find out if it is advantageous to use the modified device due to the reduced Joule heating, despite all the injection difficulties

According to the simulation, the maximum temperature assumed (26ºC) for the normal development of the embryo is achieved for an electric field of 1.43mV/µm (original device), corresponding to a voltage of 8.5V. However, experiments show that applying 10V still allow an apparently normal development of the embryo. Therefore, no more

than 10V should be applied continuously during embryogenesis. In fact, a temperature of 25ºC is already enough to induce developmental changes.

Fig. 4.19 shows clearly that there is a gain in efficiency of the system if we use the modified system, but it requires a lot of effort to inject the embryo. In addition, at the limiting temperature, the gain in efficiency is only 25.5% i.e. just a quarter of the total electric field and current, what does not justify the use of the modified device. The graph also shows that the gain of efficiency decreases with applied voltage, since the inverse of slope decreases for the two devices. On the other hand, decreasing the voltage will increase the non-linearities of the system. Therefore, the original system will be used in all the experiments for the embryo stimulation.

4.6.4. Analytical Model of the Electrode/Electrolyte Interface

Analysing the charge transfer resistance (R_{CT}) computed analytically, one can conclude that it can be neglected due to being extremely small compared to the bulk channel resistance for any applied voltage. This small value arises from the very big surface area of the electrode. The average of the charge transfer resistance measured by impedance spectroscopy for a pool of PBS is 43Ω. This value is smaller than the analytical calculation values, since the bulk resistance of a recipe filled with PBS is almost zero. In the system, the charge transfer resistance should be greater, due to the greater bulk resistance, resulting in a smaller channel current that contributes to reduce the overpotential (η_t). But the expected increase of the R_{CT} should not be significant and the measurement serves therefore as a good estimate for the system.

As for the diffusion resistance, although not knowing its exact value, we know that it is smaller than 620Ω, since the limiting current is greater than the one used in the calculations. Since it is also small when compared with the bulk resistance, we can neglect it too.

The estimated spreading resistance is also small and can be neglected, even if the electrode is considered as planar (greatest spreading resistance).

As for the interfacial capacitance, the time constant determines if it can be neglected or not. If the time constant is too small, the capacitor charges quickly and behaves as an open circuit in just a few instants. For practical purposes, when this happens, the capacitor can be neglected and considered as an open circuit and removed from the model, giving importance just to the branch of the resistive mechanisms. Being only of the order of hundreds of microsenconds, it means that the capacitor is almost instantly charged after the beginning of the voltage application. Consequently, it will behave as an open circuit almost instantly, for DC situations, and can be neglected because the experiments take several hours.

From the results, the electrode/electrolyte interface can be entirely neglected, except for the chemical reactions (as will be seen next), since, for the voltages used in the experiments, it has an impact in the channel U/I relationship that is extremely small (much less than 1%), and therefore the channel behaves mostly as a linear element. This is due mainly to the extremely large surface area of the platinum electrodes.

4.6.5. Electroosmotic Flow and pH of the Channel and Theoretical Study of the Chemical Reactions Occurring in the Electrolyte

The electroosmotic flow rate indicates that an analyte present in one extremity of the channel can reach the other extremity in just a few seconds. Thus, when adding any composite to the channel, it should be assumed that it propagates instantly to the entire channel and may interact with whatever is present there, including the embryo. This was evidenced after adding phenol red to the PBS: after turning vivid pink at the anode, it spread to the rest of the channel in just a few seconds, turning the entire channel red.

The electrode/electrolyte interface is a region where redox reactions occur independently of the type of electrode and electrolyte. These reactions are important to analyse, since the chemical products created by them can change the electrolyte pH and compromise the development of the embryo. Since PBS is mainly composed by sodium chloride [80] we can analyse the chemistry at the electrode surface considering the electrolyte as a $NaCl$ solution.

For the interface *platinum/NaCl*, the electrolysis of salt water at the platinum surface is the main concern. The electrolysis of pure water is the decomposition of water (H_2O) into oxygen (O_2) and hydrogen gas (H_2) due to an electric current passing through the water [83, 84]:

$$2H_2O(l) \rightarrow 2H_2(g) + O_2(g) \tag{4.18}$$

with the half reactions

$$\begin{aligned} &\text{Anode (oxidation):} \\ &2H_2O(l) \rightarrow O_2(g) + 4H^+(aq) + 4e^- \\ &\text{Cathode (reduction):} \\ &2H_2O(l) + 2e^- \rightarrow H_2(g) + 2OH^-(aq) \end{aligned} \tag{4.19}$$

Hydrogen is produced at the cathode while oxygen is produced at the anode, manifesting by the formation of bubbles at each electrode (more intensely at the cathode). The degree of the reactions increases with the applied voltage.

Since reduction occurs at the cathode and oxidation occurs at the anode, H^+ cations will accumulate near the cathode and OH^- anions will accumulate near the anode. Thus, the water near the cathode (-) is acidic while the water near the anode (+) is basic.

For salt water a slightly different mechanism occurs. If *NaCl* is dissolved in the water, only half the electrolysis of water occurs since the chloride ions are oxidized to chlorine rather than water being oxidized to oxygen. In this case, chloride anions from the electrolyte are in competition with hydroxide ions to give up an electron. The overall reaction is [85]:

$$2H_2O(l) + 2Cl^-(aq) \rightarrow H_2(g) + Cl_2(g) + 2OH^-(aq) \tag{4.20}$$

where the half reactions are

$$\begin{aligned} &\text{Anode(oxidation)}: \\ &2Cl^-(aq) \rightarrow Cl_2(g) + 2e^- \\ &\text{Cathode(reduction)}: \\ &2H_2O(l) + 2e^- \rightarrow H_2(g) + 2OH^-(aq) \end{aligned} \tag{4.21}$$

The Na^+ ions present in the solution may react with OH^- ions creating $NaOH$ (a strong base) and leading to the total overall reaction:

$$2NaCl(aq) + 2H_2O(l) \leftrightarrow Cl_2(g) + 2NaOH(aq) + H_2(g) \tag{4.22}$$

This leads to a very basic solution in the channel.

Other types of redox reactions also occur at the platinum surface. These mechanisms are complex and will not be described here, but from literature, it is possible to have an idea of some of the resultant products created, as platinic oxides such as PtO and PtO_2 or compounds derived from platinum and chloride such as $PtCl_4^{2-}$ and $PtCl_6^{2-}$ [79]. These compounds can eventually have an influence on the electrolyte pH and may also interact directly with the embryo with damage consequences.

The presence of $NaOH$ in the channel explains the red tone of the electrolyte when the phenol red was dissolved. Since it may disturb the development of the embryo, an agar salt bridge was placed in the inlets. With the salt bridges, the solution remained light yellow, almost transparent, typical of a neutral solution. At the inlets, the colour remained vivid pink at the anode and strong yellow at the cathode, proving that the

electrochemical reactions keep occurring there, but the resulting products are retained by the agar, not flowing into the channel. This shows that the agar salt bridges are an effective way to protect the embryo, avoiding pH changes during the development time. This was further evidenced when the mortality rate of the embryo was drastically reduced by using salt bridges.

4.7. Conclusion

From the analysis performed here, we conclude that all the physical phenomena that may affect the relationship between the applied voltage (V_0) and the electric current in the channel, other than ohmic processes, may be neglected for the voltages used (5V or greater), and we can approximate the circuit to a linear system that obeys Ohm's Law. Consequently, knowing a priori the channel resistance (2.2MΩ) and the applied voltage, allows one to compute the electric current, and the channel may be modelled by the circuit of Fig. 4.20.

Furthermore, since the channel dimensions are almost constant and can be averaged, we can precisely estimate the average current density of the channel, and from it, the electric field and voltage drop that, for an applied voltage of 5V, are in the physiological range.

Eventually, the embryo must have a greater resistivity than PBS, since it has an eggshell, permeability barriers and each cell is protected by a cell membrane, so that the voltage drop is greater at the embryo region. This way, the greater the resistance, the greater the surface charge gradient between its extremities [86]. Consequently, we can say that an excess of opposite charge accumulate at the embryo's extremities and may charge the cell membranes of the embryo cells (Fig. 4.21). It should be noted that this excess of charge results from a greater charge gradient at the embryo extremities compared to any other part of the channel, and not from the presence of negative charge on one side and positive charge on the other side of the embryo. Charge is symmetric only when seen from the embryo. Unfortunately the electric field at the embryo region could not be quantified for the real situation, since the embryo resistivity is unknown,

but we hypothesise that it may someway affect its development, by changing the membrane potential due to the charge accumulation.

Joule heating effect must be a major concern when conducting the experiments, since temperatures greater than 25ºC/26ºC might disturb the embryo development. Considering the best case scenario as 26ºC, voltages till 8.5V should not give problems related with temperature, assuming that the room where the experiments are performed has a maximum ambient temperature of 24ºC.

Finally, a theoretical analysis of the chemical reactions occurring at the electrode surfaces suggests that the electrolyte is a strong base and can disturb the embryo development. The use of a slat bridge at the inlets to avoid the contact between the electrodes and the channel electrolyte will be considered, since it seems to avoid the propagation of chemical products to the channel, maintaining an almost neutral solution in the channel, while effectively conducting the electric current.

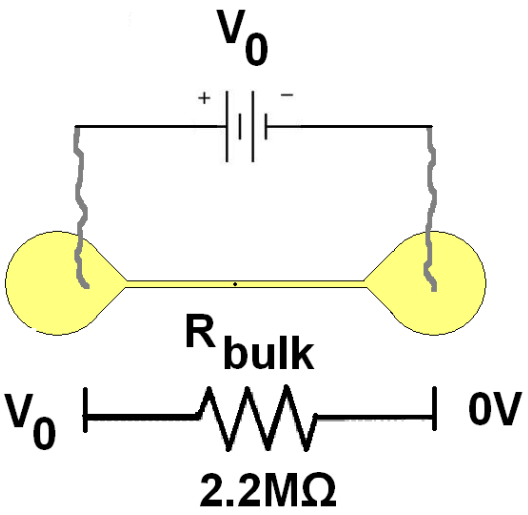

Fig. 4.20: Schematic representation of the circuit analogy of the system. The central channel is approximated by a resistor between the inlets, representing the bulk resistance $R_{bulk} = 2.2M\Omega$.

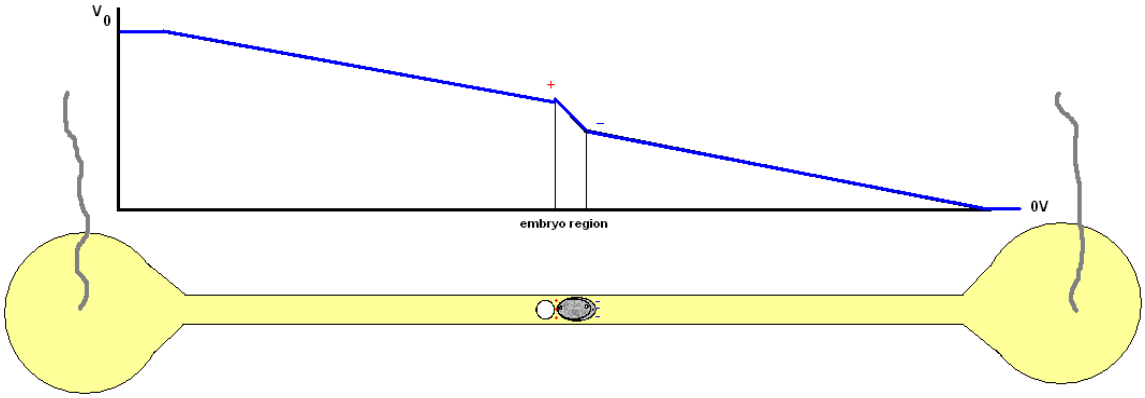

Fig. 4.21: Schematic representation of the voltage drop along the channel, evidencing the charge accumulation around the embryo.

5. Assumptions

The goal of this project is the study of the impact of a DC electric field in the embryo of *C. elegans*. From the conclusions taken when characterizing the system, we expect an excess of charge accumulation at the embryo's anterior and posterior extremities (Fig. 5.1). From what is known about bioelectricity, this electric field may change the membrane potential of the cells of the embryo. The charged membrane may, therefore, alter the function of its components, namely voltage dependent ion channels that may induce a variety of cell responses, by means of signal transduction. Through signal transduction, diverse cellular mechanisms may be activated by means of second messengers, inducing cell responses at the level of the cytoplasm or cell membrane, or even at the nuclear level itself. Since the signal may be amplified during transduction, a single electrical stimulus may induce several mechanisms that lead to diverse cellular responses.

In addition, voltage dependent ion channels may increase their conductivity to ions due to cell membrane potential variations, allowing an ionic current into the cells. It is known from the action potential propagation, for example, that those currents further contribute to change the membrane potential and contribute to activate even more channels, in a positive feedback way.

Due to the voltage drop through the embryo, the charge accumulation at the two extremities (anterior and posterior) will have opposite sign when seen by the embryo. Therefore, we expect to charge more positively (or less negatively) the membranes of one extremity of the embryo and more negatively (or less positively) the membranes of the other extremity. This may induce different responses in different cells, as for example AB and P_1 that are side by side at the AP direction, functioning as an electric analogy to the application of a temperature gradient across the embryo that is already known to alter the development of the embryo by changing the duration of the cell cycle [26]. Alternatively, the same cell, such as P_0, may be charged differently at its anterior and posterior extremities, and it might be interesting to observe different responses at the same time due to a different stimulus at each side of the cell, that even may enter in conflict.

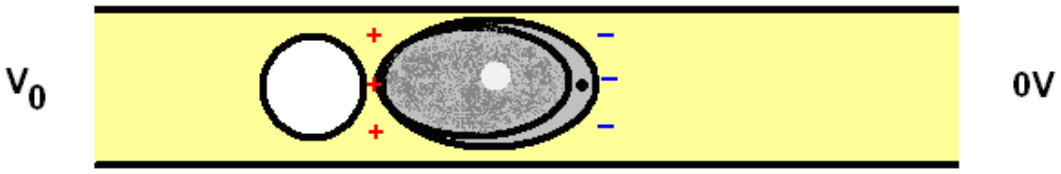

Fig. 5.1: Schematic representation of the excess of accumulation of opposite charge at the anterior and posterior extremities of the embryo (grey) that is placed next to the pillar (white). This excess of charge results from a greater charge gradient at the embryo extremities compared to any other part of the channel, and not from the presence of negative charge on one side and positive charge on the other side of the embryo.

The analysis of the impact of the electric field on embryogenesis consists in observing diverse stages of the embryo development, some of the embryo's cell cycles, divisions, growth and differentiation and maybe even the behaviour of the juvenile worm, after hatching. From the analysis, the impact of the electrical stimulus in the embryo will be assessed and it will be confirmed if the embryo of the nematode *C. elegans* is or is not an appropriate model to study the impact of bioelectricity in biological systems, at least in the form of DC electrical stimulus.

The stimulus will be applied preferentially at the beginning of embryogenesis, when the embryo is more sensitive to most kind of disturbances, compromising all the upcoming development events. The beginning of embryogenesis is also the time where it is easier to follow the embryo development.

The analysis itself consists in comparing control and stimulated embryos under the same conditions, except the existence of the electric field. This allows the most precise and accurate comparison between the two situations, essential to take accurate conclusions about the impact of the electric field on the embryo.

6. Planning of the Analysis of *C. elegans* Embryogenesis

The analysis of the impact of a DC electric field on the development of the embryo of *C. elegans* consists in analysing diverse selected stages of embryogenesis. A detailed description of the main stages to be analysed is in Appendix C, also presenting the nomenclature of the analysed cells. The stages suspected of being more susceptible to the electric field will be compared between control embryos developing with no stimulus and embryos stimulated with the electric field. Each development stage chosen will be compared in time and space: cell cycles and time intervals between development stages (ex: gastrulation to comma fold); cleavage directions and cell movements and migration (as in gastrulation, for ex.).

Briefly, the events to be analysed are the first cell cycles and divisions (P_0, AB, P_1, AB_a, AB_p, EMS and P_2 cells) till the 8-cell stage, gastrulation, comma fold, start of muscle twitches and instant of hatch. Other features to be compared are the intensity of the embryo movements inside the eggshell and the behaviour of the juvenile worm after hatching.

6.1.1. Temporal Analysis

The following nomenclature was adopted for the time of occurrence of selected development events, by order of occurrence:

- $\mathbf{t_{ncl}}$**:** pro-nuclei fusion
- $\mathbf{t_{nP0}}$**:** nuclear envelope breakdown of P_0 (signalling the beginning of mitosis)
- $\mathbf{t_{P0}}$**:** cytokinesis of P_0 cell (signalling the end of the cycle of P_0)
- $\mathbf{t_{nAB}}$**:** nuclear envelope breakdown of AB

- $\mathbf{t_{nP1}}$**:** nuclear envelope breakdown of P_1
- $\mathbf{t_{AB}}$**:** cytokinesis of AB
- $\mathbf{t_{P1}}$**:** cytokinesis of P_1
- $\mathbf{t_{ABa}}$**:** cytokinesis of AB_a
- $\mathbf{t_{ABp}}$**:** cytokinesis of AB_p
- $\mathbf{t_{EMS}}$**:** cytokinesis of EMS
- $\mathbf{t_{P2}}$**:** cytokinesis of P_2
- $\mathbf{t_{gstr}}$**:** start of gastrulation (E_a and E_p cells start ingressing)
- $\mathbf{t_{fld}}$**:** start of the first comma fold (lime-bean stage)
- $\mathbf{t_{mov}}$**:** start of muscle twitches
- $\mathbf{t_{brn}}$**:** instant of hatch (born)

Fig. 6.1 presents the event timeline showing only the selected events that will be analysed, starting with the pro-nuclei fusion.

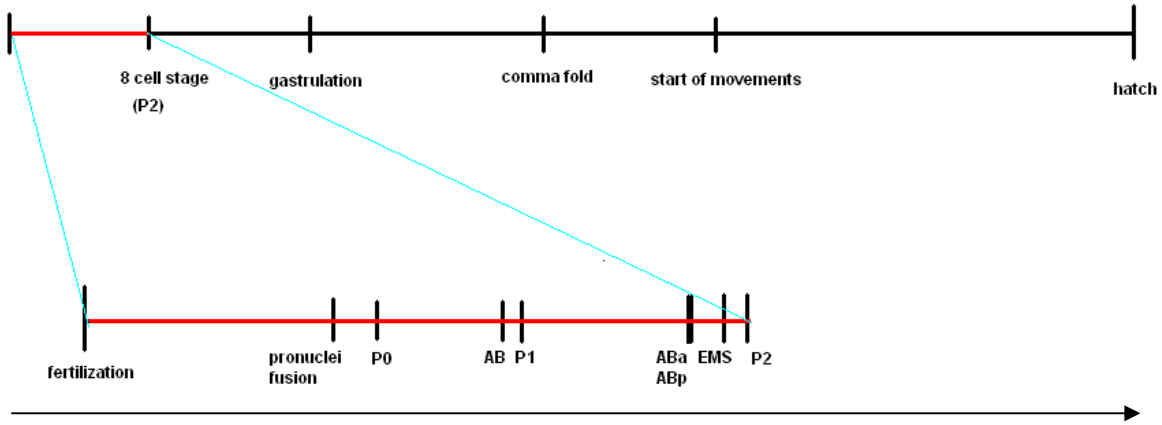

Fig. 6.1: Event timeline showing the selected events to analyse (see Table 6.2 and the list presented previously).

Table 6.1 summarizes the approximate times of the cell cycles, separating the S and M phases, for P_0, AB and P_1, for 20 experiments taken from literature [87]. Table 6.2 summarizes the times of the events present in the timeline of Fig. 6.1 in relation to the pro-nuclei fusion, based in Fig. 3.6 and Table 6.1. Table 6.3 presents the same data as Table 6.2, but each event time is relative to the event immediately before and not to the pro-nuclei fusion.

Table 6.1: Mean and standard deviation of duration (in minutes) of S and M phases in P_0, P_1 and AB determined by time-lapse DIC microscopy (20 embryos analysed) (Taken from [87])

Cell	S	M
P_0	4.9 ± 0.8 *	1.7 ± 0.3
AB	12.1 ± 1.1	1.6 ± 0.4
P_1	14.1 ± 1.1	1.7 ± 0.3

*only between pseudocleavage and nuclear envelope breakdown (NEBD)

Table 6.2: Time of events selected for analysis in relation to pro-nuclei fusion

Event	t_{ncl}	t_{P0}	t_{AB}	t_{P1}	t_{ABa}	t_{ABp}
Time	0min	7-8min	21-22min	23-24min	32-34min	32-34min
Event	t_{EMS}	t_{P2}	t_{gstr}	t_{fld}	t_{mov}	t_{brn}
Time	37-40min	40-45min	1:15-1:30h	3:30-5:00h	6:15-6:45h	12-14h

Table 6.3: Time of events selected for analysis in relation to the previous event

Event	t_{ncl}	t_{P0}	t_{AB}	t_{P1}	t_{ABa}	t_{ABp}
Time	0min	7-8min	14-15min	2-3min	10-12min	0min
Event	t_{EMS}	t_{P2}	t_{gstr}	t_{fld}	t_{mov}	t_{brn}
Time	4-5min	3-4min	30-40min	2:00-3:30h	1:30-2:30h	6-7h

6.1.2. Spatial Analysis

The embryos will be selected preferentially at the beginning of the pro-nuclei fusion (Fig. 6.2 left), or even before the pro-nuclei are visible, when the pseudocleavage contractions are still starting. In a normal situation, the two pro-nuclei will migrate

towards each other and fuse (Fig. 6.2 centre). The nucleus formed migrates to the centre of the cell where nuclear envelope breakdown (NEBD) occurs (Fig. 6.2 right), signalling the beginning of the M phase of P_0, which ends with cytokinesis. During the M phase the nucleus is not visible.

Fig. 6.3 shows the 2-cell, 4-cell and 8-cell stages of the same embryo. The position and orientation of the cells are schematized in Fig. 6.4. P_0 divides into an anterior cell (AB) and a posterior cell (P_1). When AB starts mitosis, the mitotic spindle rotates slightly around the dorso-ventral (DV) axis of the cell to put its cleavage plane nearly perpendicular to the AP plane, in such a way that the two daughters are also anterior-posterior (Fig. 6.5). The same happens with P_1 with its two daughters occupying the space left free by the AB descendants. The AB daughters are slightly more dorsal than the P_1 daughters. When AB_a and AB_p divide at the same time, they "push" EMS and P_2 to the ventral surface of the embryo, so that the AB descendants occupy the entire dorsal surface of the embryo. By their turn, EMS divides in the AP direction and P_2 divides in the DV direction (Fig. 6.4).

Fig. 6.2: DIC images of P_0 at different stages: Left: beginning of pro-nuclei migration, being visible the pseudocleavage. Centre: instant immediately after pro-nuclei fusion. Right: instant immediate before P_0 NEBD. (Image adapted from [88, 89])

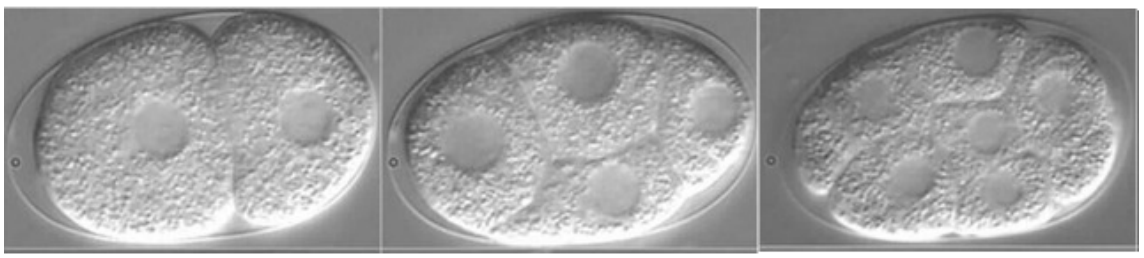

Fig. 6.3: DIC images of the 2-cell, 4-cell and 8-cell stages of the same embryo. (Image taken from [90])

Fig. 6.6 presents the E_a and E_p ingression stages during the beginning of gastrulation. From the lateral view, one MS granddaughter (referred to here as MS_{xx}) and P_4 move towards each other over the apical surfaces of E_a and E_p and flank them. These interactions result in an ingression of the two E cells to the centre of the embryo. After ingression, the flanking cells occupy almost the original positions of the E cells. From the ventral view it is seen that other cells also flank and interact with the E cells, causing their ingression.

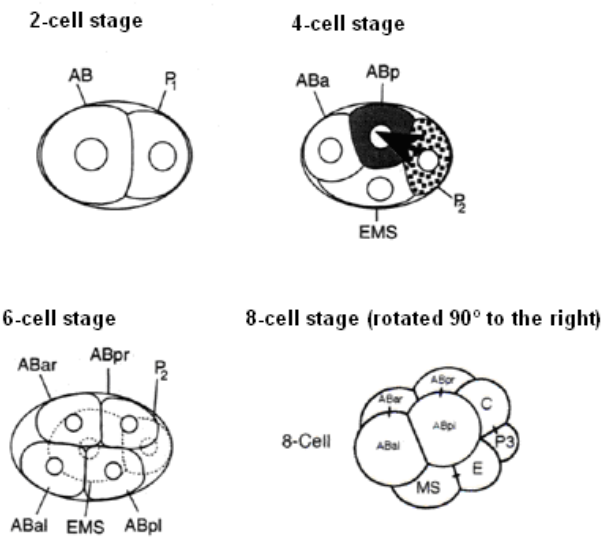

Fig. 6.4: First embryo cleavages and localization of the daughter cells. (Image adapted from [54])

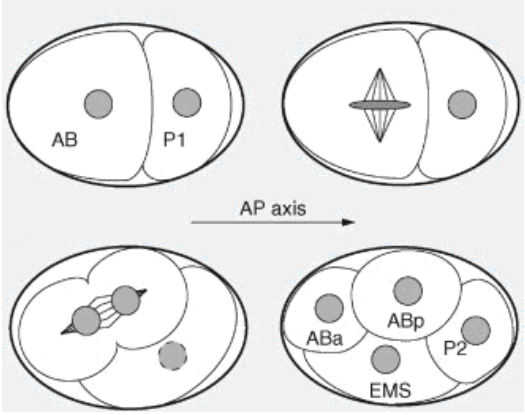

Fig. 6.5: Mitosis of AB and P_1 are accompanied by spindle rotation. This way the daughters remain oriented approximately parallel to the AP axis. (Image adapted from [91])

Fig. 6.7 shows the lime-bean stage and first fold of the embryo as they should be observed by microscopy by viewing the embryo laterally or ventrally. From the ventral view, the lime-bean shape of the embryo is not observable, but instead a constriction appears at the left and right sides of the embryo, signalling the lime-bean stage. During the first fold, that constriction becomes more accentuated.

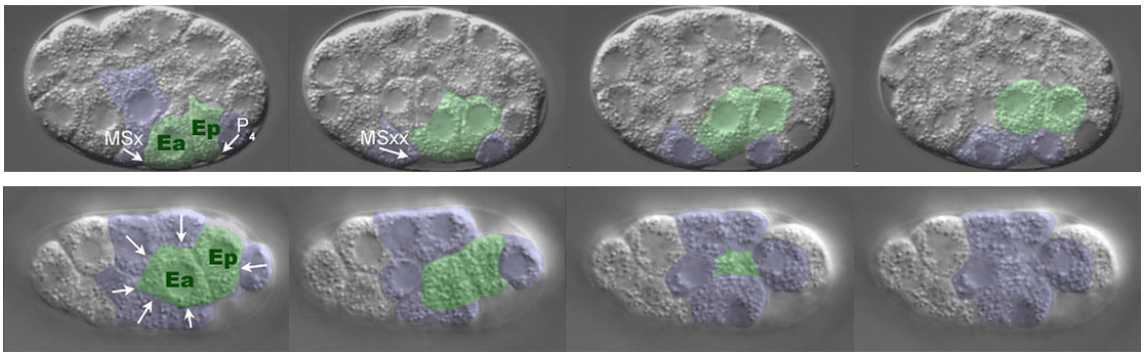

Fig. 6.6: Nomarski (DIC) time-lapse images of *C. elegans* gastrulation. E_a and E_p are pseudocoloured in green, and neighbouring cells are in blue. Arrows indicate the direction of the neighbouring cell movement. Top panel: lateral view with the P_4 and MS_{xx} labelled (MS_x is in the first image and divides between the first and second images). Bottom panel: ventral view with E_a and E_p sinking into the embryo. Embryos are oriented anterior to the left. (Image and description taken from [92])

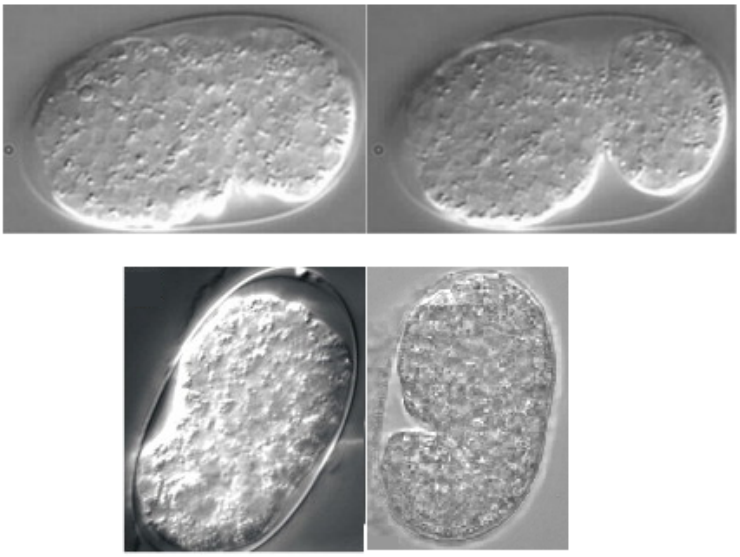

Fig. 6.7: Ventral (top) and lateral (bottom) views of the embryo at the lime-bean (left) and first comma fold (right) stages. (Image adapted from [90, 93, 94])

The start of the muscles twitches is easily identified when the embryo changes its position inside the eggshell between two time-lapse images. Finally, the embryo hatches when it breaks the eggshell and leaves the egg, letting behind a broken empty eggshell (Fig. 6.8).

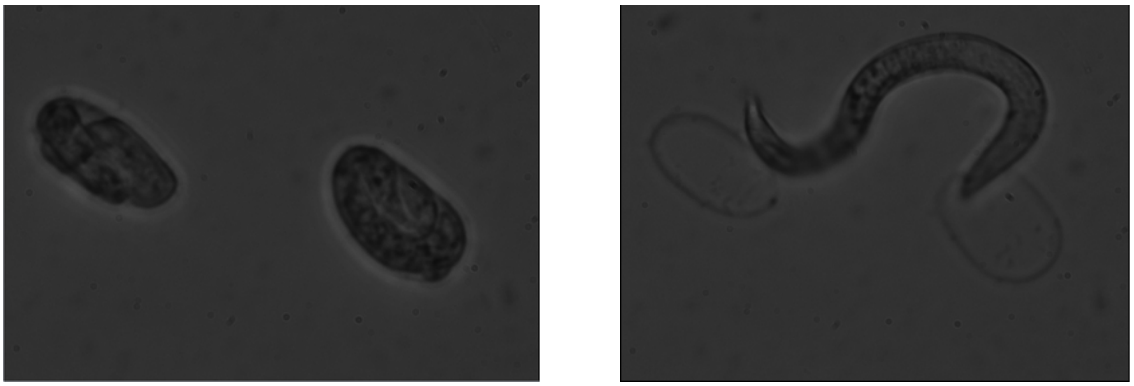

Fig. 6.8: DIC time-lapse images of two embryos before hatching (left) and after hatching (right), where the right juvenile worm is still leaving the egg. Although the images are unfocused, it is easily distinguishable the empty eggshell left after hatching.

7. Experimental Methods

7.1. Setup Preparation

Note: a detailed description of the methods presented here and of the methods to maintain the *C. elegans* culture is in Appendix D.

With the help of a microscope (*Binoculars Leica MZ6*), a 1-cell stage embryo, preferably before the pro-nuclei fusion, was selected from a dissected adult hermaphrodite (N2) *C. elegans* nematode. Then it was mouth pipetted to a small PBS drop on the top of one of the inlets of the microfluidic chip, and the drop was sucked into the channel, taking the embryo with it. The flow took the embryo into the channel till it was placed next to the pillar, where it was forced to stop since it could not go through the pillar. By this time, the sucking force on the opposite inlet was stopped and no more flow was present in the channel. Then the inlet was refilled with more PBS with the help of a syringe, with care not to let air bubbles enter into the system (Fig. 7.1).

The embryo was placed with its AP axis approximately parallel to the channel lateral walls, but since the height of the channel is superior to the embryo width, the same axis was not always parallel to the floor and roof of the channel, and was sometimes in a position slightly oblique relatively to them (Fig. 7.2).

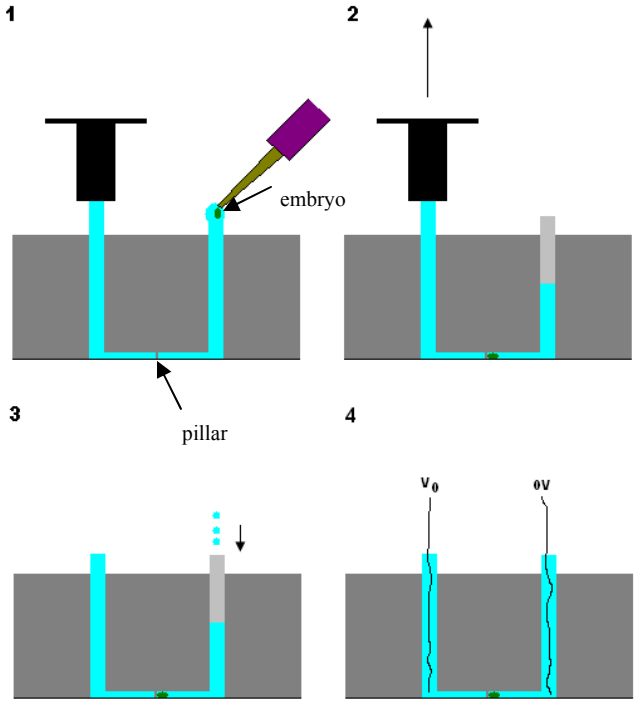

Fig. 7.1: Injection procedure. 1) The embryo is mouth pipetted to a liquid drop on the top of one inlet of the microfluidic chip already filled with PBS. 2) The drop with the embryo is sucked with the help of a syringe on the other inlet until the embryo is placed next to the pillar. 3) More liquid is injected in order to fill the inlets. 4) When the device is ready, the electrodes are inserted in the inlets and a voltage (V_0) is applied between them.

The chip was then moved do a box with a water reservoir inside (to maintain the box humid and avoid dryness of the channel), and the two platinum electrodes connected to a power generator were inserted in the inlets. The box was closed and moved to an inverted microscope (*Leica DMI 3000B* or *Leica DMIL*) already prepared. The power generator (*GW Laboratory DC Power Supply GPS-3030D*; or *Agilent HP E3631A Triple Output DC Power Supply*) was switched on and the microscope was focused at the pillar region where the embryo was. Finally, time-lapse images started to be acquired. The electric current flowing through the device was routinely monitored with an ammeter (*HP 34401A Multimeter*). In some experiments, agar salt bridges were used to avoid the contact between the electrolyte and the electrodes to avoid channel contamination, as already mentioned during the chip characterization (Fig. 7.3).

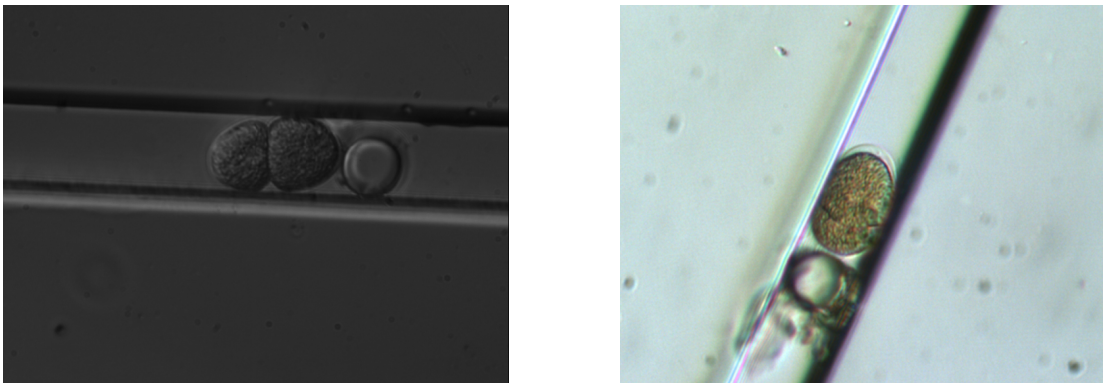

Fig. 7.2: Left: DIC image of the embryo in the correct position (psudocleavage stage). Right: Brightfield image of the 2-cell stage embryo slightly oblique in the up-down direction, resulting in part of the P_1 cell being under the AB cell.

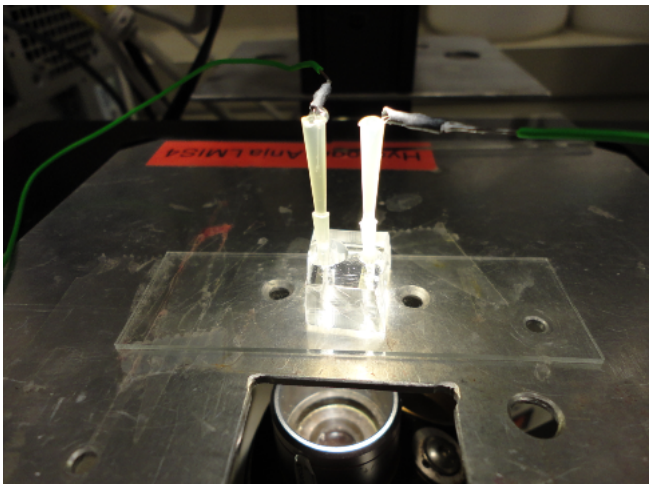

Fig. 7.3: Final setup of the system already placed at the microscope. In this experiment, salt bridges at the inlets were used to avoid channel contamination with electrode products.

For control experiments, the embryos were not transferred to the chip every time. In most cases, they were instead transferred to big PBS drops on a coverslip inside a transparent box with a water recipe inside (to maintain the box humid). This had the advantage of allowing more than one embryo to be imaged at the same time (Fig. 7.4), by transferring multiple embryos to the PBS drop and putting them together with the help of a needle. The box was then moved to the microscope and the region of the drop with the embryos was imaged.

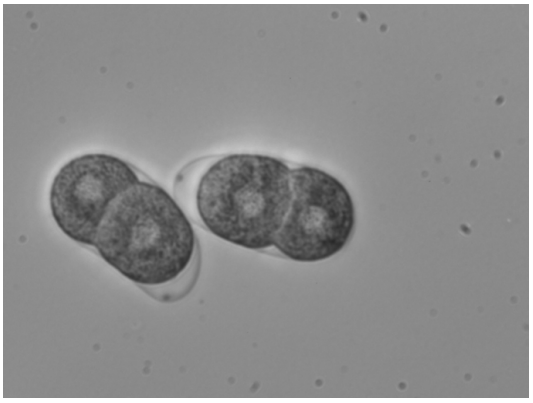

Fig. 7.4: DIC image of two embryos at the 2-cell stage in a PBS drop on a coverslip.

The applied voltage varied between different experiments. Most experiments were conducted with $V_0 = 5V$, while some of the latest experiments where conducted with 10V and 15V. In a few cases 33V were applied during only the M cell phases, since applying it continuously would kill the embryo due to the high temperature induce by Joule heating. The corresponding electric current (I) values, predicted by the system circuit model (Fig. 4.20), were respectively 2.27μA, 5.54μA, 6.81μA and 15μA. The respective average current density values are 1.14nA, 2.79nA, 3.43nA and 7.56nA; and the respective average electric field values are 0.71mV/μm, 1.73mV/μm, 2.13mV/μm and 2.69mV/μm. However, the measured current was ~ 10% smaller than what was expected by the circuit model, and also decreased with time when the agar slat bridges were used. The next day, the current was about 10% to 20% smaller than the initial value. These changes of current were neglected, since the voltage was adjusted when the current decreased and compensations were made by increasing slightly the current with antecedence when the system could not be monitored.

7.2. Data Acquisition and Analysis

Time-lapse images were acquired between every two seconds (~1200 images) for the initial development (till 8-cell stage), and between every one minute for later development (~800 images). For the initial development, the focus was continuously monitored and adjusted according to the cell wanted to visualize at a given moment, for

example, during division. Fig. 6.4 and Table 6.3 were consulted during the adjustments, to assure that the focus was at the right place at the right time. According to the position of the embryo relatively to the objective of the microscope, the cell positions could vary to the observer, which had to be in count during the observations.

Two microscopes were used (Fig. 7.5):

- *Leica DMI 3000B* equipped with DIC, and

- *Leica DM IL* equipped with phase contrast.

Although the *Leica DMI 3000B* was preferred since it was equipped with DIC, the *Leica DM IL* phase contrast also provided good quality images, suitable for the analysis (see Fig. 7.2).

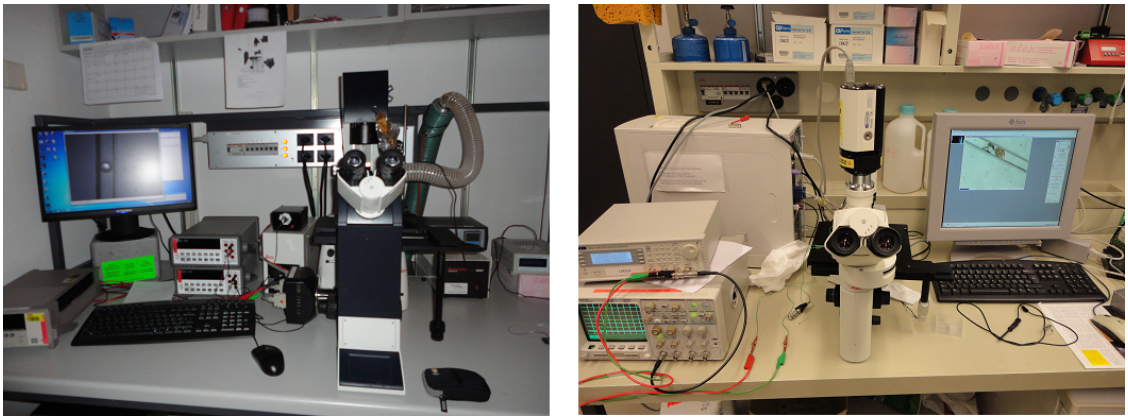

Fig. 7.5: The two microscopes used for the experiments. Left: *Leica DMI 3000B*. Right: *Leica DM IL*.

The data analysis was performed by comparing the control experiments with the experiments where the electric field was applied. For that, the image processing software *ImageJ* was used. Exactly the same criteria were used when comparing event times and cell positions between control and electric field experiments. The spatial comparison consisted in comparing cell positions and orientation relatively to other cells between control and electric field experiments. The temporal analysis consisted in comparing the selected event times between control and electric field experiments.

The time intervals between each consecutive selected event were registered in a datasheet (Datasheet 2) and from there they were statically compared by using the significance Mann-Whitney test (95% two tailed confidence interval). Comparing time differences allowed analysing between which events a particular change might occur. This way, if more than one change occurred between the control and stimulated populations, all of them could be temporally discriminated. The time differences compared were:

- $\mathbf{t_{P0} - t_{ncl}}$
- $\mathbf{t_{AB} - t_{P0}}$
- $\mathbf{t_{P1} - t_{AB}}$
- $\mathbf{t_{ABa} - t_{P1}}$
- $\mathbf{t_{EMS} - t_{ABa}}$ (AB_p divides at the same time as AB_a)
- $\mathbf{t_{P2} - t_{EMS}}$
- $\mathbf{t_{gstr} - t_{P2}}$
- $\mathbf{t_{fld} - t_{gstr}}$
- $\mathbf{t_{fld} - t_{P2}}$
- $\mathbf{t_{mov} - t_{fld}}$
- $\mathbf{t_{brn} - t_{mov}}$

The reason of using a non-parametric statistical test was its greater robustness face to parametric statistics. It does not require any assumption to be made about the population of times observed, where it is not known if the time events follow the normal distribution. Non-parametric methods are easily implementable, well perceptible and usable for small samples, and are low sensitive to measurement errors, despite having less statistical power face to parametric methods.

Cell cycles of P_0, AB and P_1 were also compared since these cells are the most susceptible of influencing all embryogenesis if their behaviour is disturbed.

Consequently, any disturbances in the cell cycle of these cells may give insight about other later disturbances in embryogenesis.

The intensity of the muscle twitches of the embryo and the movements and behaviour of the juvenile worm were also analysed, the later two only for a few experiments, since the pos-hatching part of the experiment was usually checked only the day after the experiment started and most times the juvenile worm was already dead at that time.

27 control experiments and 17 electric field experiments were conducted. However, it was not possible to observe all events and register their time for a single experiment. Consequently, different events may have a different number of observations, which must be in count during the statistical analysis. The Mann-Whitney test allows comparisons of samples with different dimensions.

8. Results

Note: all the details of the data treatment are in Datasheet 2 (files in the annex CD-ROM).

8.1. Temporal Analysis

8.1.1. Consecutive Events

Of the total 27 control experiments and 17 electric field experiments conducted, the number of observations varied for each event, being always smaller than the total number of experiments, due to the fact that, for a given experiment, not all the selected development events could be observed. Reasons that led to this were the position of the embryo in the channel, presence of dust between the embryo and the objective, or a bad focusing when the microscope was not being monitored.

Table 8.1 presents the number of observations for each of the eleven consecutive time differences used for the statistical tests. Table 8.2 presents and compares the mean time of each consecutive event analysed, for the control and electric field experiments. The comparison was done by dividing the difference between the control and electric field mean times by the control mean time, i.e. the mean time difference relatively to the control situation. Negative percentages correspond to situations where the control time is greater than the electric field time. The last column shows the Mann-Whitney test results, presenting the p-value. The details of the test are also in Datasheet 2.

Table 8.1: Number of observations of each of the eleven consecutive time differences statistically analysed (Fig. 8.2 – 8.4)

Time Difference	Control	Electric Field
t_{P0}-t_{ncl}	8	7
t_{AB}-t_{P0}	20	11
t_{P1}-t_{AB}	22	16
t_{ABa}-t_{P1}	18	15
t_{EMS}-t_{ABa}	17	15
t_{P2}-t_{EMS}	17	15
t_{gstr}-t_{P2}	17	8
t_{fld}-t_{gstr}	16	8
t_{fld}-t_{P2}	17	9
t_{mov}-t_{fld}	18	9
t_{brn}-t_{mov}	9	13

Table 8.3 presents the standard deviation of each consecutive event analysed, for the control and electric field experiments. It is given also in terms of percentage, dividing it by the mean of the same event, presented in brackets. The standard deviations were compared the same way the mean was, by dividing the difference between the control and electric field values by the control value.

Table 8.2: Temporal analysis results: Mean of the times of the events measured for control and electric field experiments; Mann-Whitney p-value for each of the eleven consecutive time differences statistically analysed

Time Difference	Control (min)	Electric Field (min)	Difference from control (%)	p-value
t_{P0}-t_{ncl}	8.32	6.86	-17.50	0.0205
t_{AB}-t_{P0}	14.86	13.14	-11.58	0.1934
t_{P1}-t_{AB}	2.29	2.24	-1.94	0.0815
t_{ABa}-t_{P1}	12.52	11.36	-9.29	0.3579
t_{EMS}-t_{ABa}	4.50	3.54	-21.37	0.0139
t_{P2}-t_{EMS}	3.33	3.72	11.66	0.1481
t_{gstr}-t_{P2}	32.37	30.95	-4.38	0.5411
t_{fld}-t_{gstr}	190.52	181.95	-4.49	0.2559
t_{fld}-t_{P2}	222.75	211.05	-5.25	0.0422
t_{mov}-t_{fld}	116.19	124.16	7.03	0.2679
t_{brn}-t_{mov}	367.92	428.97	16.43	0.2294

Table 8.3: Standard deviation of the eleven time differences for control and electric field experiments (in parenthesis is the value divided by the mean of the corresponding time event)

Time Difference	Control (min)	Electric Field (min)	Difference from control %
t_{P0}-t_{ncl}	1.47 (18%)	0.45 (7%)	-69.14
t_{AB}-t_{P0}	3.12 (21%)	1.32 (10%)	-57.61
t_{P1}-t_{AB}	0.56 (25%)	0.63 (28%)	12.70
t_{ABa}-t_{P1}	2.59 (21%)	0.78 (7%)	-70.00
t_{EMS}-t_{ABa}	1.18 (26%)	0.71 (20%)	-39.93
t_{P2}-t_{EMS}	0.67 (20%)	0.73 (19%)	8.15
t_{gstr}-t_{P2}	5.48 (17%)	4.42 (14%)	-19.28
t_{fld}-t_{gstr}	16.67 (9%)	15.37 (8%)	-7.78
t_{fld}-t_{P2}	14.71 (7%)	15.59 (7%)	5.95
t_{mov}-t_{fld}	30.62 (26%)	25.33 (20%)	-17.28
t_{brn}-t_{mov}	76.57 (21%)	136.39 (32%)	78.12

Fig. 8.1 plots the average of the times of the eleven consecutive events that participated in the statistical tests. t_{fld} - t_{P2} was not used, since that time difference is already covered by t_{gstr} - t_{P2} and t_{fld} - t_{gstr}. The graph is in logarithmic scale since the times of the later events are much higher than the times of the early events (until P_2). Each event is represented by a point matching the control mean time with the electric field mean time. Control experiments are represented by the *x* axis and electric field experiments are represented by the *y* axis.

The total average of the development time was considered as the average time from the cytokinesis of P_0 till the average time the worm hatches. For the control experiments, it is about 744min (12.4h), while for the electric field experiments it is about 798min (13.3h). The difference from the control is about 7.18%.

Fig. 8.2 compares the same results graphically but now side by side, allowing an individual event comparison, again using a logarithmic scale.

Figs. 8.3 and 8.4 separate the results for the early and latter events, avoiding the use the logarithmic scale. They amplify the comparison between the control and electric field experiments for the early and fast events and for the latter and slower events studied.

All the data may be consulted in Datasheet 2.

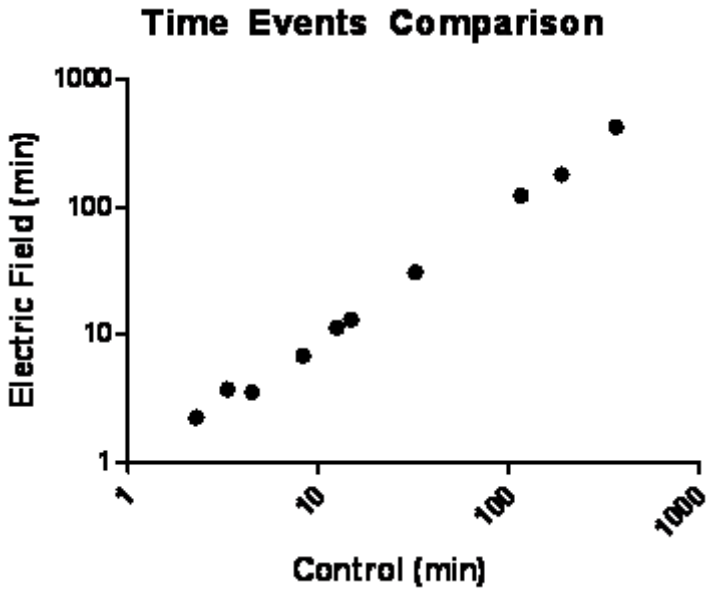

Fig. 8.1: Plot comparing the average of the control and electric field experiments temporal series. A logarithmic scale was used. From the origin to the opposite extremity, the points correspond to the following time differences: t_{P0} - t_{ncl}; t_{AB} - t_{P0}; t_{P1} - t_{AB}; t_{ABa} - t_{P1}; t_{EMS} - t_{ABa}; t_{P2} - t_{EMS}; t_{gstr} - t_{P2}; t_{fld} - t_{gstr}; t_{mov} - t_{fld}; t_{brn} - t_{mov}. Control experiments are represented by the *x* axis and electric field experiments are represented by the *y* axis.

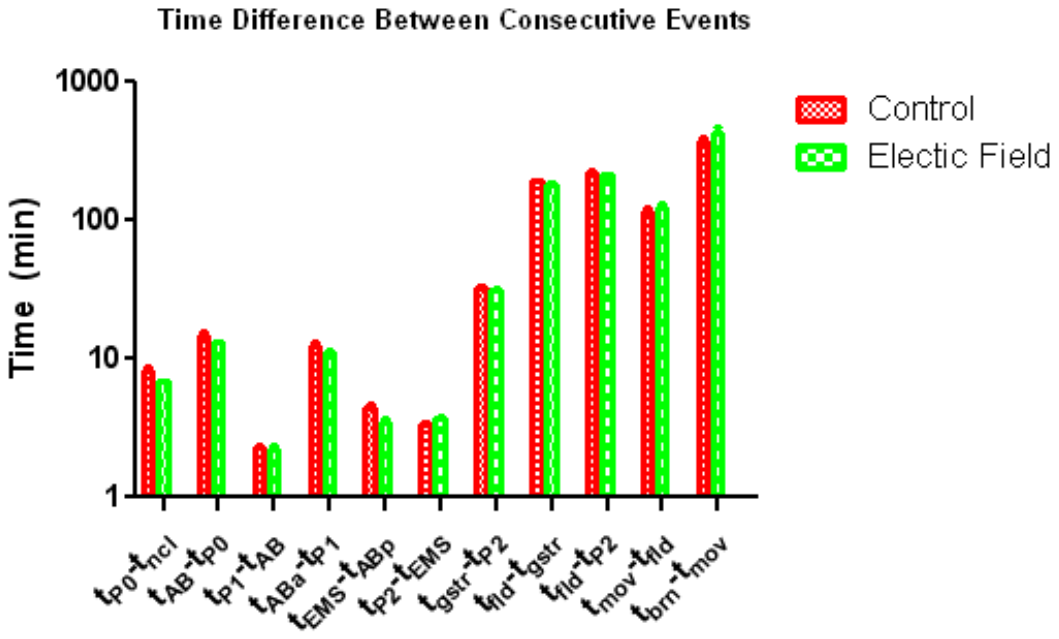

Fig. 8.2: Average of the time differences of the eleven events that were statistically analysed. A logarithmic scale was used. To compute the total average development time (since the firs cleavage), all the times must be summed. t_{P0} - t_{ncl} was not considered for this computation. The number of experiments for each event is in Table 8.1.

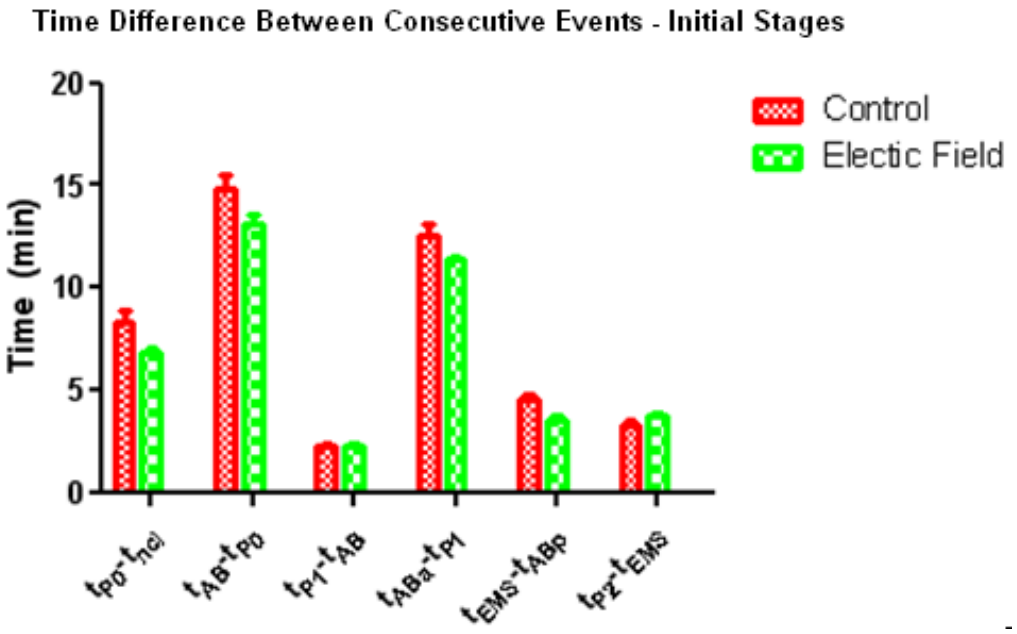

Fig. 8.3: Average of the time differences of the early events (until the division of P_2) that were statistically analysed. The number of experiments for each event is in Table 8.1.

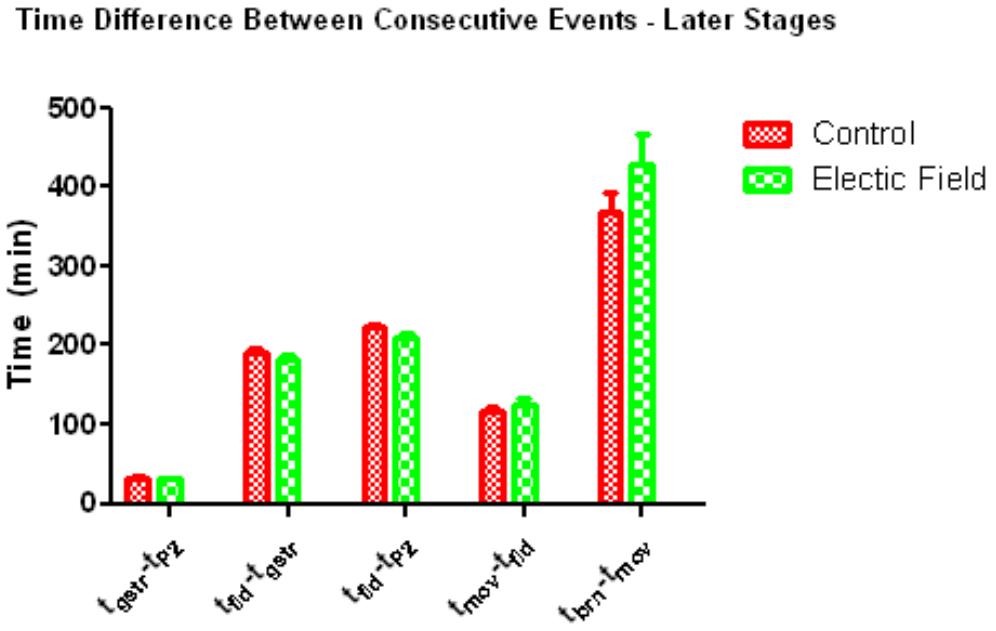

Fig. 8.4: Average of the time differences of the later events (after division of P_2) that were statistically analysed. The number of experiments for each event is in Table 8.1.

8.1.2. Cell Cycles of P_0, AB and P_1

Table 8.5 compares the cell cycle duration of the first three cells of the embryo (P_0, AB and P_1). It also splits the cycle into interphase, M-phase, separated by the NEBD. For P_0, only the cell cycle portion after at the pro-nuclei fusion was considered, since it was almost impossible to analyse this cell right after meiosis. The number of observations for these events is in Table 8.4. The data is also plotted in Fig. 8.5.

Table 8.6 compares the standard deviations of the same cell cycles. All the details are in Datasheet 2.

Table 8.4: Number of observations of the cell cycle times (Fig. 8.5)

Time Difference	Control	Electric Field
t_{P0}-t_{ncl}	8	7
t_{nP0}-t_{ncl}	8	7
t_{P0}-t_{nP0}	15	9
t_{AB}-t_{P0}	20	11
t_{nAB}-t_{P0}	19	12
t_{AB}-t_{nAB}	22	16
t_{P1}-t_{P0}	19	11
t_{nP1}-t_{P0}	18	11
t_{P1}-t_{nP1}	21	15

Table 8.5: Mean of the times of the cell cycles of the first three cells of the embryo (P_0, AB and P_1)

Time Difference	Control	Electric Field	Difference from control %
t_{P0}-t_{ncl} (P_0 Cell Cycle*)	8.32	6.86	-17.50
t_{nP0}-t_{ncl} (P_0 Interphase*)	3.29	2.80	-14.77
t_{P0}-t_{nP0} (P_0 M-phase)	4.82	4.17	-13.63
t_{AB}-t_{P0} (AB Cell Cycle)	14.86	13.14	-11.58
t_{nAB}-t_{P0} (AB Interphase)	11.25	10.00	-11.12
t_{AB}-t_{nAB} (AB M-phase)	3.61	3.28	-9.05
t_{P1}-t_{P0} (P_1 Cell Cycle)	17.26	15.33	-11.23
t_{nP1}-t_{P0} (P_1 Interphase)	14.03	12.40	-11.63
t_{P1}-t_{nP1} (P_1 M-phase)	3.37	2.96	-12.05

*for P_0 only the cell cycle portion after at the pro-nuclei fusion was considered, since it was almost impossible to analyse this cell right after meiosis.

Table 8.6: Standard deviation of the cell cycles of the first three cells of the embryo (P_0, AB and P_1) (in parenthesis is the value divided by the mean of the corresponding time event)

Time Difference	Control	Electric Field	Difference from control %
t_{P0}-t_{ncl} (P_0 Cell Cycle*)	1.47 (18%)	0.45 (7%)	-69.14
t_{nP0}-t_{ncl} (P_0 Interphase*)	0.68 (21%)	0.38 (14%)	-43.26
t_{P0}-t_{nP0} (P_0 M-phase)	1.16 (24%)	0.85 (20%)	-26.32
t_{AB}-t_{P0} (AB Cell Cycle)	3.12 (21%)	1.32 (10%)	-57.61
t_{nAB}-t_{P0} (AB Interphase)	2.51 (22%)	1.34 (13%)	-46.58
t_{AB}-t_{nAB} (AB M-phase)	0.81 (23%)	0.57 (17%)	-29.61
t_{P1}-t_{P0} (P_1 Cell Cycle)	3.63 (21%)	1.46 (10%)	-59.62
t_{nP1}-t_{P0} (P_1 Interphase)	2.70 (19%)	1.17 (9%)	-56.69
t_{P1}-t_{nP1} (P_1 M-phase)	0.96 (28%)	0.69 (23%)	-28.42

*for P_0 only the cell cycle portion after at the pro-nuclei fusion was considered, since it was almost impossible to analyse this cell right after meiosis.

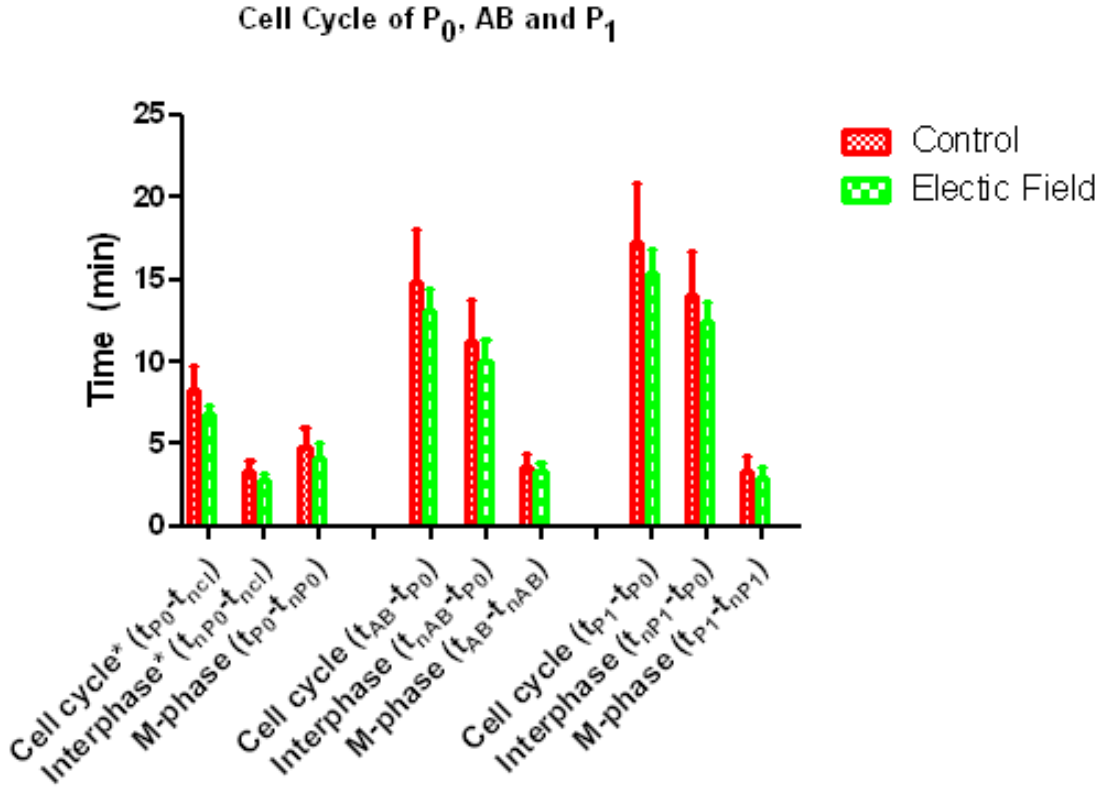

Fig. 8.5: Cell cycles of the first three cells: Interphase, M-phase and entire cell cycle. For P_0, only the Interphase after the pro-nuclei fusion was considered (*). The number of experiments for each event is in Table 8.4.

8.2. Spatial Analysis

Appendix E presents a template for the spatial analysis of the cell positions inside the eggshell, showing what is expected to be observed during each relevant stage. Only lateral views were presented, but once knowing the cell positions relatively to the others it is easy to extrapolate to other views, such as the ventral view.

No apparent differences were observed in cell positions between control and electric field experiments. All cells were approximately at the expected position at the expected time.

8.3. Other Analysis

The intensity of the movements of the embryo was not apparently different between the control and electric field experiments. However, for electric field experiments with no salt bridges used, most embryos died at the time of hatch and, in some cases, they were completely dissolved. This problem was solved after starting to use salt bridges or perfusing the channel and switching off the electric field some hours before hatch. Unfortunately this approach was used only for the last few experiments. In control experiments, the embryo only died when the PBS was almost dry, maybe due to osmotic mechanisms that dried the embryo inside the eggshell.

The worm behaviour after hatching was slightly different between control and electric field experiments. Control juveniles lived for several hours after hatching in the absence of food and moved very intensely. Juveniles of the electric field experiments lived usually for less time and the intensity of the worm movements varied between experiments. Generally, the movements were less intense (but not always) than control worms, but the channel dimensions did not allow an adequate comparison. At first sight, no deformations were found in electric field experiment worms. Since the channel restricts most of the movement of the worms, it was tried to recover the juveniles and make a culture with them, to see if they were able to reproduce. However, the worm

was lost every time during the transfer to an agar plate, since removal from the chip was extremely difficult with the available equipment.

Experiments performed with higher voltages had similar results, despite the increased stimulus intensity. In some cases, where high voltages were applied, the embryo was destroyed and collapsed due to the high temperatures. Consequently, the stimulus had to be applied discontinuously to avoid big temperature changes. It was done by applying it only during the M-phases of the first cells.

9. Discussion

9.1. Temporal Analysis

9.1.1. Mean Event Times Analysis

From the analysis of Fig. 8.2 – 8.4, it is seen that no major differences occur between control experiments and electric field experiments. The total average development time of stimulated embryos is about 7.2% longer compared to control embryos, suggesting at first sight that that the electric field may have a long term effect that retards the embryo development.

However, when observing Fig. 8.5, the cell cycles of P_0, AB and P_1 seem to be 1.5 – 2 min faster when electrically stimulated relatively to control experiments. The cell cycles are about 11%-12% shorter for AB and P_1 and between about 14% and 18% shorter for the analysed portion of the P_0 cell cycle. The M and S phases seem to be shorter in the same percentages, suggesting that the cell cycle was entirely accelerated and not just its individual phases (interphase and M-phase). The time between AB and P_1 divisions also decreased, evidencing an overall acceleration of the embryo development.

If only this data about the initial events is considered, it may be explained by the fact that, due to the Joule heating, the temperature of the channel was slightly increased during the electric field experiments, and thus accelerated these cell cycles that are sensitive to the temperature like all embryogenesis. This temperature increase was not sufficient to induce any disturbances in the development. However, the later stages of embryogenesis contradict this explanation, as will be seen below. Another explanation is the presence of chemical reaction products at the embryo region, but this is improbable, since, when not using salt bridges or perfusing the channel, the embryo developed apparently normally till the hatch time, except that it died at hatch time. As will be discussed below, it was assumed that the electrolyte contaminants only disturb the embryo at the time of hatching.

Observing again Fig. 8.2 – 8.4, it looks that the development of electrically stimulated embryos is faster only till the very last events, starting at the lime-bean stage, where the tendency inverts and the stimulated embryos develop at a slower rate, reflecting in the total development time, which is longer in electric field experiments.

From Table 8.2 and Table 8.5, it is seen that, at the beginning, embryogenesis is about 10%-20% faster for electric field experiments compared to control experiments, except between the divisions of EMS and P_2, where the time difference was about 12% greater in control experiments, and between the division of AB and P_1, where there was almost no difference. Fig. 9.1 presents a diagram comparing the times of the initial events (until the division of P_2) of control and electric field experiments, showing which events are faster or slower for each experiment.

After the division of P_2, no more times between cell divisions were measured, but instead longer times between specific events of advanced embryogenesis. Those times were only about 4%-5% shorter in electric field experiments, till the comma fold stage, where control experiments times were increasingly longer than the electric field experiments times.

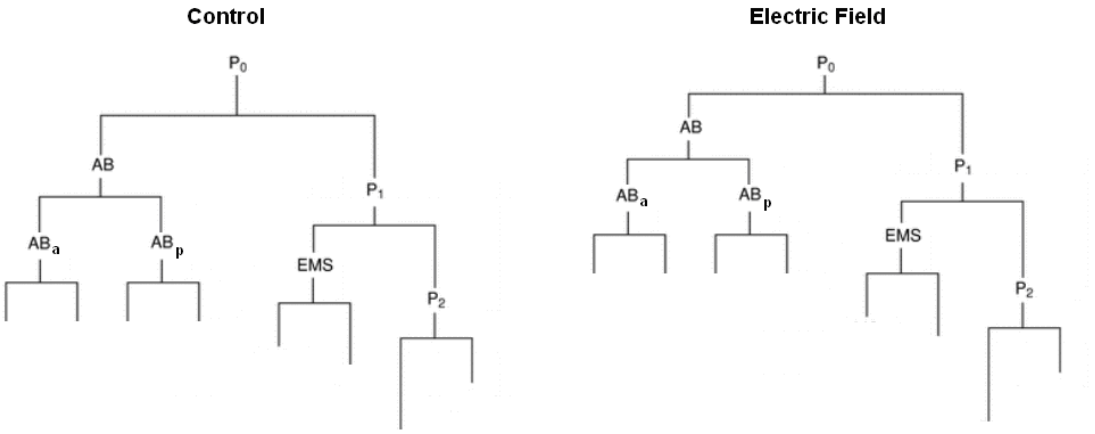

Fig. 9.1: Diagram comparing the differences in division times between control and electric field experiments, until the start of the 8-cell stage. The longer the line above the cell name, the longer is its cycle, except for P_0, were the cell cycle duration is represented by the line below the cell name (since the diagram starts there). Note: the time is not precisely scaled by the line length.

Since the temperature should be higher in electric field experiments, it can not explain why the embryo develops slower for the later stages nor the longer time difference between EMS and P_2 divisions, suggesting again that that the electric field may have a long term effect that retards, at least the later development stages and that it may be related with mechanisms occurring between the divisions of EMS and P_2. There is also the possibility that the early events are slightly accelerated by the temperature, but, due to an influence of the electric field, the later events are retarded even in the presence of a higher temperature. However, the change of total development time is small (~1h, ~7%). A difference of 1ºC in temperature is enough to induce such a change of the total embryogenesis duration and thus it would be advantageous to eliminate such temperature variations in order to have a greater certainty about how the electric field affects the embryogenesis duration.

9.1.2. Standard Deviation Analysis

From Table 8.6, the cell cycles of AB and P_1 in control experiments show more than 20% of variability (except for P_0 that is 18%), while the electric field stimulated cells show 10% or less variability. Stages of the cell cycle also have a greater variability in electric field experiments than in control ones, but the difference in variability between the two types of experiments seems to increase with the time length of the event studied, greater for interphase and entire cell cycle and smaller for the M-phase, with differences ranging between about 30% and 70% (see last column of Table 8.6). Analysing now Table 8.3, it seems the other initial events follow the same rule, except for the difference between the divisions of AB and P_1, where electric field experiments had a variability greater in about 13% compared with control experiments, and again the difference between the divisions of EMS and P_2, where electric field experiments had a variability greater in about 8%.

On the other hand, later events had more similar variabilities (differing less than 20% between control and electric field experiments), but still with the electric field stimulated embryos having a smaller variability, except for t_{brn} - t_{mov}, with a much greater variability than control embryos (~78% greater), and for t_{fld} - t_{P2}, where it is

almost 6% greater than in control embryos. This suggests whether the electric field may have an effect of reducing the variability of the embryogenesis events and also suggests that the early events may be more sensitive to external conditions, since they present the higher variability difference relatively to the control embryos.

Comparing the development speed with the variability, it seems that the initial faster developments have a greater difference in variability between control and electric field experiments, while later events have smaller differences, except for the last event that covers half of embryogenesis. Also, t_{P1} - t_{AB} is smaller in electric field experiments, while its variability is greater in those experiments, when compared to control experiments, which shows a conflict between the mean comparison and the standard deviation comparison. However, it was already stated that this event is an exception that differs only about 2% in time between the two types of experiment, compared to the other adjacent events, which differ more. Consequently, a more detailed analysis of the time lapse between AB and P_1 divisions would be a good approach for future studies.

Comparing now the standard deviation with the time difference between the events in control and electric field experiments, it is seen that in most cases, the difference between the times between the two types of experiment is smaller than the standard deviation of the event in question. This suggests that differences between the two types of experiments are hard to find, since they are concealed by the standard deviation. Consequently, in future research, it should be used a more accurate way of observing the embryogenesis events in order to minimize the most possible the standard deviation of the observations, since, according to Schnabel et al. [95], the variability of the timing of cell divisions among homologous cells in the same embryo and among different embryos is only about 10%.

9.1.3. Mann-Whitney Test Analysis

From all the eleven time differences, only three (t_{P0} - t_{ncl}, t_{EMS} - t_{ABp} and t_{fld} - t_{P2}) were significantly different according to the Mann-Whitney test since they have a p-value

smaller than 0.05. The test shows almost no significant differences between the experiments for the other events.

The first significant result was in the time of the first cell cycle, from pro-nuclei fusion till cytokinesis. It is also the time difference with the greatest difference from the mean time analysis. This event is also the most susceptible of being hit by the electric field, since it corresponds to the first cell polarization preceding the first asymmetric division of the *C. elegans* embryogenesis.

The second positive result was in the comparison between the division of EMS and AB_a. This later event did not raise any suspicion in the mean time analysis, but occurs immediately before $t_{P2} - t_{EMS}$, that is suspicious. Consequently, a detailed analysis of the cell cycle of EMS should be performed in further research.

The third significant difference was between the P_2 cytokinesis and the lime-bean stage, but not between P_2 and gastrulation, and gastrulation and the lime-bean stage, which raises the suspicion of being a false positive, since $t_{fld} - t_{P2} = t_{gstr} - t_{P2} + t_{fld} - t_{gstr}$.

Since 11 events were analysed, the Bonferroni correction should be implemented for multiple comparisons. If this correction is applied, none of the events show a significant difference between the control and electric field experiments. This puts the question whether there are really significant differences (possible if comparing only one event), or not (comparing the 11 analysed events), suggesting that the impact of the electric field on embryogenesis is very small. A greater number of observations would be advantageous in order to obtain more accurate results when comparing multiple events.

9.1.4. Other Temporal Results Analysis

Some isolate experiments manifested higher times than the expected 12h-14h of total development (16h-17h). However, this happened in both control and electric field experiments and those essays were considered as outliers, probably due to the room temperature variations at night. However, these outliers were not removed from the data analysis.

In the plot of Fig. 8.1, almost all points are in the line $y = x$, showing that the differences between the control and electric field experiments are small. Depending on the embryo position, cytokinesis may be difficult to determine exactly when occurred since the cell may be covered by other cells, relatively to the observer. Consequently, it may be hard to distinguish whether the results depend directly from the electric field, from other factors and measurement errors, or both. Therefore, a more accurate analysis should be performed in future research in order to minimize any factor that may contribute for the uncertainty of the results.

9.2. Spatial Analysis

No significant changes were observed for cell positions. Since a spatial variability is also known to occur, very small changes in cell positions were already expected. With the equipment available, it was not possible to observe those changes at the cell level. After the 8-cell stage it turned very difficult to distinguish individual cells, and only the embryo shape was observed. No significant changes were observed during gastrulation and the fold stages. All apparent changes were due to different positions of embryos relatively to the observer, from experiment to experiment. This was further increased by the fact that the embryo position changed sometimes during the same experiment due to fluid flow.

These results do not prove, however, that no spatial changes occurred between control and electric field experiments, but only that they were not observed with the available equipment. It is possible that small positional changes occurred and were not observed during the analysis.

9.3. Other Analysis

No relevant differences were detected in the intensity of embryo movements inside the eggshell between control and electric field experiments. This does not mean, however, that there were not differences in muscle twitches, but just that they were not apparent.

The juvenile worm behaviour after hatching was almost the same between control and electric field experiments. No major conclusions could be drawn form this, since in most experiments the worm was already dead when the experiment was checked the next day. However, it is to be noted that the juvenile worm movements were more vivid in control experiments when compared with electric field juveniles. Also, control juveniles seemed to live longer, staying alive for several hours after hatching even without food, what did not happen with electric field juveniles. This difference in behaviour may be due to differences in embryogenesis or due to the presence of some remains of dejects from the electrode/electrolyte chemical reactions, which were not stopped by the agar salt bridges and could damage slightly the worm. However, it was not possible to draw any major conclusion since only a few experiments were checked.

Before using the agar salt bridges, the embryo died almost every time at hatch time, probably since the high pH basic electrolyte was able to enter the eggshell after the worm started breaking it in order to come out, killing it, and, in some cases, even dissolving it entirely. This also proves that the eggshell is strong enough to protect the embryo from the contaminated electrolyte, since it developed apparently normally until the hatch time. After using salt bridges or perfusing the channel, this situation of the embryo dying at hatch time was solved, but there was still the chance that some contaminants would remain in the channel, mainly when using salt bridges, if some particles were able to bypass the agar barrier, and damage the embryo during hatching time, what even complicated the conclusions to be drawn about the behaviour of the worm after hatching.

Unfortunately, only the few last experiments were conducted using the salt bridges and perfusion techniques, which did not allow a separate statistical analysis. The results were analysed together with the other experiments, assuming that the embryo developed equally until the hatch time, using or not those techniques. Although apparently correct

from the observations and from the discussion presented in [56], there is still the possibility that this assumption is not correct and the pH changes might also contribute to alter the development times, so, for future studies, it is highly advisable to eliminate as most as possible any pH or temperature fluctuations in order to have accurate results that allow to draw elaborated conclusions. Another assumption was that the embryo immediately started dying after breaking the eggshell and entering in contact with the contaminant. If this is not true and the embryo died only some time after entering in contact with the contaminant, but still remaining in the eggshell (due to being weak to break through it), this would at least explain why the last event time is longer for the electric field experiments. Since the embryo, after breaking partially the eggshell and entering in contact with the contaminant (thus being damaged by it) remained inside the eggshell due to being weak instead of hatching, this would yield a confusion factor about the hatching time instant. The assumption about the hatching time being the same as the death time was based in the fact that the embryo moved apparently normally inside the eggshell right before dying and ceasing moving.

For higher voltage experiments, no apparent changes were observed compared to the other experiments, except that some embryos collapsed (and died) due to the greater temperatures induced by Joule heating when extreme care was not taken when switching on and off the electric field. These results suggest that the embryo is very resistant to physiological electric fields externally applied, maybe due to the eggshell.

9.4. Commentary

From the results, one may conclude that the impact of the electric field on the development of the embryo of *C. elegans* is small. It is true that errors were committed during the experiments and measurements, and also that the number of experiments is not enough to make a powerful statistical analysis. However there are some relevant differences worthy of a more detailed analysis in future research, since they may arise from the influence of the electric field on embryogenesis.

Electric field stimulated embryos develop initially faster than control embryos, which alone can be explained due to the small temperature increases of the channel medium due to the Joule heating effect, which is impossible to eliminate. A solution to this problem would be performing control experiments with a slightly greater temperature to compensate, and see if embryogenesis is accelerated the same way as in the electric field experiments. However, that would require a continuous control of the channel temperature to maintain it constant at a fixed value, what would be hard to achieve with the device used. Nevertheless, temperature control should be in count for future experiments, since the embryo development is extremely sensitive to it, and, even if disturbances do not occur, its speed will change. The final development events, on the other hand, were slower in electric field embryos than in control ones. This fact can not be explained by the temperature, once it would increase the development rate and not the contrary, as happened. This suggests that the electric field may have an influence on the embryo development, accelerating the initial events and slowing down the later events. pH changes may also influence embryogenesis, but, as explained before, it was assumed that the eggshell blocked the entry of reaction products, and thus the pH did not influence embryogenesis until the hatch time.

The difference observed between the two types of experiments is much smaller than the variability for each of them, what puts the question of the possibility to minimize the standard deviation of the observations through more accurate and precise analysis. For that, it would be necessary a greater control of the experimental conditions, such as the temperature as already mentioned, the pH, and the instant of embryogenesis when the of stimulation starts. This type of control was not possible with the available equipment. Also, more observations should allow minimizing the standard deviation, since they would reduce the influence that an outlier observation would have in the sample of observations.

The overall development time did not seem greatly affected by the electric field, differing only about 7.2% compared to the normal situation, and part of that percentage may arise from other factors other than the electric field. Together to what was discussed in the previous paragraphs, it suggests that the electric field does not have a visible significant impact in the temporal embryo development, but it does not mean that there is no impact at all, but just that it is not easily observable. In fact, the slower

development rate at later events may suggest that the electric field has a very small impact at the long term development, due to influences at the initial stages of embryogenesis. This leads again to the need of a greater control of the experimental conditions and a more accurate analysis and more observations.

Some of the development time intervals, namely the first cell cycle, time lapsed between AB and P_1 divisions and EMS cell cycle are worthy of a more detailed analysis, since they are suspicious of being different between control and electric field experiments in such a way that the temperature and observations variability cannot explain. Also, after the comma fold, embryogenesis seems to be slower, what also cannot be explained by the temperature and should be analysed with more detail. Perhaps there is a relationship between those initial events and the slower development rate at later embryogenesis.

Relatively to the cell positions and orientation in the embryo, almost no conclusions can be drawn. Spatial differences were to be expected for the first cells of the embryo, but were not observed. Whether spatial differences occurred for later events, they could not be detected with the equipment used and, even if small differences occurred, they would just provide evidence that the electric field had a very small impact on the later embryo development. If true, that impact did not avoid the embryo of hatching and behave almost normally in the perfused or salt bridged experiments.

Using higher voltages did not change any of the obtained results. This suggests that the embryo resists someway to externally applied electric fields. One explanation is the presence of the eggshell and its permeability barrier, which blocks the flow of ions to near inside it, where are the cells, thus avoiding charge accumulation on the cell membrane and consequently the change of the membrane potential. It is known that the eggshell is very resistant and impermeable to most molecules. If it blocks the passage of most ions, the electric field inside it would be extremely week to significantly charge the cell membrane and induce significant cell responses. However, only a few high voltage experiments were conducted and a statistical analysis was not performed for them.

A possible approach to solve the eggshell problem is to remove it and apply the electric field to a stripped embryo. Some publications [56] and [58] present methods to remove

the entire or portions of the eggshell, or to permeabilize it through genetic manipulation methods. However, stripped and permeabilized embryos are much more fragile and very sensitive to mechanical stresses and thus cannot be mouth pipetted. Publication [56] presents a laser treatment method to remove different eggshell layers or even the entire eggshell, but it is very complex and not a reasonable approach for this study. In addition, removing the eggshell or some layers of it induces abnormalities in embryogenesis that might conceal the effects induced by the electric field, even if known a priori. Nevertheless, there is still the possibility of removing the eggshell and collecting individual or small groups of cells to analyse how they would react when subjected to an external DC electric field. Although not allowing an entire study of embryogenesis, it would allow studying individual cells or small groups of interacting cells.

In summary, the embryo of the nematode *C. elegans* is not a good model to study the effect of DC electric fields in biological systems if precisely controlled experimental methods are not implemented and a very accurate analysis is not performed. Even if embryogenesis changes slightly due to the electric field, those changes are not easily visible to study the relationship between the DC electric field and the embryogenesis mechanisms. Therefore, a more expanded analysis should be performed, analysing more detailed events of the cell cycle instead of comparing only specific events of embryogenesis, such as cell divisions, gastrulation or embryo folds. For example, the entire cell cycle of EMS or P_0 should be carefully observed, including the localization of protein, microtubules and other cell polarizing molecules, the membrane potential, signal transduction and other detailed cellular mechanisms. It is possible that these mechanisms are related with later events and it would be interesting to match them with the mechanisms that slow down the later embryogenesis events. It is possible that everything is nothing more than just a mere coincidence and the differences are due to other factors, but there may also be an impact induced by the electric field.

Nevertheless, the *C. elegans* embryo is not as suitable for this particular kind of study as other models, such as amphibian or chick embryos, that show a much higher degree of responses to DC electric stimulation. Other alternative models that might be evaluated and used in further research are:

- Hydra,

- The squirt *Oikopleura*,
- The planarian *Schmidtea mediterranea*,
- The sea urchin *Arbacia punctulata*,
- The acoelomorpha *Symsagittifera roscoffensis*,
- The fishes *Oryzias latipes* and *Zebrafish*,
- The lancelet *Branchiostoma floridae*,
- The flatworm *Macrostomum lignano*.

Also, although not responding greatly to a DC electric field, the embryo of *C. elegans* might respond better to an AC electric field. If the eggshell also presents a capacitive effect, it would behave as an open circuit to a DC electric current after being entirely charged, assuming that it is impermeable to most ions. However, in AC circuits, RC circuits behave as filters and let pass some frequencies, perhaps allowing changing the potential inside the eggshell and maybe the membrane potential. If those frequencies are used, it would be possible to stimulate the embryo with an alternating electric field. It would an interesting approach trying to stimulate the embryo with AC electric fields in future studies, or even to try combinations of AC and DC fields.

10. Conclusion

This dissertation evaluated the impact of a DC electric field on the development of the embryo of the nematode *Caenorhabditis elegans*. This biological model was chosen due to the fact of being used in many research applications, including the study of asymmetric cell division and embryogenesis. Other embryos, such the ones of amphibians, are currently well known for being practical and efficient models to study the influence of bioelectricity in tissue development and regeneration.

The main goal of the project was to apply an electric field along AP axis of the embryo, in a similar way a temperature gradient along the same axis, known to change the embryo behaviour. The electric field would therefore induce an excess of accumulation of charge at the anterior and posterior extremities of the embryo. The main assumption was that the charge accumulation might change the polarity of the cell membrane and induce cellular responses through signal transduction and consequently affect the development of the embryo.

The electric field was applied by placing the embryo inside a microfluidic device filled with a biocompatible electrolyte (PBS) making the link between the electrodes at the channel inlets and the embryo. The embryo was fixed in the channel due to the presence of a pillar near its centre, whose dimensions were enough to block the passage of the embryo. The material of the electrodes (99.9% pure platinum) was appropriate for this application, since its high exchange current density (J_0), together with the big dimensions of the electrodes, allowed minimizing the charge transfer resistance (R_{CT}), an undesired feature in the design of electrode systems. This material also minimizes electrode/electrolyte reactions compared to other electrode materials, what was also an advantage.

The simple geometry of the channel (a parallelepiped) allowed the electric field lines to obligatorily go through the embryo or to be deflected by it in case of being insulating. The device physical characterization gave an idea of the intensity of the electric field around the embryo as well as what undesired secondary effects to the electric field application might also disturb the embryo development. The electric field and current

around the embryo were in the physiological range, being thus an appropriate stimulus to be able to change cellular behaviours, but not destroying cells and killing the embryo.

All possible measures were taken in order to minimize other physical processes that might affect embryogenesis, while maximizing the action of the electric field, in an effort to approximate the system behaviour to a simple ohmic circuit, composed by a voltage source (the electrodes) and a resistor (the electrolyte bulk resistance and the embryo resistance). Agar salt bridges were used in some experiments to avoid the direct contact between the electrodes and the electrolyte, thus decreasing the amount of chemical products from the electrode/electrolyte reactions, which were able to reach the embryo through the channel. A constant room temperature avoided major temperature changes during the about 14 hours of embryogenesis. However, it was impossible to eliminate completely temperature variations and contamination of the electrolyte with the available equipment and experimental conditions.

The embryo injection into the chip was simply done by quickly pipetting it into an electrolyte drop on one of the system inlets, and then sucking the drop into the channel till it was placed next to the pillar. Fluid flow was then suppressed so that the embryo would not move anymore, and then the electric field was applied by connecting the electrodes to a power supply. The electrical stimulation started preferentially at the beginning of embryogenesis, during the pro-nuclei migration, in order to affect a great portion of the first cell cycle and all subsequent embryogenesis stages.

The impact of the electric field was assessed by comparing control experiments, where embryos developed normally, with electric field experiments. The same criteria were used during the images analysis of both types of experiment. The comparison was based in the times of embryogenesis events, such as cell cycles and division times, and also the spatial position of cells of the embryo. Movements of the embryo in advanced development stages and the behaviour of the juvenile worm after hatching were also analysed.

The results show that the observed effect of the DC electric field on the embryo is too small to be able to draw major conclusions about its impact on the development of this particular embryo. In electric field experiments the speed of initial embryogenesis is faster than in control experiments, what alone can be explained by the effect of the

increased temperature, from to Joule heating of the electrolyte, since it is known that the *C. elegans* embryo develops faster at higher temperatures. However, it is also a fact that the electric field may have an influence on the development of the embryo, but its effect is concealed by the temperature effect. Also, for the later stages of embryogenesis, the development speed in electric field experiments decreased, contrary to the initial stages, which cannot be explained by the temperature in this case. This suggests that the electric field has a long term effect in embryogenesis.

The results also show that a more detailed analysis should be performed for the P_0 cell cycle, the time-lapse between the AB and P_1 cell divisions and the EMS cell cycle, since they presented a suspicious difference in times between the control and electric field experiments. A suggestion is to analyse with a greater detail the biological processes that occur during the cell cycle of these cells, since it is possible that the electric field induces very small changes in cellular mechanisms that are not apparently observed by just timing the cell cycles and cell positions.

The equipment used in this project did not allow to perform an analysis with big detail of cellular processes, but just to measure the time of simple cellular events, such as the interphase, M-phase and cell cycle of some of the first cells of embryogenesis, and also to observe the positions of those first cells, as well as other easily observable events, such as gastrulation or the comma fold. Since the results suggest a more detailed analysis of the cellular processes, the equipment used should allow that kind of analysis. For that, microscopes with a stronger magnification power should be used, as well as fluorescence techniques in order to target and follow particular cell components, such as specific proteins that determine cell fate (PAR complex, for example), mitotic spindles, or other susceptible of being affected by bioelectricity, since it is known that intracellular electric fields may also exist. For example, in the egg of the seaweed *fucus*, there was demonstrated the existence of transcellular currents that determine the prospective axis of germination. Those currents are caused by a stabilized separation and accumulation of cation pumps on one side of the fertilized egg and of permeability channels on the opposite side. The accompanying EF gradient was proposed to have an electrophoretic effect on the distribution of charged morphogenetic determinants within the cytoplasm [1, 96]. This way, cytoplasm flow should also be analysed, since it is known to occur in the *C. elegans* embryo, for example during the pseudocleavage [88].

Temperature and pH fluctuations, as well as the reduced number of observations are the greatest limitations of this project. A greater control of the experimental conditions would be preferred for future experiments, since undesired factors, even if minimal, can greatly influence the results. The proof is that the standard deviation of the obtained results is much higher than the variability predicted by Schnabel et al. [95]. Consequently, in order to obtain accurate results and draw elaborated conclusions, it should be a priority to minimize to the most possible any temperature fluctuations and alterations of the electrolyte composition, what could not be achieved with the available equipment.

A most accurate way of determining the exact time an embryogenesis event occurs would be also advisable, since cell positions vary more or less relatively to the observer, between the experiments, and sometimes it is difficult to determine exactly if the same criteria is being used to time a same event. For example, the completion of the cytokinesis furrow signals the end of the cell cycle, but when the two daughter cells are superposed, it is hard to determine accurately when the furrow is complete, turning it hard to apply always the same criteria when measuring the times. Another example are the different embryo positions relatively to the observer, as the AP or DV positions, that may also induce slightly involuntary changes in the analysis criteria. Increasing the number of observations would also help to minimize this criteria issue.

A particular factor suspected for minimizing the impact of the electric field on embryogenesis is the action of the eggshell and its permeability barrier. Removing this eggshell could provide a great advantage in applying the electric field to the embryo, since more ions would be able to flow into its cells. Although removing it may compromise normal embryogenesis, this option should not be discarded, since there is yet the possibility to compare embryogenesis processes with and without the electric field, even if the overall embryogenesis is disturbed; or to collect single cells or small groups of cells that could be solely subjected to the influence of the DC electric field and analysed individually. In addition, a recent investigation, [61], provides a new view for the *C. elegans* eggshell, which opens the possibility of the development of new methods of manipulating its structure and function.

In summary, there is not a great impact of the DC electric field on the development of the embryo of *C. elegans*, when comparing it to other embryos, such the ones of

amphibians. However, it must not be discarded the hypothesis of existing an impact at all, but just that a more precise and detailed analysis should be performed. The results show that some stages of embryogenesis need an analysis with a great detail, and that the removal of the eggshell could be a considerable help for future similar research. Also, the hypothesis of trying to use AC electric fields in future research about the impact of bioelectricity on the development of the embryo of the nematode *C. elegans* should still be considered. *C. elegans* is one of the most used biological models and several methods may be in development to facilitate new ways of manipulating it, and who knows, to allow a better stimulation of its embryo with bioelectricity. Alternatively, other models may be used to evaluate the impact of DC electric fields in tissue development. Depending on the application, a particular model may be advantageous to use face to other models.

Appendix A – Materials Used

Chip Microfabrication

- Latex gloves
- System SU8 master previously treated with trichloro(1H,1H,2H,2H-perfluorooctyl)silane (Sigma-Aldrich 448931) to turn it hydrophobic
- Small square or rectangular box
- Silicon elastomer: base + curing agent (Dow Corning , Sylgard 184 silicon elastomer kit)
- Box for elastomer
- Pasteur pipettes
- Precision balance (PB3002-S FACT Seven Easy, Mettler Toledo)
- Desiccator
- Oven (Heraeus-Sorvall, Kendro)
- Material to cut (scalpel or cutter)
- Coverglass or coverslip
- Pen to punch holes PDMS (1.5mm or 1.25mm diameter)
- Plasma bath machine (Diener Electronic, Femto)

Agar Plates Preparation

- Reagents:
    - Distilled water – H_2O
    - Ethanol – EtOH
    - Calcium chloride – $CaCl_2$ – (Sigma-Aldrich C1016)

  - Magnesium sulphate– $MgSO_4$ – (Sigma-Aldrich M7506)
  - Cholesterol (Sigma-Aldrich C75209)
  - Peptone (Sigma-Aldrich 70173)
  - Glycerol (Sigma-Aldrich G9012)
  - Luria Broth (Miller) – LM – (Sigma-Aldrich L2542)
  - Sodium chloride – NaCl – (Fluka 71378)
  - Dipotassium hydrogenphosphate – K_2HPO_4 – (Fluka 60355)
  - Potassium dihydrogen phosphate – KH_2PO_4 – (Fluka 60230)
  - Sodium phosphate dibasic – Na_2HPO_4 – (Fluka 71642)
  - Agar (Fluka 05040)

- Spatula
- Clock glass
- Precision balance (PB3002-S FACT Seven Easy, Mettler Toledo)
- Volumetric flasks (different volumes)
- Glass bottles (different volumes between 200mL, and 1L)
- Ultrasound mixer (Elma Transsonic TI-H-10) or magnetic mixer (Variomag Electronicrührer Compact HP1)
- Autoclave machine (Systec DB-45)
- Petri plates
- Wet bench (Skan AG)
- Escherichia coli colony (OP50)
- Automatic pipette (Biohit Proline for small quantities; battery powered pipette controller (1-100 mL), Pipetboy acu, IBS, for great quantities)
- Falcon tubes (2mL and 50mL)
- Fridge (-4ºC)
- Freezer (-18ºC)
- Parafilm (Parafilm M Laboratory Film, 4in width)

C. elegans Culture

- Prepared agar plates
- *C. elegans* hermaphrodite adult N2 individual (for the first culture) or old *C. elegans* culture
- Toothpick
- Parafilm (Parafilm M Laboratory Film, 4in width)

System Characterization and Mounting

- Microsystems design software CleWin 4.3
- Microfluidic chip
- Platinum wire (electrodes) (0.3mm diameter)
- Rigid plastic tubes (1.5mm diameter)
- Pipette tips
- Agar solution 0.1%
- Microwave and oven
- Plastic syringe
- Needles for syringe
- Glass syringe (Mikroliter Spritzer, ILS 250 μL)
- Phosphate buffered saline (PBS)
- Conductivity meter (S30 Seven Easy, Mettler Toledo)
- Electric connectors and cables
- DC generator (two models were used: GW Laboratory DC Power Supply GPS-3030D; Agilent (HP) E3631A Triple Output DC Power Supply)
- Multimeter (HP 34401A Multimeter)
- Current amplifier (Stanford SR570)

- Impedance spectromer (two models were used: Agilent 4294 A and Agilent 4284 A)
- MATLAB R2010a
- Binoculars (Leica MZ6)
- Phenol red solution
- *C. elegans* embryo (see next section)
- Software to perform mathematical computations (Microsoft Excel)

System Simulation

- Microsystems design software CleWin 4.3
- Finite element method software COMSOL Multiphysics 3.5

Experiments with Embryo and Data Processing

- Binoculars (Leica MZ6)
- Already mounted system (including the necessary materials, such as the electrodes, power supply, etc, see section before)
- *C. elegans* culture (reproducing)
- Tweezers
- Clock glass
- PBS
- Needle or scalpel
- Mouth pipette (Sigma-Aldrich A5177-5EA)
- Transparent glue tape
- Transparent box

- Cover glass
- Coverslip
- Inverted microscope (two models were used: Leica DMI 3000B equipped with RT Monochrome SPOT camera (Laboratory Instruments); Leica DMIL equipped with Q-Imaging QICAM camera)
- Software of image acquisition (two software were used, one for each camera model used: Micro Manager 1.3; Q-Capture Pro 6.0)
- Software for image processing and analysis (ImageJ 1.45s)
- Software for statistical analysis (Microsoft Excel and GraphPadPrism 5)

System Cleaning

- Lab cleaning napkins
- Isopropanol
- Dish washing soap
- Tap water

Relevant Material Properties

- PBS measured resistivity (ρ_{PBS}) – 62.10×10^{-2} Ω.m at 22ºC (from S30 Seven Easy, Mettler Toledo)
- Platinum resistivity (ρ_{Pt}) – 105×10^{-9} Ω.m (Taken from [97])
- PDMS properties (Taken from [78]):
  - PDMS resistivity (ρ_{PDMS}) – 4×10^{13} Ω.m
  - PDMS thermal conductivity (k_{PDMS}) – 0.15 W/m K
  - PDMS specific heat at constant pressure (C_{pPDMS}) – 1.46 kJ/kg K

Appendix B – Simulation Details

Note: Check the file "contants.txt" to consult the parameters used for the simulations. In the constants file, the only changeable parameter is V_0.

2D Simulation – Empty Channel, Default Model

File: "2D Channel (standard model).mph"

In this simulation, the system is empty (no embryo) and the channel is filled with PBS. The two platinum electrodes are inserted in the inlets and the input voltage (V_0) is applied at a point at the centre of the electrodes. The channel walls are electrically insulating, but can transfer heat. The interface between the channel medium and the pillar and electrodes was set to the condition boundary of continuity. The pillar and the channel walls are made of PDMS. The height of the channel is 41µm. A height of 41µm was chosen for all the structures based on the channel height (this parameter is needed for 2D simulations to find the cross sectional area necessary to compute the current density). The external temperature is 24ºC.

The heat transfer coefficient of the channel walls was calculated from the thermal conductivity divided by the thickness of the channel PDMS wall. Assuming the base of the chip as a 1cm × 1cm square, the thickness was assumed 1mm for the external walls of the inlets (because they are near the lateral surfaces of the chip) and 5mm for all the other walls (the central channel is far away from the chip lateral surface).

All the simulations were performed considering an external temperature of 24ºC. The applied voltage (V_0) varied between 1V and 15V.

Geometry

The geometric structures of the model were designed with the most possible fidelity to the *ClenWin* design. For design simplicity, the channel was centred at the middle of the *x* axis (*x = 0µm*) and *y* axis (*y = 0µm*). This way, the channel starts at about *x = -3.5mm* and ends at about *x = 3.5mm*. It was drawn from a rectangle centred at the origin (*x = 0* and *y = 0*), with length 6870µm (from *x = -3435µm* to *x = 3435µm*) (Fig. B.1). From *x = -3435µm* to *x = 365µm*, the channel has a width of 50µm (from *y = -25µm* to *y = 25µm*), corresponding to segment 1. Between *x = 365µm* and *x = 1435µm* the channel has a width of 40µm (from *y = -20µm* to *y = 20µm*), corresponding to segments 2 and 2'. Between *x = 1435µm* and *x = 3435µm*, the channel has again a width of *x = 50µm*, corresponding to segment 1'. The pillar is a circle of 10µm radius centred at *x = 525µm* and *y = 0* (Fig. B.2).

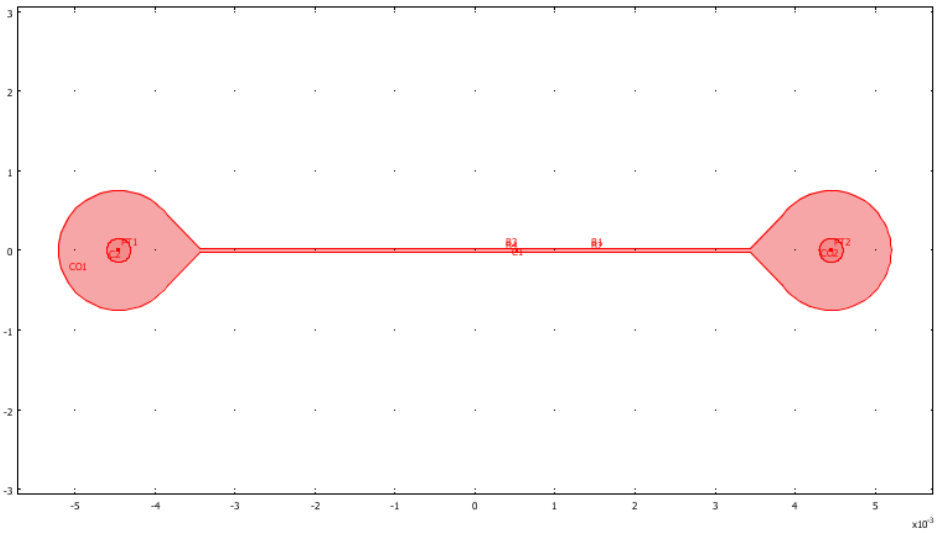

Fig. B.1: Geometry design overview for the 2D simulation, default model. The coordinate axes are in 10^{-3}m.

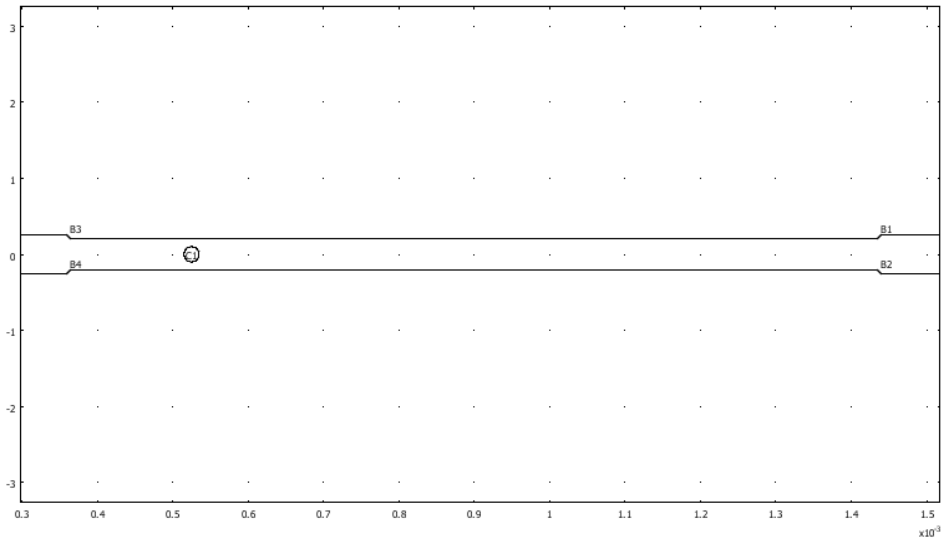

Fig. B.2: Geometry design zoomed at segments 2/2', default model. The coordinate axes are in 10^{-3}m.

The inlets are adapted from a circle of 1.5mm diameter (0.75mm radius) centred at $x = -445\mu m$ and $y = 0$ and at $x = 445\mu m$ and $y = 0$. They are connected to the channel by a mouth made manually with triangles. Each electrode is a circle of radius 150µm centred at $x = -445\mu m$ and $y = 0$ and at $x = 445\mu m$ and $y = 0$. At the centre each electrode is defined a point where the input voltage (V_0) will be applied (Fig. B.3).

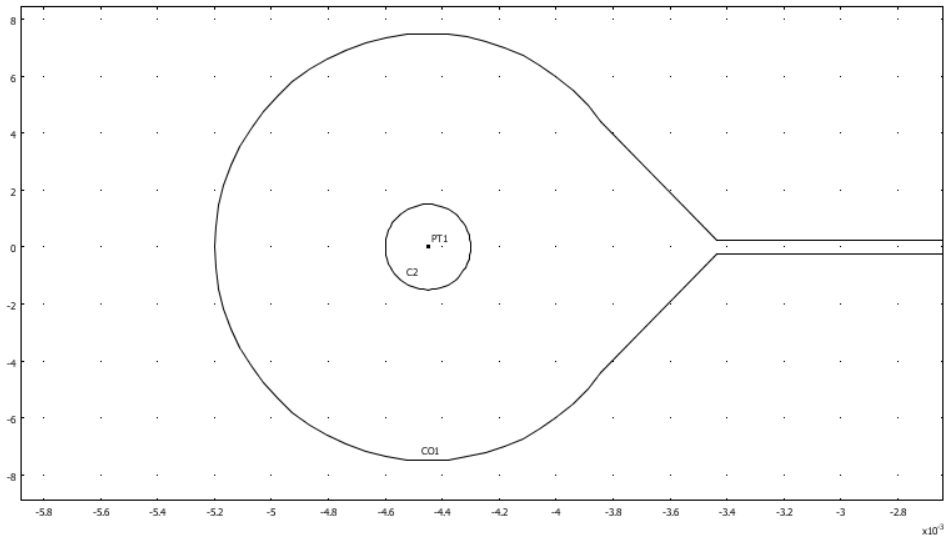

Fig. B.3: Geometry design zoomed at left inlet, default model. The left semi-circumference corresponds to the inlet back walls. The coordinate axes are in 10^{-3}m.

Physical Settings for the *Conductive Media DC Module*

Note: The settings referred here are only the ones changed from their default values.

Subdomain Settings

- Channel height: $d = 41\mu m$ (constants file)
- Channel conductivity*: $\sigma_{PBS} = 1.601\ S/m$ (constants file)
- Electrodes conductivity*: $\sigma_{Pt} = 9.524\ E6\ S/m$ (constants file)
- Pillar conductivity*: $\sigma_{PDMS} = 2.5 \times 10^{12}\ S/m$ (constants file)

(* conductivities taken from Appendix A)

There are no initial conditions.

Boundary Settings

Note: external boundaries correspond to the channel walls and internal boundaries correspond to the pillar/channel medium and electrode/channel medium interfaces.

- Boundaries with the exterior: Electric insulation
- Internal boundaries: Continuity

Point Settings

Only two points were changed: the point at the centre of the left inlet was set with V_0 and the point at centre of the right inlet was set with 0V.

Physical Settings for the *General Heat Transfer Module*

Subdomain Settings

- Platinum thermal properties taken from the built-in materials library of COMSOL - material chosen: platinum in solid state)
- PBS properties taken from the built-in materials library of COMSOL - material chosen: water in liquid state (since PBS is an aqueous solution and the ions present almost do not affect the thermal properties)
- PDMS properties (taken from Appendix A):
    - PDMS thermal conductivity: $k = 0.15\ W/(m.K)$ (constants file)
    - PDMS density: $\rho = 0.97\ kg/m^3$ (constants file)
    - PDMS heat capacity: $C_p = 1460\ J/(kg.K)$ (constants file)
- Heat source (Q): computed by COMSOL from the coupling of the *Conductive Media DC Module* and *General Heat Transfer Module*

Initial conditions

- Initial temperature: $T_i = 24ºC = 297.15\ ºK$

Boundary Settings

Note: external boundaries correspond to the channel walls and internal boundaries correspond to the pillar/channel medium and electrode/channel medium interfaces.

- Boundaries with the exterior: Heat flux
    - Material: silicon:
    - Heat transfer coefficient: $0.15/wall\_width\ W/(m^2.K)$ (where $wall\_width = 1cm$ (*w1* in constants file) for the inlet back walls (turned to the chip surface, Fig. B.1 and Fig. B.3) and $wall\_width = 5cm$ for the other walls of the system (*w2* in constants file). The heat transfer coefficient was calculated dividing the PDMS thermal conductivity by the wall width.
    - External temperature: $T_{ext} = 24ºC = 297.15\ ºK$ (constants file)

- Internal boundaries: Continuity
    - Material chosen: silicon for the pillar and platinum for the electrodes

Mesh

The model was meshed with the default mesh settings and the mesh was refined once.

Solution

The model was solved with the default settings.

Postprocessing

The simulation results were analysed by computing the electric field and current density values by clicking in the region of the channel wanted to compute. The chosen unit was A/m^2 for the current density and mV/µm for the electric field. The regions chosen for the measurements were the middle of segments 1/1' and 2/2' where the values

computed were almost equal to the average values for the entire segment. The following coordinates were chosen to compute the current density, electric field and temperature:

- Current density and electric field at segments:
  - Segment 1/1': $x = -300\mu m$, $y = 0$
  - Segment 2/2': $x = 90\mu m$, $y = 0$
- Temperature and electric field at the embryo region: $x = 57\mu m$, $y = 0$

2D Simulation – Empty Channel, Modified Device

File: "2D Channel with near electrodes (modified system).mph"

The model is almost unchanged relatively to the default model. Only the geometry was slightly changed. Two new inlets with 1.25mm diameter were drawn manually at about the interface between segments 1 and 2 or 1 and 2'. The exact position was not geometrically controlled, but only visually, to mimic the experimental situation. The electrodes, along with their central point where the input voltage was set, were moved to about the centre of the new inlets (Fig. B.4). The position of the new inlets has no influence in the direction of either the electric current or the electrolyte flow since the original inlets are not connected to the exterior and thus are a dead end for the propagation of the current and fluid flow.

The physical conditions of the new inlets are the same as the original inlets, except that for the boundary settings for the heat transfer coefficient it was assumed a wall 5cm thick (w2), since the inlet is at the centre of the system, and thus far away from the external lateral surfaces.

The mesh settings, solution settings and postprocessing remained unchanged.

The applied voltage (V_0) varied between 1V and 5V.

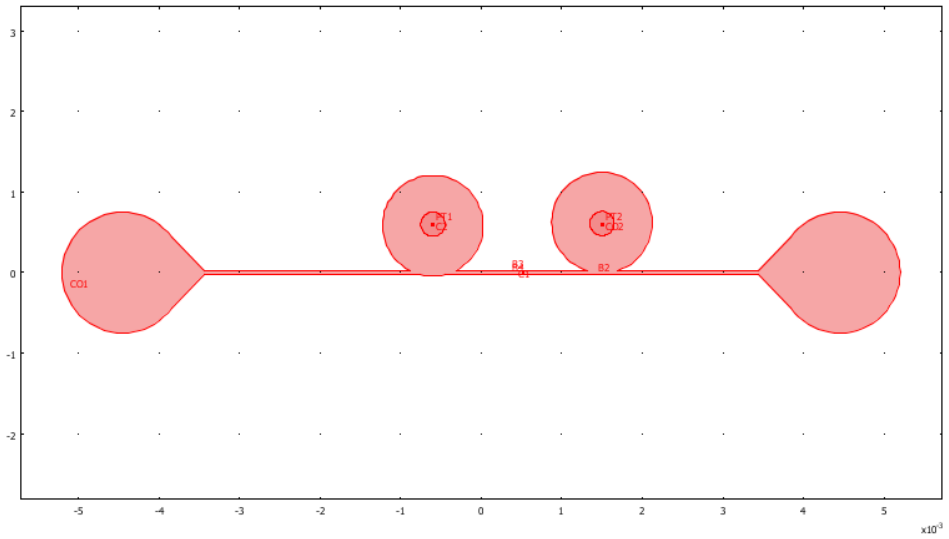

Fig. B.4: Geometry design overview for the 2D simulation, modified device model. The coordinate axes are in 10^{-3}m.

2D Simulation – Channel with Embryo

File: "2D Channel with embryo.mph"

Model unchanged relatively to the default model, except that the embryo was inserted next to the pillar, at its right (Fig. B.5). The embryo is an ellipse with semiaxis 15µm × 25µm (the embryo dimensions are 30µm × 30µm × 60µm), centred at $x = 565\mu m$ and $y = 0$. An external ellipse centred at the same point, but 0.4µm outside the first ellipse was designed to simulate the embryo eggshell, but was not used and considered as part of a homogeneous embryo.

The relevant physical conditions of the embryo (the same for the eggshell) are the electric conductivity and boundary conditions. The boundary conditions were set to "Continuity", since the embryo is an internal structure. The conductivity, *ci*, taken from [77], is 200Ω.cm.

The mesh settings, solution settings and postprocessing remained unchanged, except that for this case, no temperature analysis was done.

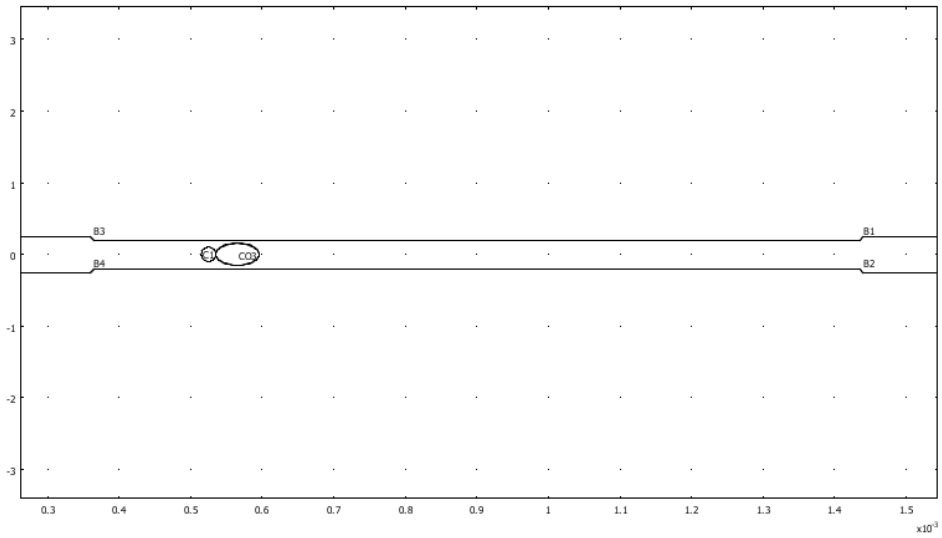

Fig. B.5: Geometry design zoomed at segments 2/2', with embryo model. The coordinate axes are in 10^{-3}m.

3D Simulation – Empty Channel

File: "3D Channel.mph"

The geometry of the 3D simulation was built starting from the 2D geometry model and extruding it for a height of 41µm. The inlets and electrodes were extruded for 7mm to create the vertical pathways connecting the system to the exterior where the electrodes are inserted. Thus, the default model was extruded to 3D, by extruding the inlets and corresponding electrodes by a height $z = 7mm$ (Fig. B.6), and the channel and pillar by a height $z = 41\mu m$ (Fig. B.7).

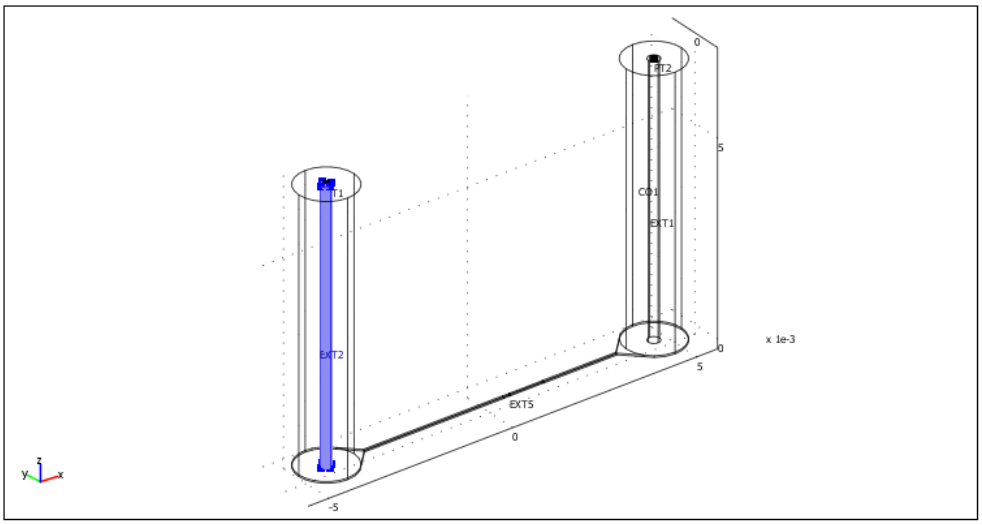

Fig. B.6: Geometry design overview for the 3D simulation, 3D model. The coordinate axes are in 10^{-3}m.

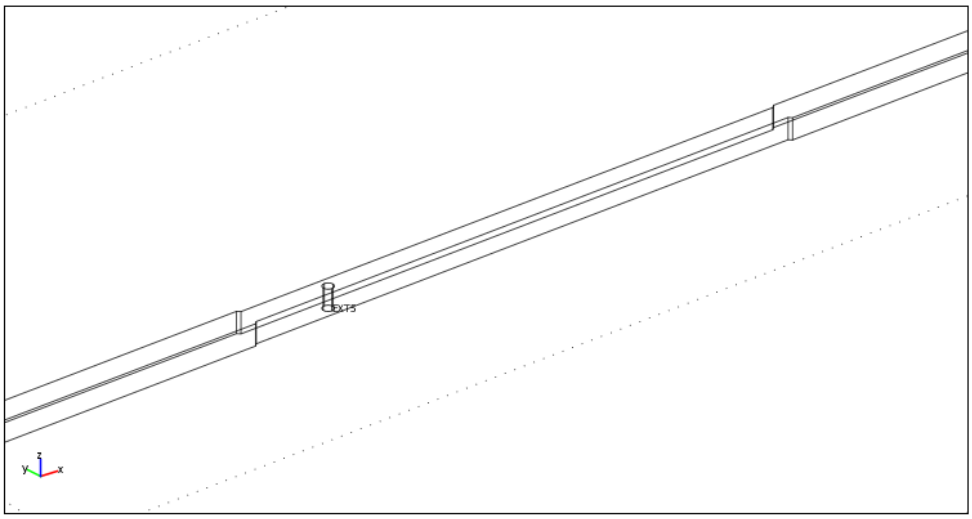

Fig. B.7: Geometry design zoomed at segments 2/2' with the pillar now as a cylinder, 3D model.

The input voltage was set at the central point, now located at the centre of the cross section of the top of one of the electrodes. The point was set at (*x = -445µm*, *y=0* and *z = 7mm*).

The physical conditions, the mesh settings, solution settings and postprocessing remained unchanged, except that for this case, no temperature analysis was done.

The values of the current density and electric field were extracted the same way as for the 2D case, with the difference that a z coordinate had also to be specified. It was chosen near the middle of the cross section of the segment measured, at $z = 20\mu m$.

Appendix C – *C. elegans* Embryogenesis Details

First Cleavage Divisions

After fertilization, the embryo is composed only by one zygote (egg) cell P_0, which starts dividing asymmetrically by mitosis. In *C. elegans*, all embryonic cell divisions are cleavage divisions[5]. The early mitotic divisions occur rapidly, with cell cycles completed in less than 20 min [52]. The divisions do not involve cell growth and the cell volumes decrease during each division, as cytoplasm is distributed between the daughter cells. The earliest embryonic cell divisions contain only S phase and mitosis [49].

The events happening before the end of meiosis II will not be described here, but detailed descriptions about the oocyte to embryo transition can be found at [98, 99]. Briefly, the oocyte to embryo transition refers to the process whereby a fully grown, relatively quiescent oocyte undergoes maturation, fertilization, and is converted into a developmentally active embryo that starts dividing by mitosis. This transition occurs very rapidly in *C. elegans*, with a fertilization of a new oocyte occurring every 23min and the first mitotic division occurring 45min later [100].

After meiosis II, the zygote P_0 divides asymmetrically into a larger anterior blastomere (AB) and a smaller posterior blastomere (P_1). This division is common for all nematodes. AB is the stem cell for the primary ectoderm. In turn, P_1 undergoes another asymmetric division that yields EMS and P_2. Further asymmetric divisions of EMS into MS and E, of P_2 into C and P_3, and then of P_3 into D and P_4, complete a generation of six founder cells (AB, MS, E, C, D and P_4) whose descendants each produce a specific subset of cell types [54] (Fig. C.1 a). EMS is the precursor of the endoderm, mesoderm,

[5] Cleavage is the division of cells in the early embryo, where the zygote and their descendants undergo rapid cell cycles with no significant growth, producing a cluster of cells that, together, have the same size of the original zygote. Each cleavage division produces two cells that are smaller than the original cell. The different cells derived from cleavage are called blastomeres. Cleavage ends with the formation of the blastula [101].

and stomodeum. It divides into separate stem cells for the endoderm (E) and mesoderm and stomodeum (MS). C and D are respectively the stem cells for secondary ectoderm and secondary mesoderm. P_4 is the progenitor of the entire germline and the only lineage that does not end in somatic cells [102]. All six stem cells and their daughters divide equally and synchronously a number of times. However, the offspring of each stem cell divide at a different characteristic rate (Fig. C.1 b), i.e. the number of successive equal cell divisions is different for the various stem cell lineages [53].

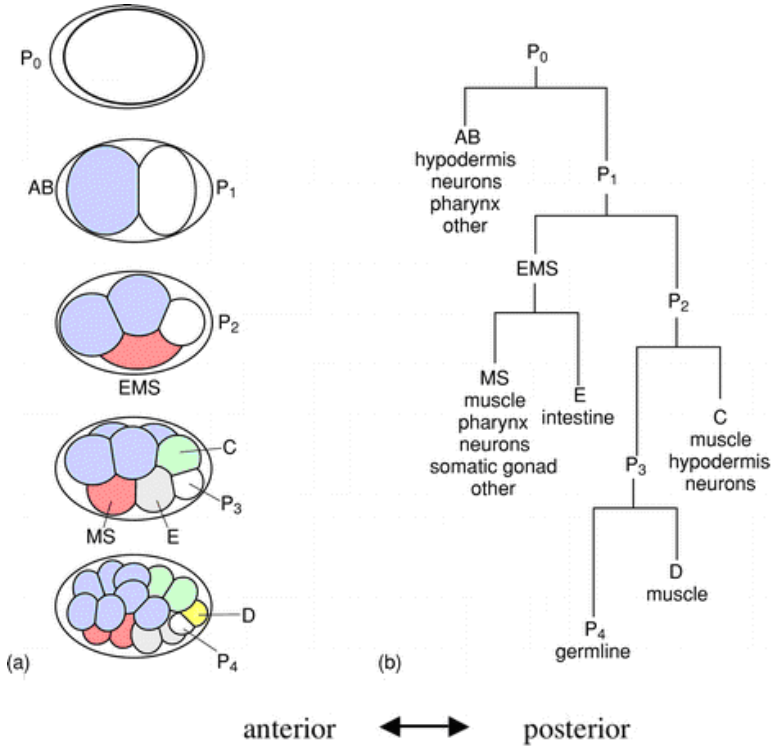

Fig. C.1: Initial development cell tree. Asymmetric cell divisions produce blastomeres with distinct fates. Posterior is to the right. (a) The invariant division pattern leads to a precise arrangement of cells and the birth of six founder cells. The founder cells and the germline precursor cells (P cells) are labelled, and cells derived from each founder are indicated by shading. For simplicity, the 16-cell embryo at bottom does not show the daughter cells of the fourth AB cleavage, which occurs at about the same time as the P_3 division. (b) Diagrammatic representation of the early lineage, showing the major cell types produced by each founder cell. Horizontal lines indicate cell divisions, and the lengths of the vertical lines indicate relative differences in cell cycle rates of each blastomere. (Image and description taken from [103])

The worm community adopted a nomenclature, adapted from the postembryonic lineage, to name all the cells of the embryo [53]. Stem cells are named with uppercase letters according to their group of destiny: AB (ectoderm); C (secondary ectoderm); D

(secondary mesoderm); E (endoderm); MS, (mesoderm and stomodeum); P_4 (primordial germ cell). Stem cell daughters are named by adding a period and one lowercase letter per division. This letter represents its position immediately after division relative to its sister cell. Anterior-posterior sisters are designated by "a" and "p"; dorsal-ventral by "d" and "v"; and left-right by "l" and "r". In oblique divisions only the predominant axis is indicated. Lineage tree branches are labelled by the same letters: the "a", "d", or "1" sister is always put on the left branch and the “p”, “v” or “r” sister is put on the right branch (Fig. C.1 b). Two letters are allowed for oblique divisions.

First Cell Cycle

The first cell cycle of the embryo of *C. elegans* is an important model to study asymmetric division. Thanks to genetic manipulation, some of the polarization mechanisms are already well understood and can be reviewed at [6, 49, 50, 104, 105].

After the completion of the two meiotic events of P_0, the maternal pro-nucleus (o) migrates from the anterior part of the zygote in direction to the paternal pro-nucleus (s), located in the posterior of the embryo. During this period, the DNA of the two pro-nuclei is replicated to generate sister chromatids, increasing the ploidy from 1n to 2n [49]. Initially, the oocyte pro-nucleus moves at a slow rate. As it approaches the sperm pro-nucleus, it accelerates, moving about 5 to 10 times its initial speed. The sperm pro-nucleus begins its migration later than its female counterpart and travels at a slow rate till it meets the oocyte pro-nucleus near the embryo centre. When the maternal and paternal pro-nuclei meet, they move towards the centre of the zygote and enter the first mitosis (Fig. C.2 A, B and C) [105].

After the pro-nuclei meet, the nuclear centrossome complex moves to the centre of the embryo and rotates to align with the long (AP) axis of the embryo. The mitotic spindle begins to move towards the embryo posterior during metaphase and asymmetric elongation during anaphase contributes to its posterior displacement. Since the cleavage furrow bisects the mitotic spindle, this displacement results in an asymmetric first cleavage (Fig. C.2 C, D and E, Fig. C.3) [105].

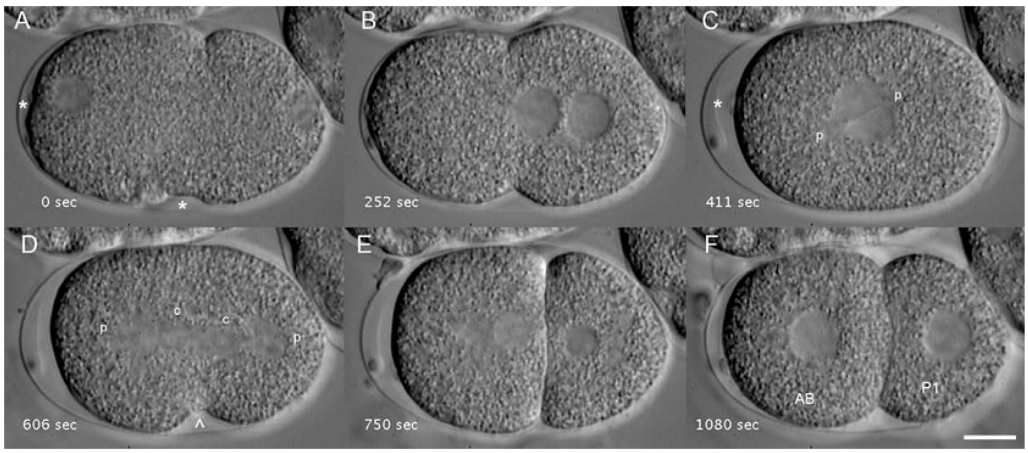

Fig. C.2: DIC time-lapse images of the first cell cycle (P_0 cell). The first frame of the time-lapse was set at 0s. A: the embryo just after meiosis. The anterior female pro-nucleus is on the left and the posterior male pro-nucleus is on the right. B: the embryo is at the end of pronuclear migration (the invagination of the cortex is called pseudocleavage and not the beginning of cytokinesis). C: nuclear envelope breakdown (NEBD), signalling the start of mitosis. Spindle poles are visible and are marked with a "p". D: the embryo is near the beginning of cytokinesis. The cleavage furrow is marked with a "^", spindle poles are marked with a "p" and the segregating chromatin is marked with a "c" just above each spot. E: the embryo at approximately the end of the first division. F: the anterior cell (AB) is just beginning the second round of cell divisions, about 5min after the first. The posterior cell (P_1) will divide a few minutes later. (Image and description taken from [41])

Polarization of the cell is governed by PAR proteins and their downstream effectors (see Fig. 1.3). PAR proteins control the orientation and asymmetric posterior localization of the spindle. They regulate the forces applied on the mitotic spindle through a localized regulation of heterotrimeric G proteins. They also regulate indirectly the segregation of a variety of cell fate determinants including proteins, mRNA or larger ribonucleoproteic complexes [6]. A more detailed description of the control mechanisms of the first asymmetric division can be found at [6, 49, 50, 104, 105].

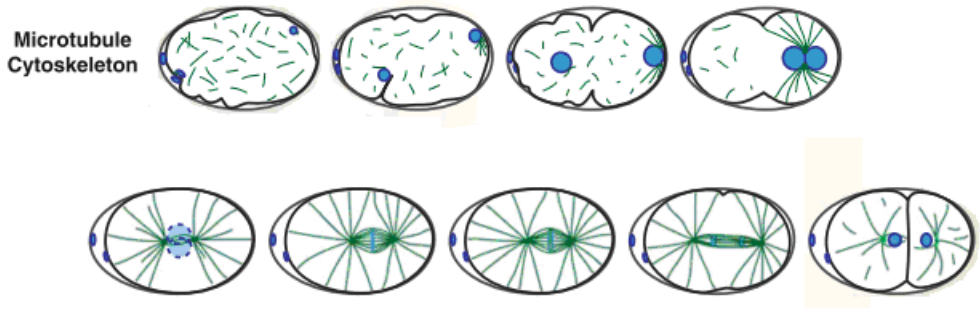

Fig. C.3: Outline of the mitotic cell cycle in the 1-cell *C. elegans* embryo. The microtubule cytoskeleton (green) reorganizes into the mitotic spindle to segregate the sister chromatids. The anterior of the embryo is to the left, the posterior to the right. (Image taken from [50])

A process called pseudocleavage occurs during the first cell cycle, before the two pro-nuclei meet (Fig. C.2 A and B). In consists in anterior cortical contractions that culminate in a single partial constriction of the embryo called the pseudocleavage furrow. The pseudocleavage contractions and furrow do not seem essential for the localization of cell fate determinants and normal embryogenesis can occur when the pseudocleavage is inhibited [88].

Gastrulation

Gastrulation plays an essential role in development of most animals. It consists in an internalization of endodermal, mesodermal and germline precursors and occurs when small groups of cells ingress into the small blastocyst cavity (also called blastocoele), at the centre of the blastula. Before gastrulation, the embryo is just a round mass of cells. The blastocyst cavity forms when specific surfaces of cells separate from one another in the interior of the embryo. Cells acquire an apical-basal polarity that is important for the asymmetric pattern of adhesions that produce the cavity [92].

In *C. elegans*, cells ingress at reproducible times and positions throughout the gastrulation. The cell movements of gastrulation begin at the 26-cell stage when the two endodermal precursors, E_a and E_p, move from the surface of the embryo into the very small blastocyst cavity. The endoderm is the first tissue to internalize during

gastrulation. E_a and E_p constrict their outer (apical) surfaces as they ingress. Their ingression occurs at approximately 90min after the first cleavage (Fig. C.4). After the endodermal cells have completed their ingression, the mesodermal cells and the germ cells ingress from various positions on the ventral surface over the next 200min.

With gastrulation, cells of the embryo have now three different possible surfaces: an outer surface that faces the eggshell (apical surface), the surfaces that contact adjacent cells (lateral surfaces), and a surface that faces cells on the opposite side of the blastocyst cavity (basal surface) [92].

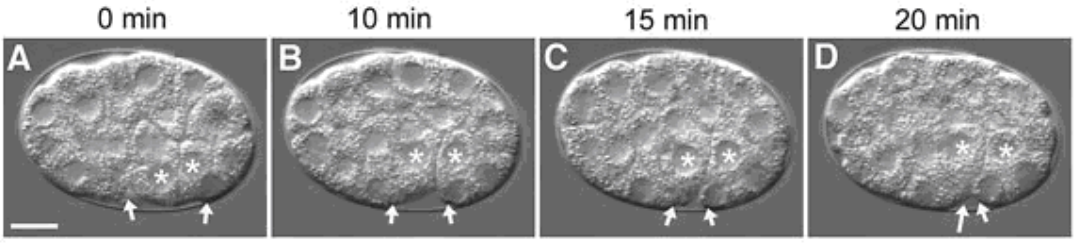

Fig. C.4: Initial stages of the gastrulation of the *C. elegans* embryo. 0min indicates the start of the gastrulation movements. The E cells are signalled with asterisks and the ingression area is highlighted by arrows. (Image taken from [92])

Temporal Cell Arrangement

The cells of a given lineage have their own inherent rhythm of cell divisions or endogenous cell cycle clocks. Cells that descend from the same stem cell divide at the same rate. A more anterior position in the embryo corresponds to a shorter cell cycle, and apparent waves of mitosis pass over the cleaving egg from anterior to posterior. The cells of the AB lineage have the shortest cell cycle and the cells of the P lineage have the longest. Each doubling of the cells of the six lineages constitutes a round of division. Each round is initiated by a doubling of the AB descendants, followed by the division of MS, C, E, and D, in that order. An early sign that a given lineage is approaching its final cell number may be the lengthening of its cell cycle [53].

According to [51], for a given lineage, cell cycle lengths follow a geometric sequence:

$$Cycle_{daughter} = \frac{1}{1-k} Cycle_{mother} \quad , \tag{C.1}$$

where $k < 1$ reflects the clock of the lineage and must be experimentally determined. From Eq.(C.1) it is clear that the cell cycle duration increases progressively while embryogenesis advances.

Early research of Sulston et al. [52] suggested an invariant cell lineage where every cell divides at specific times. However a more recent research conducted by Schnabel et al. [95] shows that in fact, there is a small variability (~10%) of the timing of cell divisions among homologous cells in the same embryo and among different embryos (Fig. C.5). The variance increases with developmental time.

They also show that division timing correlates linearly between embryos, suggesting that each embryo has also its own general clock, and each cell adjusts proportionally according to that clock. This way, there are two layers of variability: the variation of the general clock from embryo to embryo and the deviation of individual cells of an embryo from its general clock. According to [51], the embryo general clock has a relative standard deviation of 4.5%.

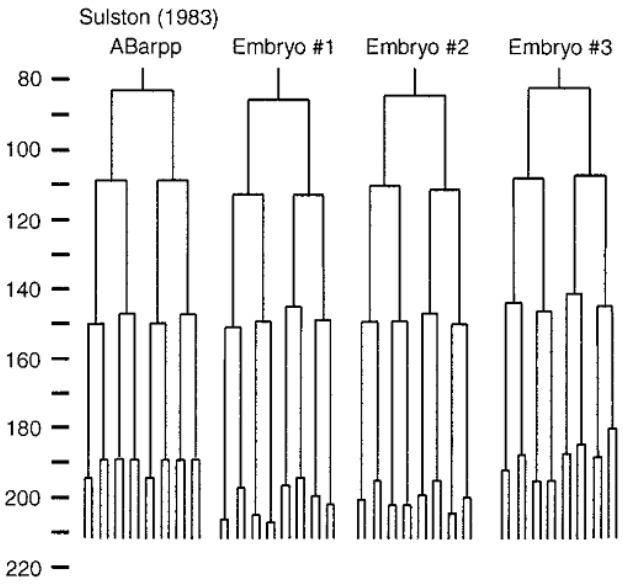

Fig. C.5: Example of variability of the cell division times in wild type embryos, according to Schnabel [57]. The figure shows the AB_{arpp} lineage according to Sulston and co-workers [52] and the same lineages in three embryos analysed with a 4D microscope. The vertical axis is the time axis, every cell division being indicated by a horizontal bar creating a branch in the lineage tree. The anterior sister is always to the left. AB_{arpp} produces 16 bilaterally homologous cells on the left (anterior eight cells) and the right side (posterior eight cells) of the embryo. According to Schnabel [57], a similar variability of cleavage times was observed in all lineages. (Image and description taken from [57])

Spatial Cell Arrangement

During the early cleavage divisions, the three main axes of the worm body plan are established (Fig. C.6). The AP axis is set up in the 1-cell stage. The DV axis becomes apparent at the transition between the 2- and 4-cell stage, with EMS defining the ventral side of the embryo. The left-right axis is detectable at the transition between the 4- and 6-cell stage, with the location of two granddaughters of AB (AB_{al} and AB_{pl}) defining the left side of the embryo [104]. Fig. C.7 presents the sequence of the firsts cell divisions, projecting their localizations in the egg.

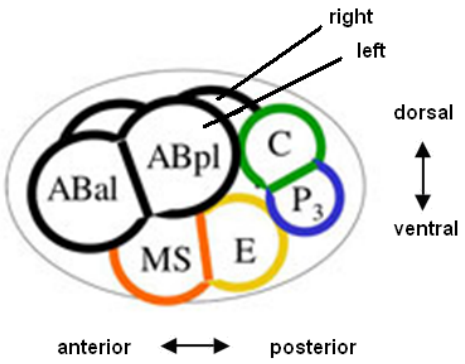

Fig. C.6: The three main axes of the worm body plan. (Image adapted from [104])

Cell movements are slow (maximally, 2 µm/min), easy to follow and do not interfere with the construction of the lineage. After completion of cell division, the two daughter cells round off, but never detach completely from one another [53].

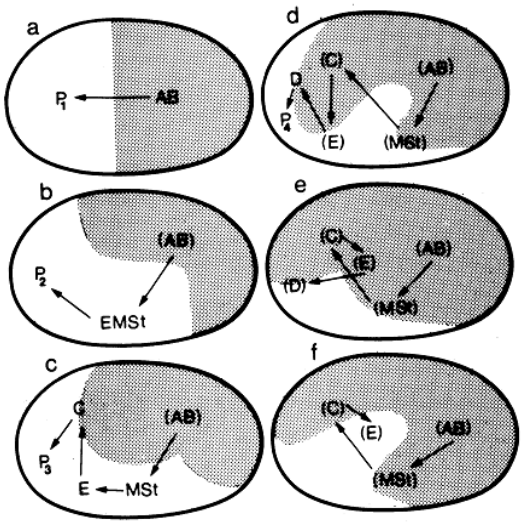

Fig. C.7: Sequence of cell divisions projected onto the egg. a-f indicate the sequence in the 2nd to the 7th division round, respectively. Eggs are in standard orientation (anterior, right; dorsal, top). Individual stem cells are named without parentheses and their descendants are grouped in regions named with their progenitor stem cell in parentheses. The stippled area is the region occupied by the AB descendants (in two-dimensional projection). The E descendants move inside and anterior during gastrulation (between stages d and e). (Image and description taken from [53])

The spatial arrangement of cells in the embryo is almost invariant, but as happens with the temporal arrangement, there is also some spatial variability. Until about 200min of development (~350 cells), the arrangement of blastomeres varies greatly among different embryos. As a consequence, up to 50% of the cell–cell contacts of blastomeres may vary. This is solved since there is a tight control of cleavage directions during the first five cleavage divisions and a stereotyped arrangement of blastomeres is already produced when these contact interactions occur, assuring stereotyped interactions between single blastomeres. This way, the same blastomere always acquires the same fate. Therefore, cells are not placed in their final positions by an invariant cell cleavage pattern but by active cell migrations due to interactions, which sort cells relatively to each other [57].

The Eggshell

Initially, it was proposed that the outside layer of the eggshell is composed by three layers (Fig. C.8):

- The external layer, thin and rich in protein and fibres, being called the vitelline layer (VL). It has the protein receptors needed for sperm to bind, which in turn are bound to sperm plasma membrane receptors. The species specificity between these receptors contributes to prevention of breeding between different species [62].

- The middle layer is thick and contains both chitin and protein and is named the chitin layer (CL). An important function of this layer is to provide structural strength to the eggshell (mechanical rigidity) and to prevent polyspermy [106]. According to [56], removing this layer is compatible with normal embryogenesis if care is taken, since the embryo becomes more sensitive to mechanical pressure. Also, without this layer the environment where the embryo is placed may affect the development as it develops normally in PBS but not in distilled water.

- The inner layer contains lipids and proteolipids and some collagen molecules being called the lipid rich layer (LrL). It is an osmotic barrier created by yolk secreted by the intestine of the progenitor [62, 107]. It is hydrolyzed before hatching, making the egg more permeable. According to [56], this layer can be reversibly laser perforated not affecting the development. However, when irreversibly opened, it prevents normal gastrulation, which suggests that it provides a proper microenvironment and hydrostatic pressure for cell-cell interactions and morphogenic movements. Removing both the LrL and the CL leads to a string-like arrangement of cells.

Inside the eggshell, a clear zone separates the LrL and the embryo plasma membrane. This region is variably called the perivitelline fluid/space, the perimembrane space, or the extraembryonic matrix (EEM) [108]. It is comprised by an outer clear zone and an inner filamentous embryonic layer (EmL) (Fig. C.8). Surrounding the embryo, the later is the immediate extracellular environment of the plasma membrane of the late stage zygote and the apical plasma membrane of the early embryo [108].

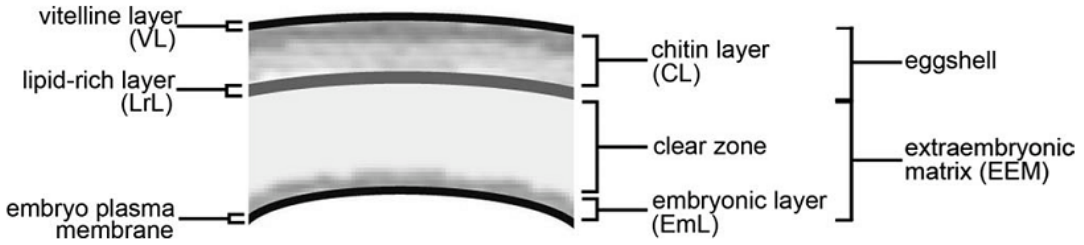

Fig. C.8: Schematic drawing of the *C. elegans* eggshell and extraembryonic matrix (EEM). Three major eggshell layers are visible by electron microscopy: an outer vitelline layer (VL), a middle chitin layer (CL) and an inner lipid-rich layer (LrL) [93]. Within the CL, a band of higher electron density just below the VL suggests the presence of distinct CL sub-layers. The EEM separates the eggshell from the embryo plasma membrane and has two distinct bands visible by electron microscopy: an outer clear zone and an inner fibrous embryonic layer (EmL). (Image and description taken from [62])

A recent investigation, [61], refutes some affirmations about the structure of the eggshell, principally the inner layer and the osmotic barrier. They suggested that the inner layer contains instead chondroitin proteoglycans (CPG-1 and CPG-2) which are required for the eggshell impermeability, calling it the CPG layer. They also suggest

that the permeability barrier is a distinct envelope formed in a separate step that requires fatty acid synthesis, the sugar-modifying enzyme PERM-1, and the acylchain transfer enzyme DGTR-1. These molecular requirements suggest that an ascaroside glycolipid may be an essential constituent of the permeability barrier. A previous study, [58], had already shown that the inhibition of genes related with the synthesis of PERM-1 and DGTR-1 results in loss of about 75% of the eggshell permeability. The inner CPG layer prevents plasma membrane adhesion to the chitin layer and expands the fluid filled perivitelline space, and the permeability barrier isolates the embryo from the environment.

The permeability barrier itself is a distinct envelope that assembles between the embryo plasma membrane and the trilaminar eggshell. The space between the CPG layer and the permeability barriers is called the perivitelline space. Inner to it is the periembryonic space that separates the embryo and the permeability barrier. The space between the embryo plasma membrane and the eggshell, previously termed the perivitelline space or extraembryonic matrix (EEM), was proposed to be named by perivitelline space for the region between the eggshell and the permeability barrier and the term periembryonic space for the region between the permeability barrier and embryo plasma membrane (Fig. C.9) [61].

The trilaminar shell does not block the entry of small molecules but prevents the entry/exit of larger molecules. It may thus serve as a filter to prevent the entry of larger proteins/molecules from the environment or to allow the retention of exocytosed molecules within the perivitelline space. The perivitelline space and the periembryonic space may provide an ideally cushioned and buffered environment for embryonic development. In addition to protecting the embryo by maintaining proper osmotic conditions and preventing the entry of potentially harmful small molecules from the environment, the permeability barrier may also allow the embryo to maintain secreted molecules that signal between embryonic cells in close proximity [61].

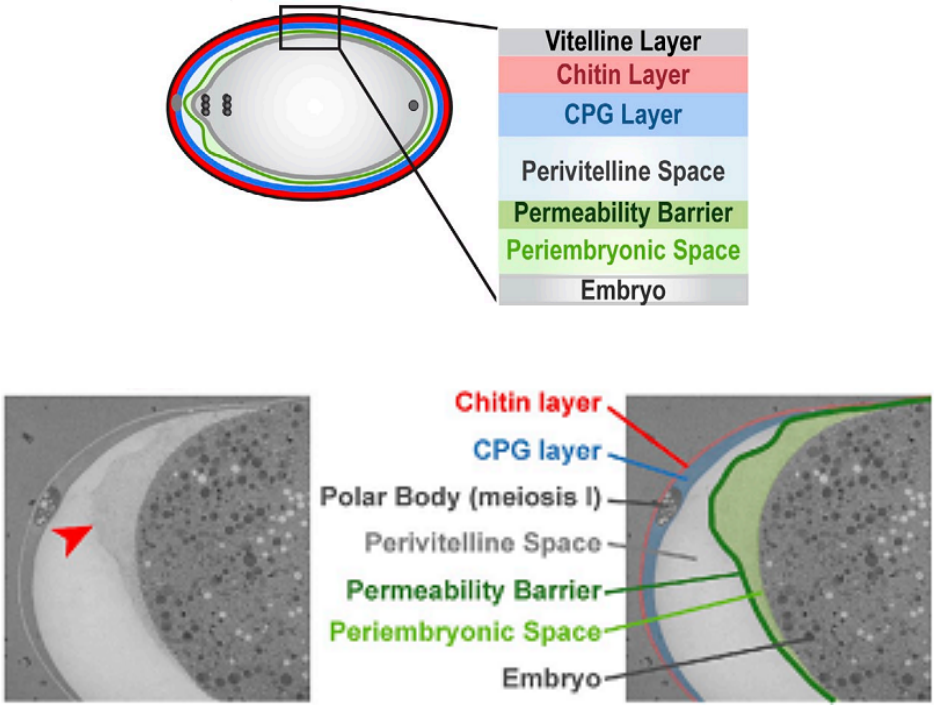

Fig. C.9: Top: schematic representation of the eggshell structures according to [61]. Bottom: transmission electron micrograph image showing the different components of the eggshell and permeability barrier. The vitelline layer is not seen, but is referred in the image at the top. The structures are named according to [61]. (Image taken from [61])

Appendix D – Auxiliary Methods

C. elegans Culture

Preparation of the Culture Plates

Embryos of wild type (N2) hermaphrodite individuals were chosen as a model for the study conducted in this project. In order to acquire them, a N2 *C. elegans* population culture was maintained monoaxenically in the laboratory, using *E. coli* strain OP50 as a food source, as described by Brenner, 1974 [28].

The *C. elegans* culture was maintained inside Petri plates (100mm radius, 15mm thickness) with Nematode Growth Medium (NGM) agar, seeded with *E. coli* OP50. The NGM agar was synthesised from normal agar according to the following protocol [28]:

1 – Take:

- 3g NaCl,
- 2.5g peptone,
- 20g agar,
- 975ml of DI water.

2 – After mixing, autoclave.

3 – Cool to 55ºC and add in order:

- 4ml cholesterol (5mg/ml in ethanol),
- 1ml of 1M $CaCl_2$ (previously autoclaved),
- 1ml of $MgSO_4$ (previously autoclaved),
- 25ml of 1M potassium phosphate buffer, pH 6.0 (13.2 ml K_2HPO_4 1M + 86.8 ml KH_2PO_4 1M for each 100ml) (previously autoclaved).

The prepared agar was then heated till the melting point and was poured, in a wetbench, into the Preti plates till filling about two thirds of the their height. The plates were left in the wetbench for 4-5 hours for the agar to dry and solidify.

The *E. coli* OP50 colony was prepared from a bacteria sample taken from a previous prepared colony according to the following protocol [28]:

1 – Prepare a falcon tube with 50ml of LB (Luria Broth) medium.

2 – Take an *E. coli* sample from a previous prepared bacteria solution, or from an agar plate seeded with a colony and drop in into the LB solution.

3 – Close the falcon tube and let a bacteria colony grow by placing the seeded solution one night at 37ºC or 2 days at room temperature.

1mL of the colony solution was pipetted into each prepared agar plate (preferentially at the centre to avoid worm migration to the borders of the Petri dish) and led dry in the wetbench for one day (the plates should not be sealed with parafilm in order to allow the culture solution to dry). The remaining bacteria solution that was not used was stored at -20ºC fur future use. Finally, the ready agar plates were sealed with parafilm and stored at 2ºC until needed for use [109].

Maintenance of the *C. elegans* Culture

To start a *C. elegans* culture, an adult N2 hermaphrodite was placed inside a ready agar plate and allowed to reproduce for one day at room temperature, creating a colony. When not in use, the culture plates were sealed with parafilm to avoid the nematodes to exit the culture and contaminate the laboratory, since in high humidity conditions some of them might climb the walls of the plate can crawl out of it. Every culture was stored at about room temperature (between 22ºC and 24ºC).

Every two days (as suggested in [109]), a chunked segment of agar with adult worms was transferred to a new empty agar plate (Fig. D.1), in order to maintain a culture with

a relatively young population. After that time, the culture plate would be predominantly populated with old nematodes not able to reproduce properly and Dauer state juvenile worms, again not able to reproduce. The latter are due to population being overcrowded and the absence of enough bacteria to feed it. One day after seeding the new agar plate, the nematodes were already in the N2 stage (reproducing) and ready for dissection and extraction of embryos.

When not possible to transfer the culture to a new plate every two days, a starving culture was chunked to a new plate with bacteria and stored for one day, to allow the worms to develop out of the Dauer stage and grow into the adult stage (N2). This method allows having starving populations for several weeks between the transfers while not losing the culture [109].

Old and useless culture plates were sealed with parafilm and properly disposed away.

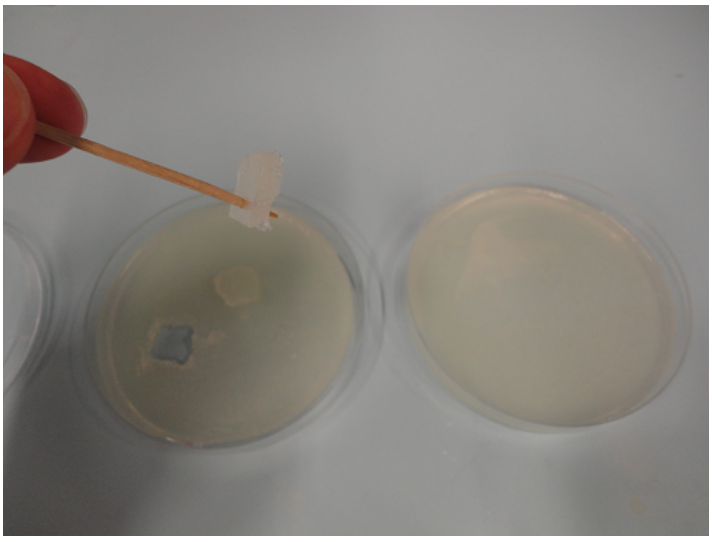

Fig. D.1: The chunking method used to transfer cultures from a used agar plate to a new empty one. A chunk was removed from the original agar plate with the help of a tooth stick, and then transferred to the new plate. The up surface of the chunk (where the worms usually lay) should be in contact with the agar surface of the new plate.

Device Microfabrication

The microfluidic chip was fabricated by soft lithography (Fig. D.2) [110].The master had previously been fabricated (courtesy of S. Baranek), so only the PDMS preparation was required. A PDMS elastomer solution 10:1 was prepared, defoamed and poured over a master[6] (with the structures designed according to the *CleWin* file [S. Baranek]) that was inside a box, till filling about 50-70mm of the box height (Fig. D.3). The box was then put in an oven for about 1h, for the PDMS to solidify.

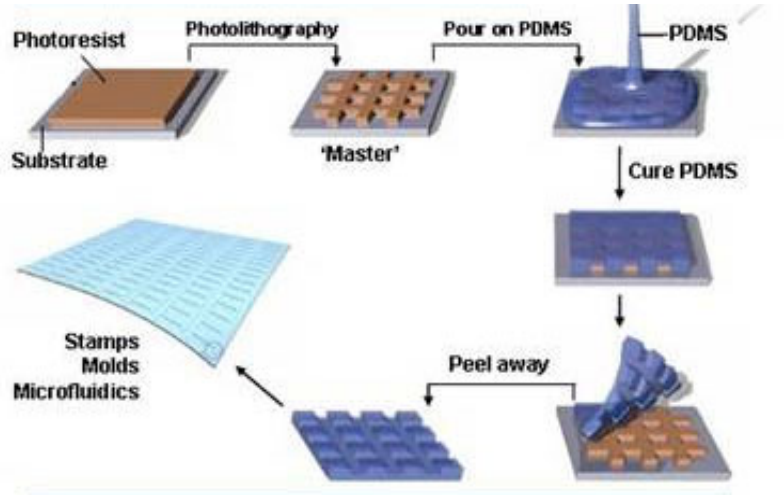

Fig. D.2: The soft lithography method. The master had previously been fabricated. The final structure was bounded to a cover glass to create a microfluidic channel. (Image taken from [110])

After solidifying, the PDMS was sliced off the box using a scalpel (Fig. D.4) and the master was then very carefully removed from the PDMS surface, using a spatula. To create the vertical pathway of the inlets, a special pen to pierce PDMS was used. The diameter of each hole is 1.5mm, or 1.25mm, when using the modified device (near inlets). The inlet holes were tested by inserting a pipette tip into them till it exited at the opposite side of the block. The blocks were finally sliced using a scalpel till the block

[6] The master had also been previously treated with trichloro(1H,1H,2H,2H-perfluorooctyl)silane. This turned it hydrophobic to make easier the removal of the solidified PDMS from it.

had the desired dimensions and subsequently sealed with glue tape and stored till they were needed.

To complete the system, the surface of the PDMS block with the geometric structures was plasma bounded (using the *Diener Electronic, Femto* plasma bath machine with parameters 0.6mbar, 0.1min, 100W) against a cover glass. The resultant chip (Fig. D.5) was stored until used.

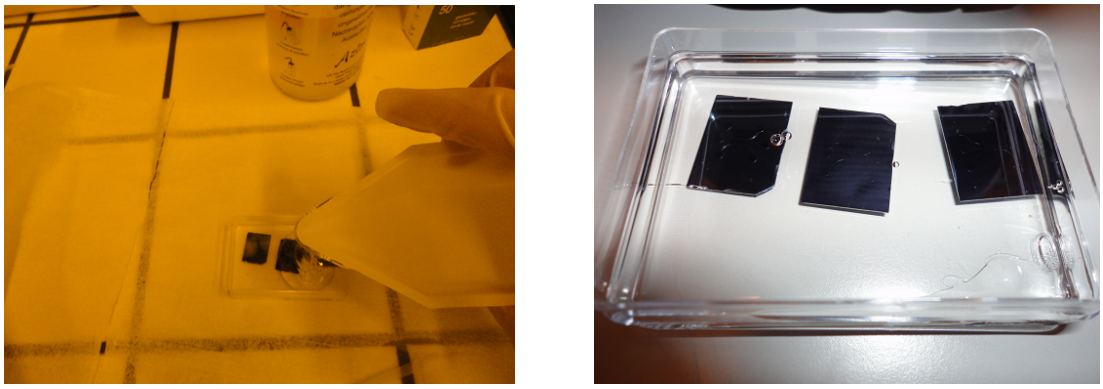

Fig. D.3: Left: the PDMS being poured against the master. Right: three masters already covered by PDMS.

Fig. D.4: The solid PDMS on the left was sliced using a scalpel, creating the block on the right. The inlet holes were made with a special pen to pierce PDMS (diameter of the holes: 1.5mm).

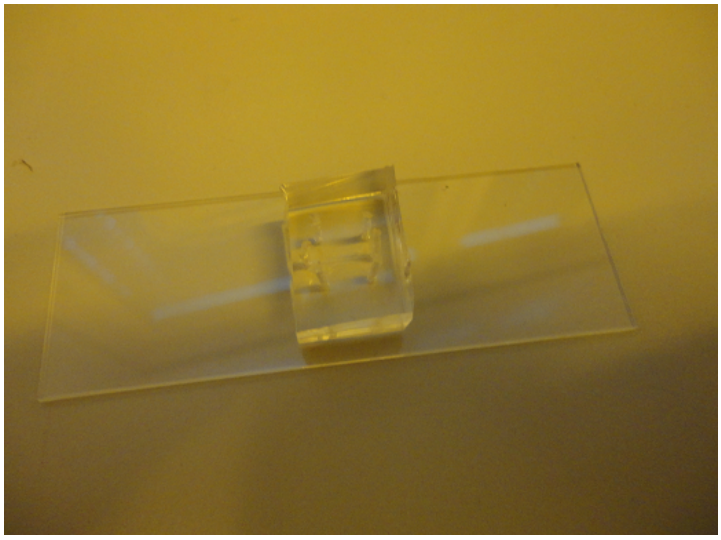

Fig. D.5: The final configuration of the microfluidic chip.

Preparation of Experiments

Chip Configuration

To inject the embryo into the chip, a small drop of liquid had to be previously created on the external entrance of one of the inlets, to where the embryo was pipetted. The embryo entered the system by sucking back the drop into it, and, once caught in the fluid flow, the embryo was able to move into the channel.

To provide the best injection conditions, segments of pipette tips were inserted in the inlets, to facilitate the connection to the tubing and to allow a better structural support to the liquid drop. The segments were fabricated from ordinary automatic pipette disposable tips that were cut near their thinner ending (Fig. D.6). That same tip end was then obliquely cut in order to direct the flow slightly laterally (to the channel). A cut pipette was inserted into each inlet of the chip (Fig. D.8). The two inlet tips should have approximately the same height, to minimize pressure driven flow in the channel.

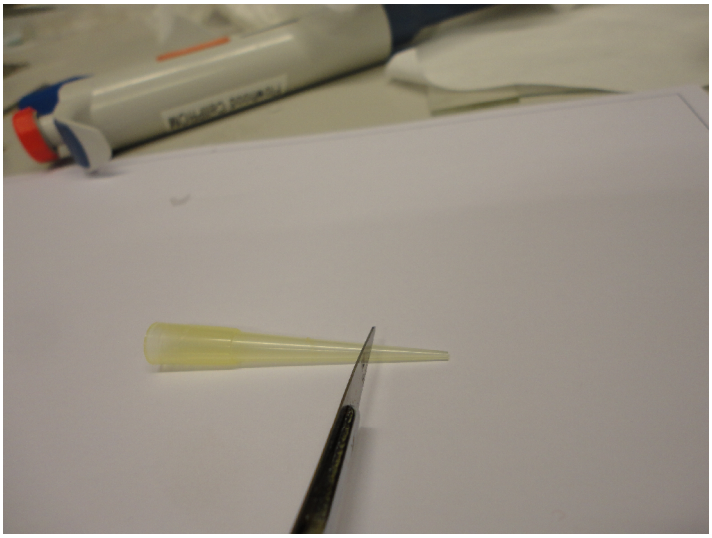

Fig. D.6: Cut pipette segment of automatic pipette tips were used for the system inlet vertical pathways. An automatic pipette is in background.

To fill the chip with liquid, a plastic tube (1.5mm diameter) connected to a glass syringe (glass does not expand) filled with the liquid to inject, was inserted inside one of the pipette tips and the liquid was pushed slowly (to avoid damaging the channel), till it filled the channel (Fig. D.7).

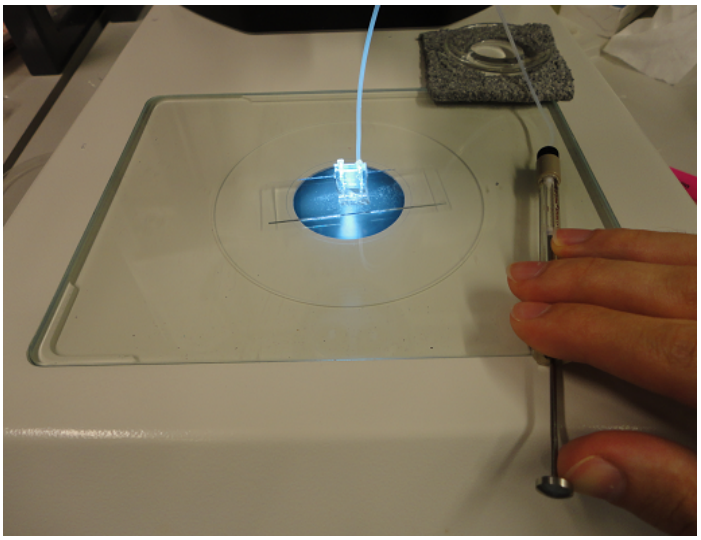

Fig. D.7: The injecting procedure. The liquid was pushed slowly, to avoid damaging the channels and causing leakage.

The channel was filled when the liquid came out from the other pipette tip. Afterwards, the tube connected to the inlet was removed, resulting in a filled chip with liquid forming a drop at the entrance of the vertical inlet pathways (Fig. D.8).

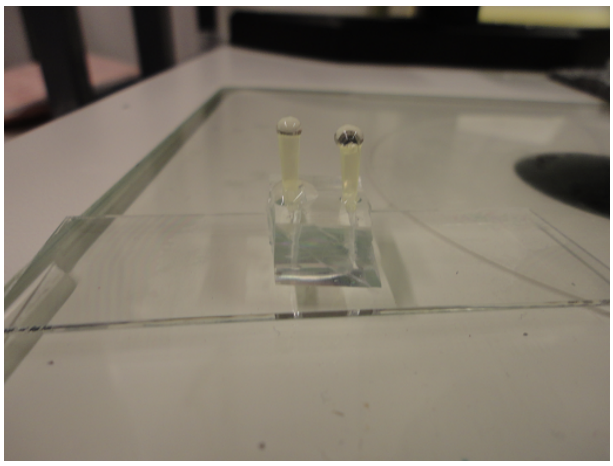

Fig. D.8: The chip filled with liquid after removing the tubing.

Embryo Injection

To inject the embryo into the chip, the system was first filled with PBS, till the liquid exited at the outlet, creating a small drop on its extremity, according to the method presented in the previous section (Fig. D.9). Next, the chip was placed inside a box in order to avoid contamination of the inlets by dust present in the air that might contribute to block of the channels.

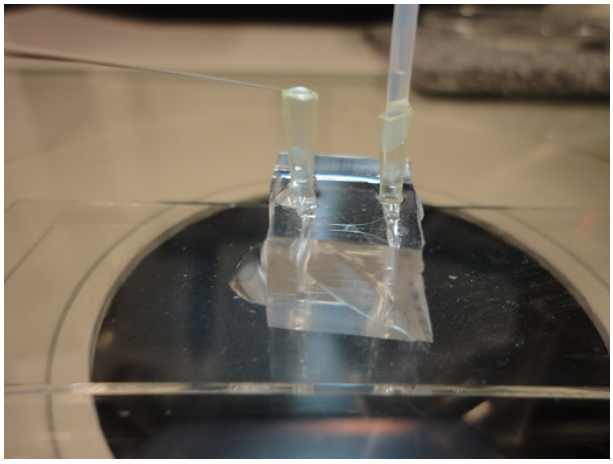

Fig. D.9: The liquid was injected until a small drop was formed at the extremity of one of the inlets (in this case the left inlet).

An adult reproducing worm was selected and collected from a culture agar plate (with the help of tweezers) (Fig. D.10) and moved into a clock glass with some PBS on it (Fig. D.11). Then, the worm was dissected using a small needle till the embryos left the carcass and laid at the bottom of the pool of PBS (Fig. D.12).

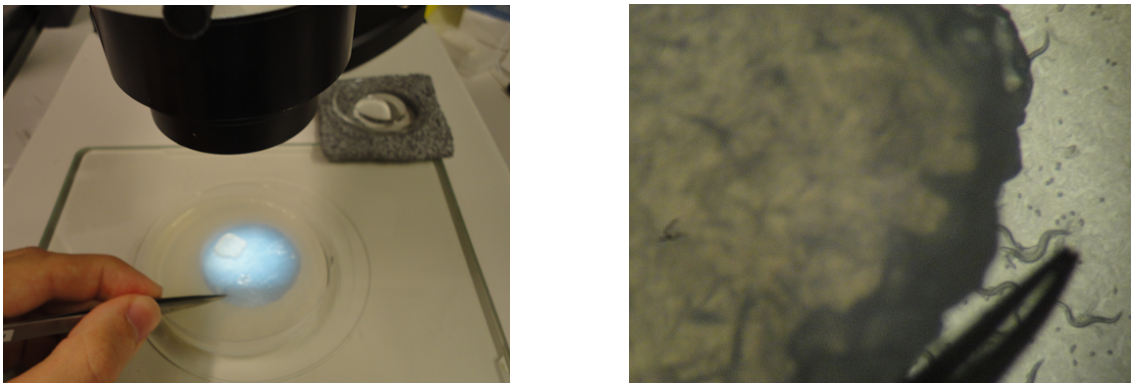

Fig. D.10: Worm selection from the culture plate. Left: an adult hermaphrodite worm was collected with the help of tweezers. Right: the same procedure now amplified with binoculars (*Leica MZ6*).

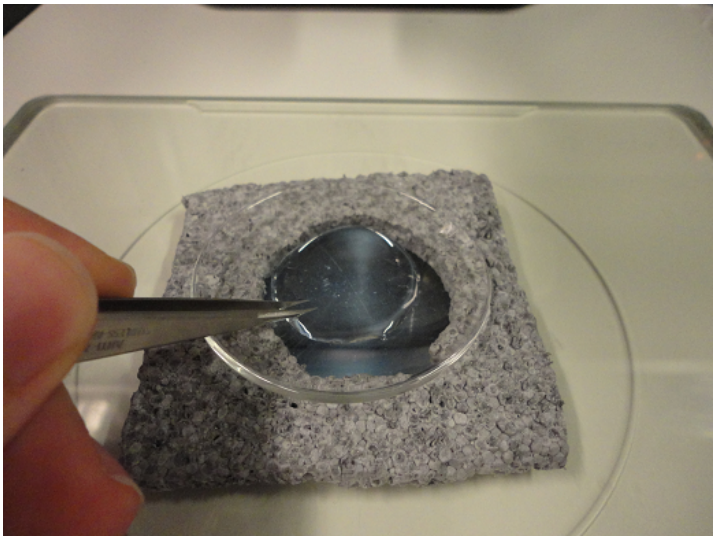

Fig. D.11: The selected worm was moved to a clock glass. The worm was transferred to the liquid by immersing into it the tweezers that were holding the worm.

Healthy 1-cell stage embryos (preferably right after meiosis II, at the start of pseudocleavage contractions) were localized and mouth pipetted into the drop of PBS on the chosen inlet extremity of the chip (preferably the cleanest one), here called the inlet (Fig. D.13). Healthy embryos could be distinguished by observing the eggshell around them (easily observable).

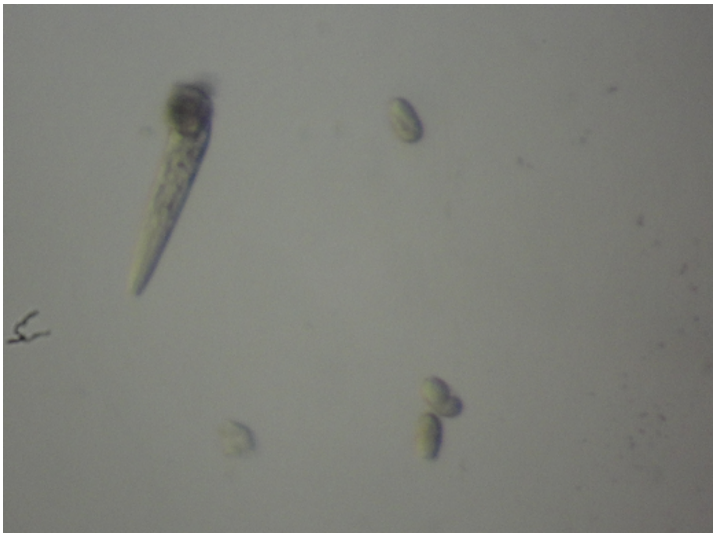

Fig. D.12: Binoculars (*Leica MZ6*) image of the worm carcass (left) and three embryos (right) lying at the bottom of the PBS pool, on the clock glass.

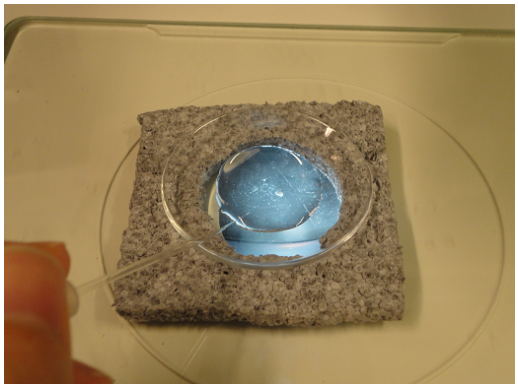

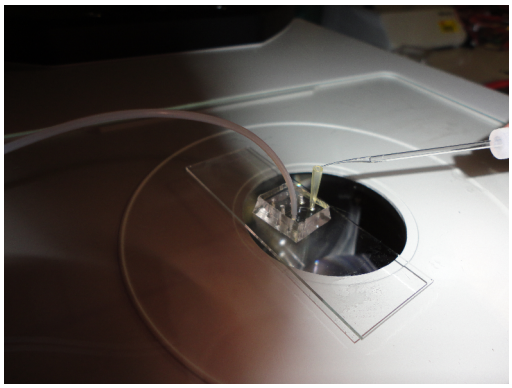

Fig. D.13: The selected healthy 1-cell stage embryo was mouth pipetted to the PBS drop on the top of the chosen inlet. In this case the tube at the other inlet (the outlet) was already connected to suck the embryo in, afterwards.

Next, the tube connected to a syringe (mentioned in the previous section) was connected to the remaining inlet (here called the outlet) and by pulling slightly the syringe, the drop on the inlet was sucked back, taking the embryo inside with it. Driven by the flow, the embryo entered the channel till it was placed next to the pillar, where it could not go further (Fig. D.14). The flow was stopped and the tube was removed from the outlet, very carefully to avoid any displacement of the embryo already placed in the correct position (next to the pillar) due to pressure changes induced by its removal (extremely important when using the closer inlets in the modified device). In such situations, inducing a small flow in the inverse direction might force the embryo to return to its correct location.

After injecting the embryo, the two inlet vertical pathways connecting the exterior to the channel should be filled with the same level of liquid, in order to have the same level of liquid in both of them to minimize pressure driven flow. Therefore, when necessary, the inlets were filled with liquid by inserting a syringe connected to an ordinary syringe needle and pushing liquid till the pathway was completely filled (Fig. D.15).

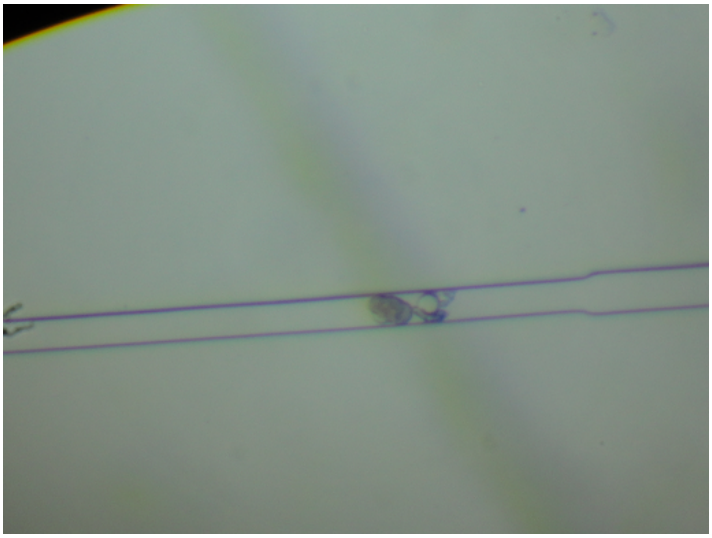

Fig. D.14: Binoculars (*Leica MZ6*) image of the embryo inside the channel, next to the pillar. The embryo does not move anymore, since the flow forces it against the pillar, which does not let the embryo pass.

Extreme care had to be taken to assure that no air bubbles entered the chip, since they function as an insulator to the electric current. Filling the inlets with PBS also granted that the inlets were completely filled with conductive medium.

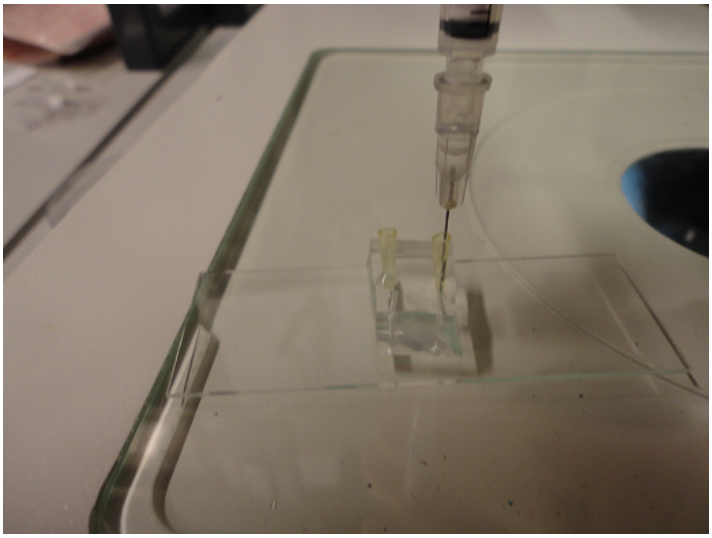

Fig. D.15: The vertical pathways of the inlets could be filled till the top with the help of an ordinary syringe with a normal tip.

After injecting the embryo, the system was rapidly moved to a box with a water reservoir inside, and moved to the microscope. Two platinum wires connected to a DC power generator (*GW Laboratory DC Power Supply GPS-3030D*; or *Agilent (HP) E3631A Triple Output DC Power Supply*) were inserted into the inlets. The generator was then switched on to induce a voltage driven electric current in the channel, and consequently also the wanted electric field. The basic steps of the injection procedure are in Fig. D.16.

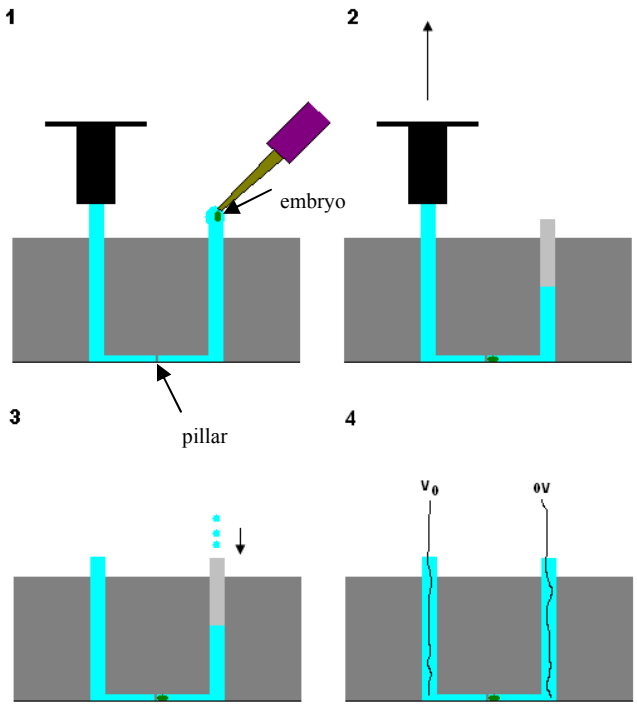

Fig. D.16: Injection procedure. 1) The embryo is mouth pipetted to a liquid drop on the top of one inlet of the microfluidic chip already filled with PBS. 2) The drop with the embryo is sucked with the help of a syringe on the other inlet till the embryo is placed next to the pillar. 3) More liquid is injected in order to fill the inlets. 4) When the device is ready, the electrodes are inserted in the inlets and a voltage (V_0) is applied between them.

Immediately after switching on the electric field, the box was closed, sealing the chip environment. The box was used to avoid the channels to dry by evaporation in long time experiments, and could be dispensed for short time experiments and for experiments using the salt bridges. The water reservoir had the function of maintaining humid the environment inside the box. To avoid light polarization by the plastic roof and floor of

the box, they were cut and replaced by glass. The floor of the chip served as the floor of the box and a glued coverslip served as the roof. Two small holes were made for the electric wires to pass without compromising the closed environment of the box (Fig. D.17).

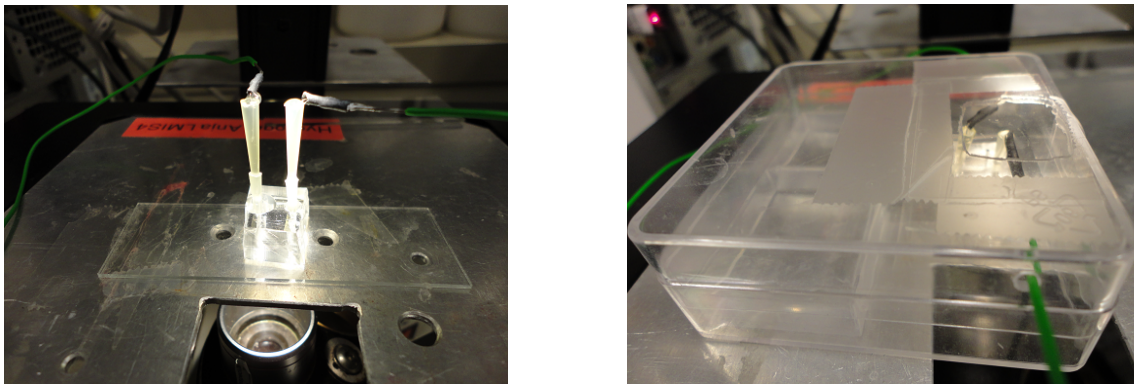

Fig. D.17: The mounted system, already at the microscope. Left: chip with the wires inserted into the salt bridges (box was not needed). Right: chip inside the sealing box where the wires entered inside it through holes made especially for that purpose.

Right after switching on the electric field, the embryo was imaged and time-lapse images were acquired by a computer (every 2 seconds for the initial development and every 1 minute from the 8-cell stage till hatch).

All the embryo injection procedure had to be performed very quickly (preferably in 5 minutes or less), before the first mitosis occurred, assuring that the experiment would start still during the first cell cycle, preferably before the pro-nuclear fusion. If any of these steps failed, all the procedure had to be repeated from the worm selection.

A binocular (*Leica MZ6*) was used to help with all the process, from the worm selection (allowing to select adult reproducing embryos by observing eggs in their uterus), dissection and egg selection (allowing the choice of a 1-cell stage embryo), mouth pipetting into the chip (allowing to observe the embryo transfer from the pipette to the drop) and injection to inside the chip (allowing to see the embryo in the pillar zone inside the channel). The binocular could detect easily if any of these steps failed, and also allowed in checking if the channels were blocked with dust, hairs or other dejects.

Agar Salt Bridges Preparation

Some experiments used agar salt bridges in the inlets, to avoid pH changes of the channel during the experiment. Also, this method avoided the necessity of the use of a box to seal the system, since the agar performed efficiently that function.

The salt bridges were built by directly injecting a liquid (above the melting point) solution of 1% agar in PBS into the inlet, exactly the same way as described for the PBS injection. Then, another and bigger pipette tip segment was inserted into the ones that were already there, and more agar was injected, increasing the height of the salt bridge (Fig. D.18). Extra care had to be taken since the agar is dense and changes easily the pressure inside the channels, displacing the embryo.

The platinum wires were inserted into the salt bridges, being sure they were short enough not to contact directly the pure PBS at the bottom of the inlets. There were no constraints with the time the agar had to cool down and solidify, since solidification occurs after some tens of seconds, and almost no agar in the liquid state had chance to flow into the channels and block them.

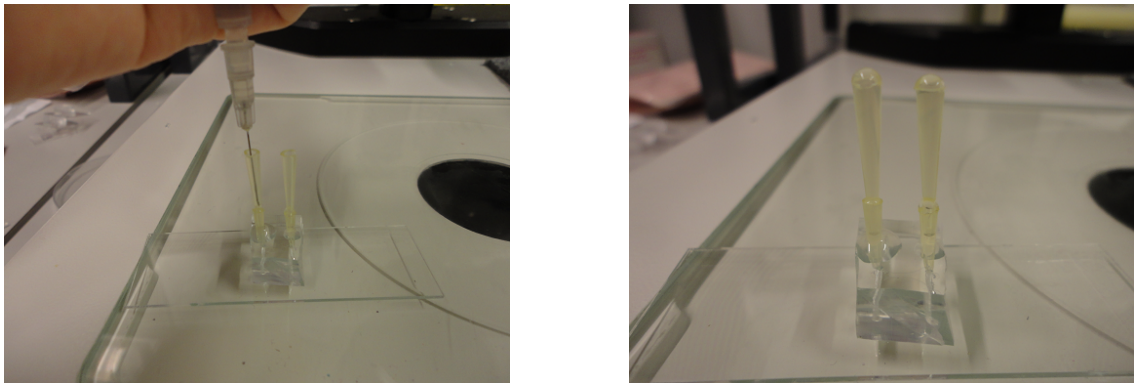

Fig. D.18: Preparation of the salt bridges. Left: a second pipette tip connected over the original inlet pipette tip is being filled with a liquid solution of 1% agar in PBS. Right: the ready salt bridge, where the platinum electrode wires will be inserted.

Chip Cleaning

In case of blockage, by dust, agar, dead embryos or other unwanted particles, the channels were cleaned (when possible) by passing a strong flow (PBS, DI water or isopropanol) in the desired direction, but not strong enough to damage the system. The flow was induced until all dejects left the channel in direction to the inlets. Then, the contaminated liquid at that inlet was sucked with a syringe. If any dejects still appeared in the channel, this procedure was repeated till it was reasonably cleaned or it was concluded that the chip could not be cleaned, being disposed in that case.

Embryo Imaging and Image Acquisition

The experimenters were imaged using two inverted microscopes, both equipped with a camera and time-lapse acquisition software:

- *Leica DMI 3000B* with DIC, equipped with a *RT Monochrome SPOT* camera (*Laboratory Instruments*) (Fig. D.19 left);
- *Leica DMIL* with phase contrast, equipped with a *Q-Imaging QICAM* camera (Fig. D.19 right).

Both microscopes offered good quality images with good contrast and resolution (Fig. D.20), although the DIC microscopy was preferred every time the microscope was available.

DIC (Differential interference contrast microscopy or Nomarski microscopy) is an optical microscopy technique used to enhance the contrast in unstained transparent samples, which contain little or no optical contrast when viewed using brightfield illumination. DIC is a widely used technique to visualize cellular features, most notably nuclei and nucleoli, but also microtubules, chromosomes and cytokinesis furrows. Cells above or below the DIC focal plane are not visible, making this technique perfect to observe and follow individual cells. DIC microscopy is superb for investigating living cells, as it is non-invasive and real-time and optical sectioning possibilities allow the movement of tiny organelles to be followed with ease. It is suitable to analyse the embryo of *C. elegans* since it provides information on the cell number, cell morphology, and details of cell cycle and division [41]. Reviews about DIC microscopy can be found [40, 111].

During imaging of the first cell cycles, the experiment had to be followed continuously, since cell and cell components may change position very frequently, and several small changes of focus might be needed. Consequently, each time-lapse image was acquired every two seconds. Image quality was optimized by knowing a priori the approximate division times and cleavage planes and some of the nuclei movements, allowing to follow the behaviour of individual cells.

After entering the 8-cell stage, the acquisition time was changed to one minute. Individual cells were not followed anymore, and only special events, such as the gastrulation, start of the comma fold and embryo movements inside the eggshell were analysed. Since most of these events affect the entire embryo, they could be easily followed even with the image slightly unfocused relatively to the ideal.

The experiments took more than half a day (12h-14h), so that they were set in such a way the initial development could be followed (about 40min), and the later stages were imaged at night. The experimental setup was placed in a way to avoid any bump, tap or another way to bother the microscope or the table it sits on.

Finally, all the images were saved in the native .tiff format and stored in a hard drive. The software used was *Micro Manager 1.3* for the *Monochrome SPOT* camera (*Leica DMI 3000B*) and *Q-Capture Pro 6.0* for the *Q-Imaging QICAM* camera (*Leica DMIL*).

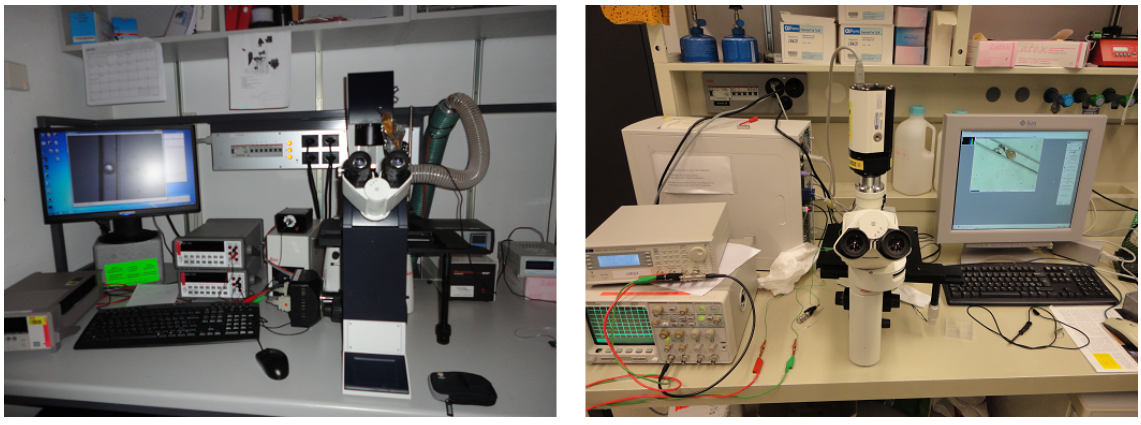

Fig. D.19: The inverted microscopes used for the image acquisition. Left: *Leica DMI 3000B* with DIC. Right: *Leica DMIL* with phase contrast.

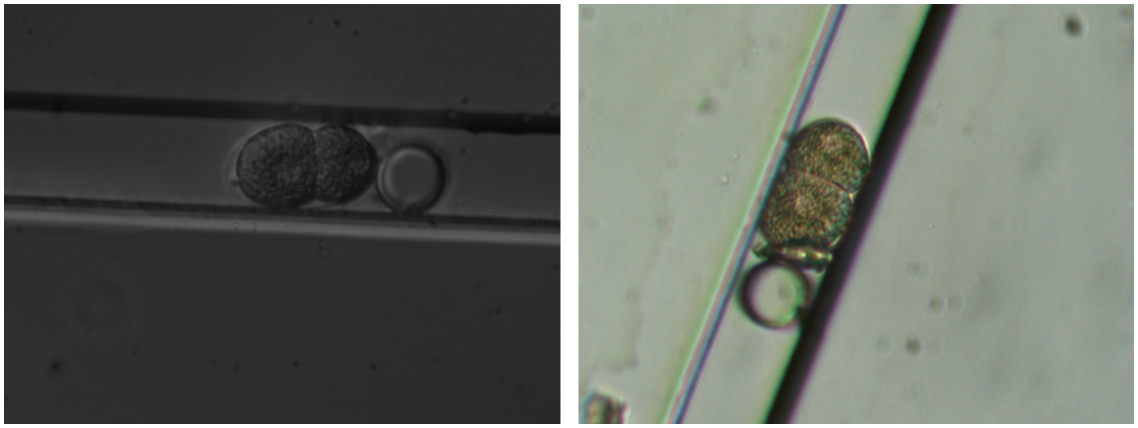

Fig. D.20: Image of a 2-cell stage embryo as seen by the *Leica DMI 3000B* (left) and *Leica DMIL* (right).

Image and Data Analysis

All images were analysed using the image analysis and processing software *ImageJ 1.45s*. Using the software, images were observed in sequence. The brightness and contrast were adjusted when necessary. Event times and positions were observed and the times were analysed and recorded in a datasheet (*Microsoft Excel 2003*), for future comparison with other experiments and statistical analysis.

The statistical analysis of the data was performed using statistical software. The Mann-Whitney test was performed using *GraphPadPrism 5*. Averages, standard deviations and other necessary parameters for the analysis were computed by the datasheet (*Microsoft Excel*). Graphs were built using *GraphPadPrism 5*.

Appendix E - Image Samples of the Observed Events

This appendix presents a DIC image sample, as seen during the observation, for each analysed event in chronologic order.

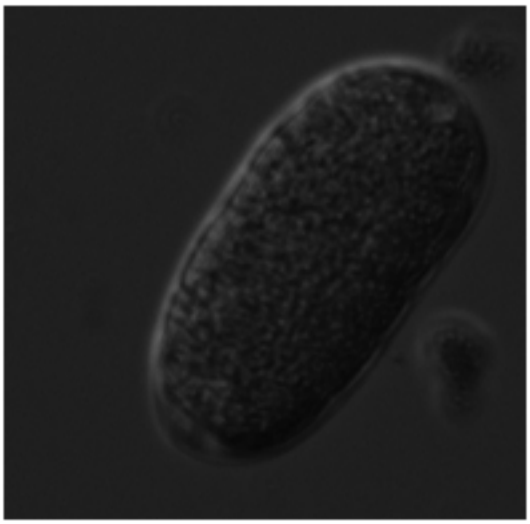

Fig. E.1: Start of pseudocleavage contractions. The pro-nuclei are starting to be visible at the extremities of the P_0 cell.

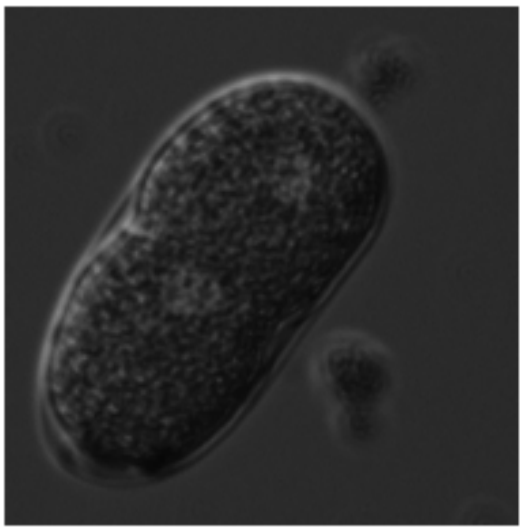

Fig. E.2: Pro-nuclei migration. Pseudocleavage furrow observable at about the middle of the cell.

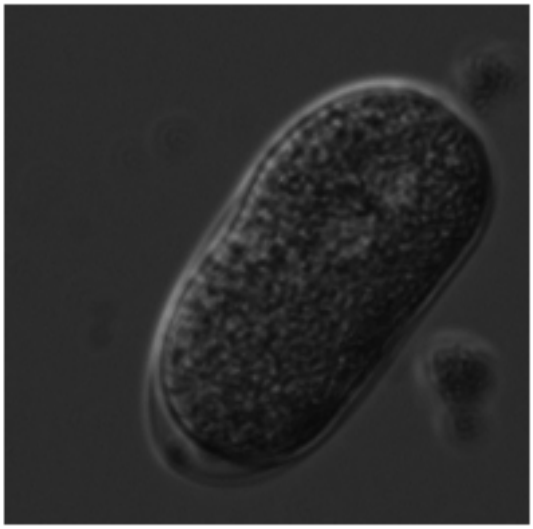

Fig. E.3: Pro-nuclei fusion. Pseudocleavage furrow almost disappeared.

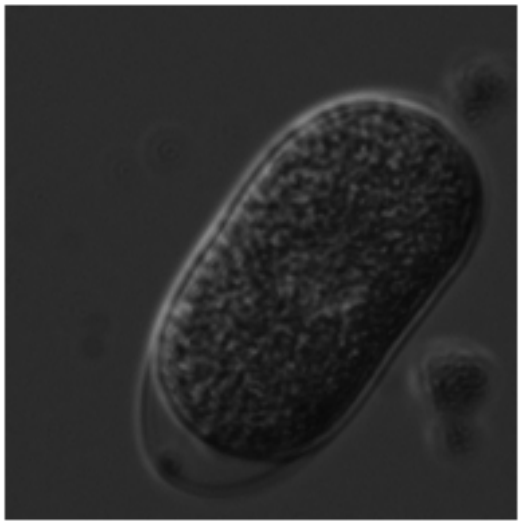

Fig. E.4: 1-cell stage just before nuclear envelope breakdown. After it, the nucleus will disappear.

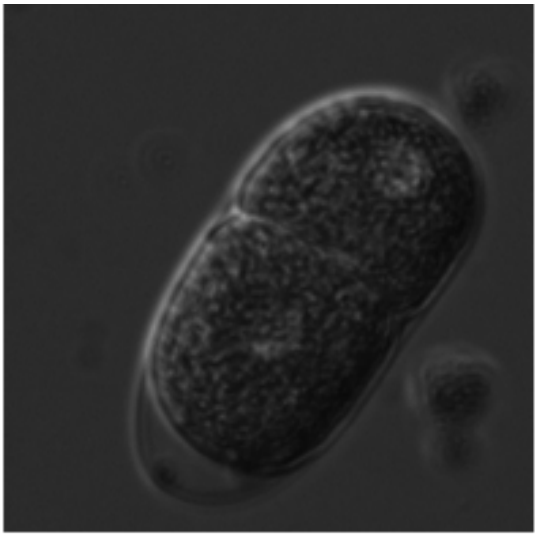

Fig. E.5g: 2-cell stage (AB and P_1).

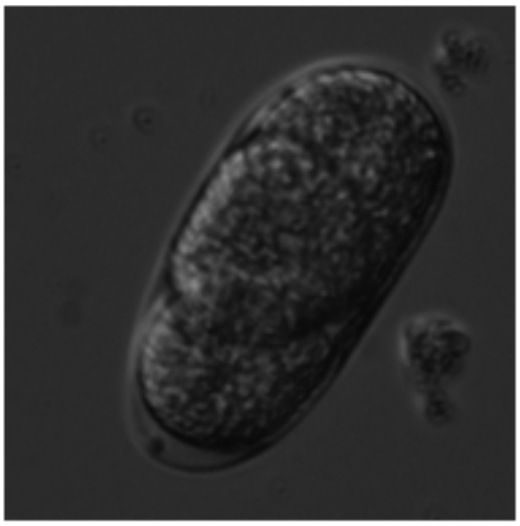

Fig. E.6: 3-cell stage (AB_a, AB_p and P_1).

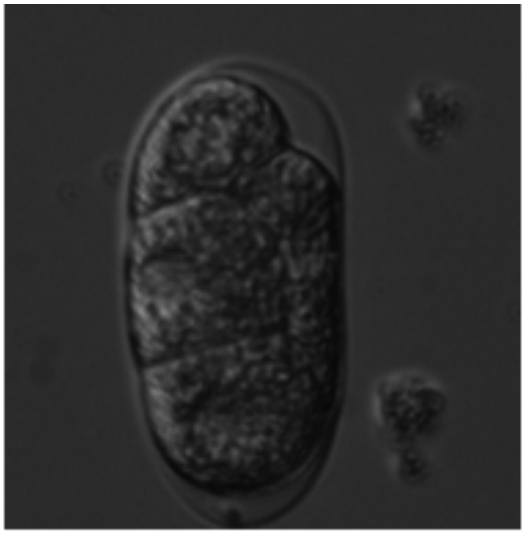

Fig. E.7: 4-cell stage (AB_a, AB_p, EMS and P_1).

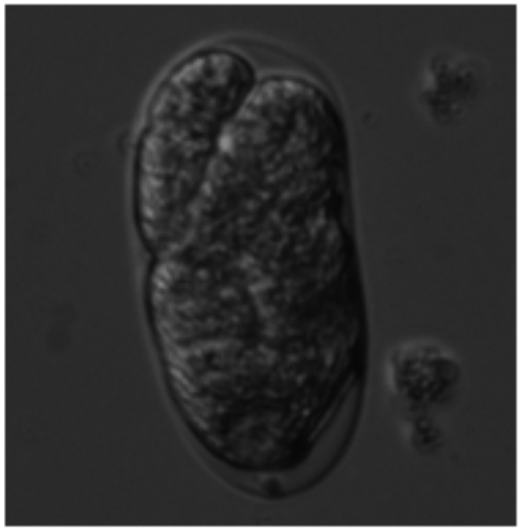

Fig. E.8: 8-cell stage.

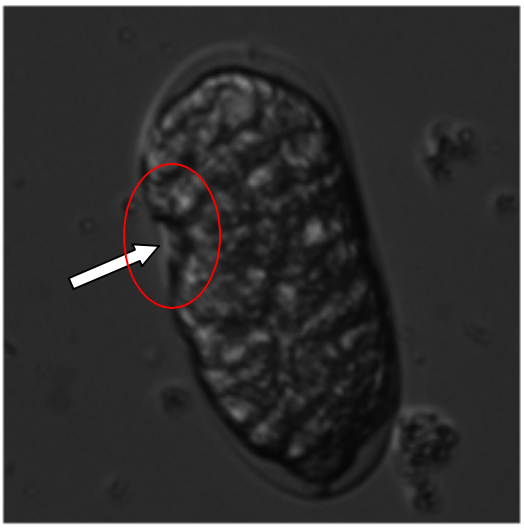

Fig. E.9: Gastrulation. The ingression area of the E cells is pointed.

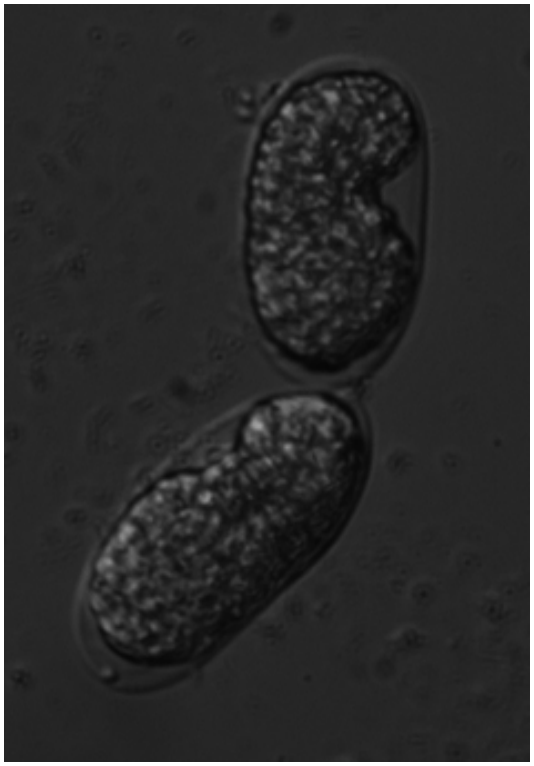

Fig. E.10: Two embryos at the lime-bean stage.

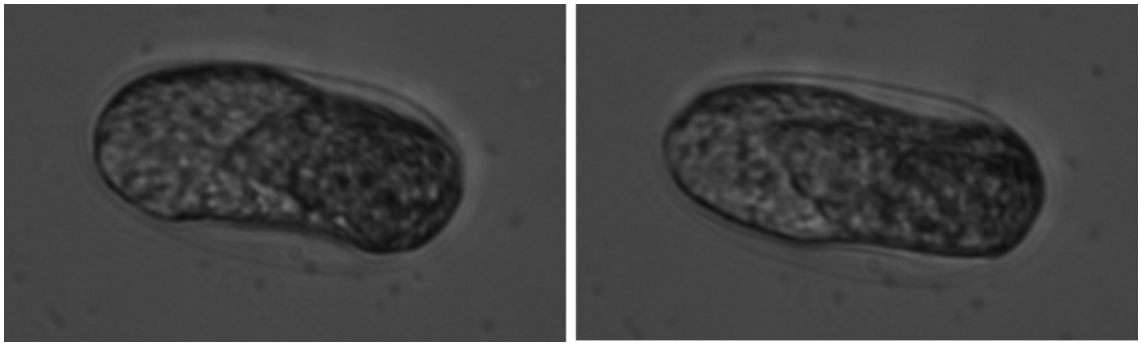

Fig. E.11: The embryo moves inside the eggshell, due to muscle twitches. Note that the embryo changes position from the left panel to the right panel.

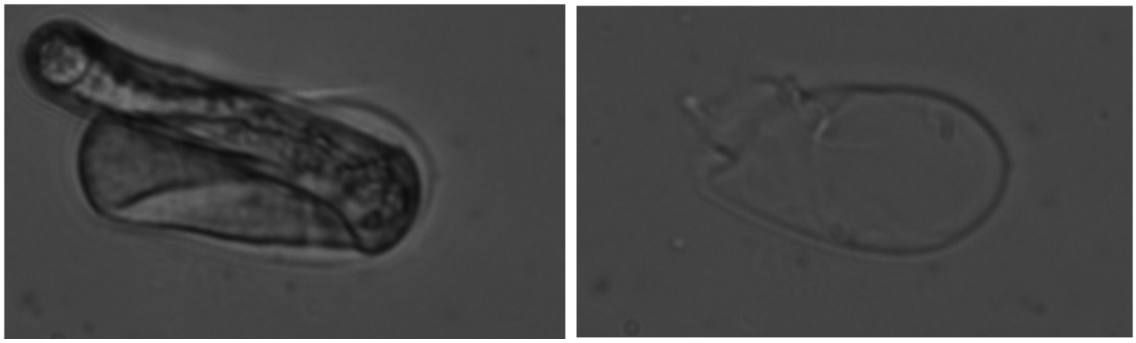

Fig. E.12: The embryo hatches and the juvenile worm leaves the eggshell.

References

Note 1: all websites were last accessed in July 2012.

Note 2: website address text may be wrapped between lines.

[1] Caig, C. D. M. C., Rajnicek, A. N. N. M., Song, B., Zhao, M. I. N. (2005). "Controlling Cell Behavior Electrically: Current Views and Future Potential". Physiological Reviews, 85, 943–978.

[2] Sabbatini, R. M. E. (1998). "The Discovery of Bioelectricity". Brain & Mind Magazine, 6, *http://www.cerebromente.org.br/n06/historia/bioelectr_i.htm*.

[3] Encyclopedia Britannica (Keyword: "bioelectricity"), *http://www.britannica.com /EBchecked/topic/65834/bioelectricity*.

[4] Kandel, E. R. Schwartz, J. H. Jessell, T. M. (2000). "Principles of neural science", 4 ed, chap 7. New York: McGraw-Hill.

[5] Plonsey, R., Barr, R. C. (2007). "Bioelectricity: a quantitative approach", 3 ed, chap 3. New York: Springer.

[6] Hyenne, V., Chartier, N. T., Labbé, J.-C. (2010). "Understanding the role of asymmetric cell division in cancer using C. elegans". Developmental dynamics: an official publication of the American Association of Anatomists, 239, 1378–1387.

[7] Wikipedia (Keyword: "cell polarity"), *http://en.wikipedia.org/wiki/Cell_pol arity*.

[8] Gönczy, P. (2008). "Mechanisms of asymmetric cell division: flies and worms pave the way". Nature Reviews Molecular Cell Biology, 9, 355-366, *http://www. nature.com/nrm/journal/v9/n5/fig_tab/nrm2388_F2.html*.

[9] Rajnicek A. M., Ireland J., Smith L. E., McCaig C. D. (2000). "Actin microfilaments and microtubules are required for Xenopus growth cone turning in a physiological electric field". J Physiol 528P: 78P.

[10] Zhao, M., Forrester, J. V., McCaig, C. D. (1999). "A small, physiological electric field orients cell division". Proceedings of the National Academy of Sciences of the United States of America, 96, 4942–4946.

[11] Farboud, B., Nuccitelli, R., Schwab, I. R., Isseroff, R. R. (2000). "DC electric fields induce rapid directional migration in cultured human corneal epithelial cells". Experimental eye research, 70, 667–673.

[12] Song B., Zhao M., Forrester J. V., McCaig C. D. (2002) "Electrical cues regulate the orientation and frequency of cell division and the rate of wound healing in vivo". Proc Natl Acad Sci USA, 99, 13577–13582.

[13] Reid, B., Song, B., McCaig, C. D., Zhao, M. (2005). "Wound healing in rat cornea: the role of electric currents". The FASEB journal: official publication of the Federation of American Societies for Experimental Biology, 19, 379–386.

[14] Reid, B., Vieira, A. C., Cao, L., Mannis, M. J., Schwab, I. R., Zhao, M. (2011). "Specific ion fluxes generate cornea wound electric currents". Communicative & integrative biology, 4, 462–465.

[15] Metcalf, M. E. M., Borgens, R. B. (1994). "Weak applied voltages interfere with amphibian morphogenesis and pattern". J Exp Zool, 268, 322– 338.

[16] Borgens, R. B., Vanable, J. W. Jr., Jaffe, L. F. (1977). "Bioelectricity and regeneration: large currents leave the stumps of regenerating newt limbs". Proc Natl Acad Sci USA, 74, 4528–4532.

[17] Messerli, M. a, Graham, D. M. (2011). "Extracellular electrical fields direct wound healing and regeneration". The Biological bulletin, 221, 79–92.

[18] Pullar, C. E., (2011). "The Physiology of Bioelectricity in Development, Tissue Regeneration and Cancer". CRC Press.

[19] Cuzick, J., Holland, R., Barth, V., Davies, R., Faupel, M., Fentiman, I., Frischbier, H. J., LaMarque, J. L., Merson, M., Sacchini, V., Vanel, D., Veronesi, U. (1998) "Electropotential measurements as a new diagnostic modality for breast cancer". Lancet, 352, 359–363.

[20] Djamgoz, M. B. A. (2011). "Bioelectricty of Cancer Voltage-Gated Ion Channels and Direct-Current Electric Fields". in Pullar, C. E.. "The Physiology of Bioelectricity in Development, Tissue Regeneration and Cancer", 1 ed, chap 12. CRC Press.

[21] Mycielska, M. E., Djamgoz, M. B. A. (2004). "Cellular mechanisms of direct-current electric field effects: galvanotaxis and metastatic disease". J. Cell Sci, 117, 1631–1639.

[22] Djamgoz, M. B. A., Mycielska, M., Madeja, Z., Fraser, S. P., Kohorada, W. (2001). "Directional movement of rat prostate cancer cells in direct-current electric field: involvement of voltage-gated Na+ channel activity". J Cell Sci, 114, 2697–2705.

[23] Borgens, R. B. (1999). "Electrically-mediated regeneration and guidance of adult mammalian spinal axons into polymeric channels". Neuro- science, 91, 251–264.

[24] Borgens, R. B., Blight, A. R., McGinnis, M. E. (1987). "Behavioral recovery induced by applied electric fields after spinal cord hemisection in guinea pig". Science, 238, 366–369.

[25] Borgens, R. B., Metcalf, M. E., Blight, A. R. (1993). "Delayed application of direct current electric fields in experimental spinal cord injuries". Restor Neurol Neurosci, 162, 1–7

[26] Baranek, S., Bezler, A., Adamczyk, C., Gönczy, P., Renaud, P. (2010). "Temperature Gradient Stimulation for Cell Division in C. elegans Embryos on Chip". 4th International Conference on Miniaturized Systems for Chemistry and Life Sciences, Groningen, The Netherlands.

[27] Model Organisms for Biomedical Research, National Institute of Health, *http://www.nih.gov/science/models/*.

[28] Brenner, S. (1973) "The genetics of behaviour". Br. Med. Bull., 29, 269–271.

[29] Caenorhabditis elegans WWW Server, *http://elegans.som.vcu.edu/*.

[30] Riddle Laboratory, *http://riddlelab.msl.ubc.ca/*.

[31] "What are C. elegans?". Web of Life NASA, *http://weboflife.nasa.gov/celegans/questionsshow.htm*.

[32] "Introduction to C. elegans Anatomy". Wormatlas, *http://www.wormatlas.org/ver1/handbook/anatomyintro/anatomyintro.htm*.

[33] Fielenbach, N., Antebi, A. (2008). "C. elegans dauer formation and the molecular basis of plasticity". Genes & Dev, 22, 2149-2165.

[34] Rankin C. H. (2002). "From gene to identified neuron to behaviour in Caenorhabditis elegans". Nat Rev Genet, 3, 622-630.

[35] de Bono M., (2003). "Molecular approaches to aggregation behavior and social attachment". J Neurobiol., 54, 78-92.

[36] WormBook - The Online Review of C. elegans Biology, *http://www.wormbook.org/*.

[37] Riddle, D. L., Blumenthal, T., Meyer, B. J., Priess, J. R. (1997). "C. elegans II", 2 ed. New York: Cold Spring Harbor Laboratory Press.

[38] Caenorhabditis elegans Resources, *http://jtenlen.drizzlehosting.com/celegans.html*.

[39] WormMethods, WormBook, *http://www.wormbook.org/toc_wormmethods.html*.

[40] Murphy, D. B. et al. "Differential Interference Contrast". Davidson, M. W. and The Florida State University, *http://micro.magnet.fsu.edu/primer/techniques/dic/dichome.html*.

[41] Powers, J. a (2010). "Live-cell imaging of mitosis in Caenorhabditis elegans embryos". Methods (San Diego, Calif.), 51, 197–205.

[42] Browder, L., Iten, L. (1998). "Development of the Nematode Caenorhabditis elegans". Dynamic Development, *http://people.ucalgary.ca/~browder/virtualembryo/worms.html*.

[43] Henahan, S. (1997). "Worms, Longevity and Diabetes". Access Excellence, *http://www.accessexcellence.org/WN/SUA11/worm897.php*.

[44] Mahlrab, P. "Caenowhat?". University of Arizona, *http://www.mcb.arizona.edu/wardlab/Caenowhat.html*.

[45] The Worm Breeder's Gazette, WormBook, *http://www.wormbook.org/wbg/*.

[46] C. elegans Movies, *http://labs.bio.unc.edu/Goldstein/movies.html#.UHdiXpHAz9o*.

[47] Wormbase, *http://www.wormbase.org/*.

[48] "The Wednesday Post (29/09/10)". Disease of the Week, *http://diseaseoftheweek.wordpress.com/2010/09/29/the-wednesday-post-290910/*.

[49] Heuvel, S. V. D., Kipreos, E. T. (2012). "C. elegans Cell Cycle Analysis". in Rothman J., Singson, A. "Caenorhabditis Elegans: Cell Biology and Physiology", 2 ed, vol 107, chap 9. Elsevier Inc.

[50] Begasse, M. L., Hyman, A. A. (2011). "The First Cell Cycle of the Caenorhabditis elegans Embryo: Spatial and Temporal Control of an Asymmetric Cell Division". in J.Z. Kubiak. "Cell Cycle in Development", vol 53, chap 6. Berlin Heidelberg: Springer-Verlag.

[51] Bao, Z., Zhao, Z., Boyle, T. J., Murray, J. I., Waterston, R. H. (2008). "Control of cell cycle timing during C. elegans embryogenesis". Developmental biology, 318, 65–72.

[52] Sulston, J. E., Schierenberg, E., White, J. G., Thomson, J. N. (1983). "The embryonic cell lineage of the nematode Caenorhabditis elegans". Developmental biology, 100, 64–119.

[53] Deppe, U., Schierenberg, E., Cole, T., Krieg, C., Schmitt, D., Yoder, B., von Ehrenstein, G. (1978). "Cell lineages of the embryo of the nematode Caenorhabditis elegans". Proceedings of the National Academy of Sciences of the United States of America, 75, 376–380.

[54] Riddle, D. L., Blumenthal, T., Meyer, B. J., Priess, J. R. (1997). "C. elegans II", 2 ed, chap 14. New York: Cold Spring Harbor Laboratory Press.

[55] Porta-de-la-Riva, M., Fontrodona, L., Villanueva, A., Cerón, J.(2012). "Basic Caenorhabditis elegans Methods: Synchronization and Observation". J. Vis. Exp, 64, e4019, *http://www.jove.com/video/4019/basic-caenorhabditis-elegans-methods-synchronization-and-observation*.

[56] Schierenberg, E., Junkersdorf, B. (1992). "The role of eggshell and underlying vitelline membrane for normal pattern formation in the early C. elegans embryo". Roux's Archives of Developmental Biology, 202, 10–16.

[57] Schnabel, R. (1997). "Why does a nematode have an invariant cell lineage?" Seminars in cell & developmental biology, 8, 341–349.

[58] Carvalho, A., Olson, S. K., Gutierrez, E., Zhang, K., Noble, L. B., Zanin, E., Desai, A., et al. (2011). "Acute drug treatment in the early C. elegans embryo". PloS one, 6, e24656.

[59] Ambros, V. R. (2000). "Control of developmental timing in Caenorhabditis elegans". Curr Opin Genet Dev, 10, 428-433.

[60] Rappleye, C. a, Paredez, a R., Smith, C. W., McDonald, K. L., & Aroian, R. V. (1999). "The coronin-like protein POD-1 is required for anterior-posterior axis formation and cellular architecture in the nematode caenorhabditis elegans". Genes & development, 13, 2838–2851.

[61] Olson, S. K., Greenan, G., Desai, A., Müller-reichert, T., Oegema, K. (2012). "Hierarchical assembly of the eggshell and permeability barrier in C. elegans", J. Cell Biol. 198, 731-748.

[62] Johnston, W. L., Dennis, J. W. (2011). "The eggshell in the C. elegans oocyte-to-embryo transition". Genesis, 17, 1–17.

[63] Hall DH, Altun ZF. (2008). "C. elegans Atlas". Cold Spring Harbor: Cold Spring Harbor Laboratory Press.

[64] Lab Videos, Caldwell Lab, *http://www.bama.ua.edu/~gcaldwel/video.html*.

[65] El-ali, J., Sorger, P. K., Jensen, K. F. (2006). "Cells on chips". Nature, 442, 403-411.

[66] Khanna, N., Cressman III, C. P., Tatara, C. P., Williams, P. L. (1997). "Tolerance of the Nematode Caenorhabditis elegans to pH, Salinity, and Hardness in Aquatic Media". Archives of Environmental Contamination and Toxicology, 32, 110-114.

[67] Plonsey, R., Barr, R. C. (2007). "Bioelectricity: a quantitative approach", 3 ed, chap 2. New York: Springer.

[68] Serway, R. A., Jewett, J. W. (2004). "Physics for scientists and engineers", 6 ed, chap 25. Belmont: Thomson-Brooks/Cole.

[69] Serway, R. A., Jewett, J. W. (2004). "Physics for scientists and engineers", 6 ed, chap 27. Belmont: Thomson-Brooks/Cole.

[70] Kovacs, G. T. A. "Introduction to the Theory, Design and Modeling of Thin-Film Microelectrodes for Neural Interfaces". in D. A. Stenger, T. McKenna (1994) "Enabling Technologies for Cultured Neural Networks", chap 7. San Diego: Academic Press.

[71] Wikipedia, *http://en.wikipedia.org/wiki/File:Diagram_of_zeta_potential_and_slipping_planeV2.svg*.

[72] Module Five, Distance Learning Corrosion Course, *http://corrosion-doctors.org/Corrosion-Kinetics/Overpotential-definition.htm*.

[73] Wikipedia (Keywords: "exchange current density"), *http://en.wikipedia.org/wiki/Exchange_current_density*.

[74] Wikipedia (Keyword: "overpotential"), *http://en.wikipedia.org/wiki/Overpotential*.

[75] Tamiasso-Martinhon, P., Cachet, H., Debiemme-Chouvy, C., Deslouis, C. (2008). "Thin films of amorphous nitrogenated carbon a-CNx: Electron transfer and surface reactivity". Electrochimica Acta, 53, 5752–5759.

[76] "Kelvin (4-wire) resistance measurement" in "All about Circuits", vol 1, *http://www.allaboutcircuits.com/vol_1/chpt_8/9.html*.

[77] Geddes, L. A., Baker, L. E. (1967). "The Specific Resistance of Biological Material - A Compendium of Data for the Biomedical Engineer and Physiologist". Med. & bioL Engng, 5, 271–293.

[78] Mark, J. E. (1999). "Polymer data handbook", online version. New York: Oxford University Press.

[79] Liticaubr, E. L., Shreir, L. L. (1966). "Anodic Polarization of Platinum in Sodium Chloride Solutions". Electrochimica Acta, 11, 527–536.

[80] Wikipedia (Keywords: "phosphate buffered saline"), *http://en.wikipedia.org/wiki/Phosphate_buffered_saline*.

[81] Hauch, A., Georg, A. (2001). "Diffusion in the electrolyte and charge-transfer reaction at the platinum electrode in dye-sensitized solar cells". Electrochimica Acta, 46, 3457–3466.

[82] Elert, G. "Thickness of a Cell Membrane". in Elert, G. "The Physics Factbook", *http://hypertextbook.com/facts/2001/JenniferShloming.shtml*.

[83] Wikipedia (Keywords: "electrolysis of water"), *http://en.wikipedia.org/wiki/Electrolysis_of_water*.

[84] With Friendship.com, *http://withfriendship.com/user/mithunss/electrolysis-of-water.php*.

[85] "Electrolysis of Brine". Student Resources for General Chemistry, *http://chemed.chem.wisc.edu/chempaths/GenChem-Textbook/Electrolysis-of-Brine-991.html*.

[86] Chabay, R., Sherwood, B. (2006). "Matter and Interactions Vol. 2 Electric and Magnetic Interactions", chap 18. Wiley.

[87] Brauchle, M., Baumer, K., Gönczy, P., (2003). "Differential Activation of the DNA Replication Checkpoint Contributes to Asynchrony of Cell Division in C. elegans Embryos". Current Biology, 13, 819–827.

[88] Rose, L., Lamb, M., Hird, S. (1995). "Pseudocleavage is dispensable for polarity and development in C. elegans embryos". Developmental biology, 168, 479–489.

[89] Micro-Optik, *http://www.micro-optik.com/htm/zeiss_axioplan2imaging.php*.

[90] WormClassroom, *http://www.wormclassroom.org/image/embryonic-development-dic*.

[91] Schumacher, B., Alpi, A., Garter, A. (2003). "Cell Cycle: Check for Asynchrony". Current Biology, 13, 560-562.

[92] Nance, J., Lee, J.-Y., Goldstein, B. (2005). "Gastrulation in C. elegans". WormBook.

[93] Wormatlas Glossary, Wormatlas, *http://wormatlas.psc.edu/ver1/glossaries/lglossary.htm*.

[94] Antoshechkin, I., Han, M. (2002). "The C. elegans evl-20 Gene Is a Homolog of the Small GTPase ARL2 and Regulates Cytoskeleton Dynamics during Cytokinesis and Morphogenesis". Developmental Cell, 2, 579-591.

[95] Schnabel, R., Hutter, H., Moerman, D., Schnabel, H. (1997). "Assessing normal embryogenesis in Caenorhabditis elegans using a 4D microscope: variability of development and regional specification". Developmental biology, 184, 234–65.

[96] Jaffe LF. "Electrical currents through the developing Fucus egg". Proc Natl Acad Sci USA, 56, 1102–1109.

[97] "Resistivity, Conductivity and Temperature Coefficients for some Common Materials". The Engineering ToolBox, *http://www.engineeringtoolbox.com/resistivity-conductivity-d_418.html*.

[98] Schedl, T. (2013). "Germ Cell Development in C. elegans". St. Louis: Springer.

[99] Riddle, D. L., Blumenthal, T., Meyer, B. J., Priess, J. R. (1997). "C. elegans II", 2 ed, chap 10. New York: Cold Spring Harbor Laboratory Press.

[100] Robertson, S., Lin, R. "The Oocyte-to-Embryo Transition". in, Schedl, T. (2013). "Germ Cell Development in C. elegans". St. Louis: Springer.

[101] Wikipedia (Keywords: "Cleavage (embryo)", *http://en.wikipedia.org/wiki/Cleavage_(embryo)*.

[102] Seydoux,G., Strome, S. (1999). "Launching the germline in Caenorhabditis elegans: regulation of gene expression in early germ cells". Development, 126, 3275-3283.

[103] Rose, L. S., Basham, S. E. (2006). "Caenorhabditis elegans Embryo: Establishment of Asymmetry". eLS. John Wiley & Sons Ltd.

[104] Gönczy, P., Rose, L. S. (2005). "Asymmetric cell division and axis formation in the embryo". WormBook.

[105] Oegema, K., Hyman, A. A. (2006). "Cell Division". WormBook.

[106] Johnston, W. L., Krizus, A., Dennis, J. W. (2010). "Eggshell Chitin and Chitin-Interacting Proteins Prevent Polyspermy in C. elegans". Current Biology, 20, 1932-1937.

[107] Paupard M. C., Miller A., Grant B., Hirsh D., Hall D. H. (2001). "Immuno-EM localization of GFP-tagged yolk proteins in C. elegans using microwave fixation". J Histochem Cytochem, 49, 949–956.

[108] Benenati G., Penkov S., Muller-Reichert T., Entchev E. V., Kurzcalia T. V. (2009). "Two cytochrome P450s in Caenorhabditis elegans are essential for the organization of eggshell, correct execution of meiosis and the polarization of embryo". Mech Dev, 126, 382–393.

[109] Stiernagle, T. (2006). "Maintenance of C. elegans". WormBook.

[110] "Soft Lithography". Nanoterra, *http://www.nanoterra.com/soft_lithography.asp*.

[111] Ruzin, S. E. "Differential Interference Contrast (DIC)", in Ruzin, S. E. (1999). "Plant microtechnique and microscopy". New York: Oxford University Press, (chapter available in *http://microscopy.berkeley.edu/Resources/instruction/DIC.html*).